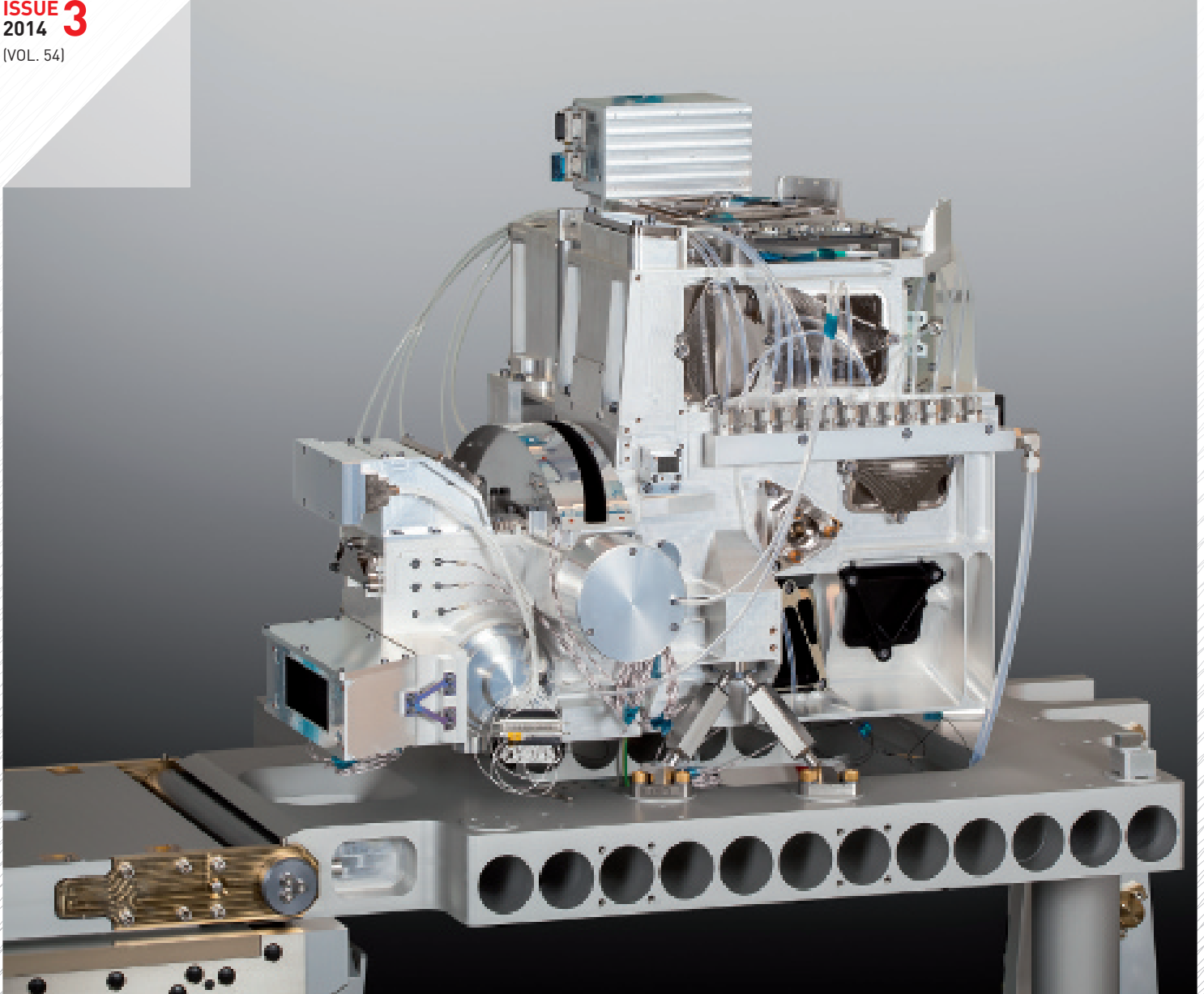


PROFESSIONAL JOURNAL ON PRECISION ENGINEERING

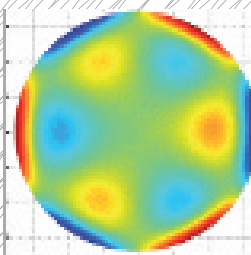
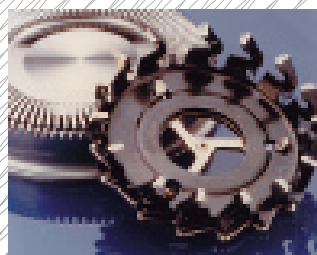


MIKRONIEK

ISSUE 3
2014
(VOL. 54)

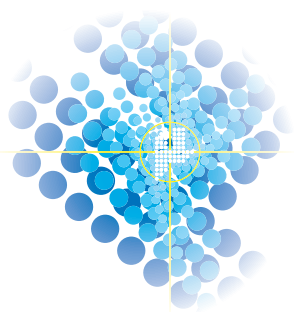


SPECIAL ISSUE: **THERMO-MECHANICS** – DESIGN, ANALYSIS AND VALIDATION
■ PRECISION **ECM** ■ FROM **SIGNAL** ANALYSIS TO **SYSTEM** ANALYSIS



Mikroniek is a publication of the DUTCH SOCIETY FOR PRECISION ENGINEERING www.dspe.nl

DSPE



Komt u ook?

Precisiebeurs 2014

Hét trefpunt voor precisietechnologie!

- Nieuwe technologieën, oplossingen en producten
- Expositie van 275 specialistische bedrijven en kennisinstellingen
- Gratis 50 innoverende, inspirerende en onafhankelijke lezingen
- Inclusief internationaal Brokerage Event

www.precisiebeurs.nl



14^e editie
gratis toegang

Vakbeurs & Congres

Woensdag 12 en donderdag 13 november 2014
NH Conference Centre Koningshof, Veldhoven

Met ondersteuning van:

PUBLICATION INFORMATION

Objective

Professional journal on precision engineering and the official organ of DSPE, the Dutch Society for Precision Engineering. Mikroniek provides current information about scientific, technical and business developments in the fields of precision engineering, mechatronics and optics.

The journal is read by researchers and professionals in charge of the development and realisation of advanced precision machinery.



Publisher

DSPE
High Tech Campus 1, 5656 AE Eindhoven
PO Box 80036, 5600 JW Eindhoven
info@dspe.nl, www.dspe.nl

Editorial board

Ir. Herman Soemers (chairman, University of Twente, Philips Innovation Services), ir.ing. Bert Brals (CCM), dr.ir. Dannis Brouwer (University of Twente), ir. Bart Dirkx (coordinator, WittyWorX), ir. Jos Gensing (MaromeTech, Avans), ir. Rob van Haendel (Additive Industries), ir. Huub Janssen (Janssen Precision Engineering), ir. Henk Kiela (Opteq, Fontys), ir. Casper Kruijer, MBI (FEI), ing. Ronald Lamers, M.Sc. (MI-Partners), ir. Piet van Rens (Settels Savenije van Amelsvoort), ir. Ad Vermeer (SoLayTec, Adinsyde)

Editor

Hans van Eerden, hans.vaneerden@dspe.nl

Advertising canvasser

Gerrit Kulsdom, Sales & Services
+31 (0)229 – 211 211, gerrit@salesandservices.nl

Design and realisation

Twin Media, Culemborg
+31 (0)345 – 470 500, info@twinmediabv.nl

Subscription costs

The Netherlands	€ 70.00 (excl. VAT) per year
Europe	€ 80.00 (excl. VAT) per year
Outside Europe	€ 70.00 + postage (excl. VAT) per year

Mikroniek appears six times a year.

© Nothing from this publication may be reproduced or copied without the express permission of the publisher.

ISSN 0026-3699



The main cover photo (Ultraviolet-Visible-Near infrared (UVN) spectrometer module of the TROPOMI instrument) is courtesy of TNO/Leo Ploeg.

IN THIS ISSUE

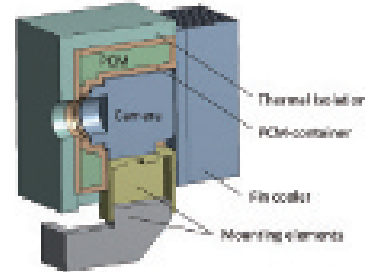
ISSUE **3**
2014

05

Thermo-mechanical stability of TROPOMI

The Tropospheric Monitoring Instrument.

15



11

Design of an AM for EUV lithography

Counteracting thermal aberrations using an adaptive optics system.

15

PCMs for improving measurement and manufacturing precision

Thermal stabilisation by means of solid-liquid phase changes.

22

Back-of-the-envelope thermo-mechanics

Beam equations under thermal load.

27

Report on SIG meeting in Zurich

Euspen Special Interest Group Thermal Issues.



60

32

From signal analysis to system analysis

Introduction to Frequency Response Function measurements – Part 2.

39

Thermal position stability in mechatronic systems

Transient thermal validation for much more system insight.

43

Where no movement is possible

Positioning solutions for cryogenic environments.

48

Upgrading to PEM

Precision electrochemical machining.

54

Not to lose sight of a sub-micron sample

Design of a variable-temperature STM.

60

Proper handling of thermal errors

Topology optimisation for thermo-mechanical systems.

FEATURES

04 EDITORIAL

Theo Ruijl (CTO, MI-Partners) on the competence of managing thermal effects in mechatronic systems.

20 DSPE

www.dspe.nl/knowledge-base/thermomechanics

26 CPE COURSE CALENDAR

Overview of Certified Precision Engineer courses.

67 DSPE CONFERENCE

Programme.

68 NEWS

Including: Roadmap for Digital Fabrication.

71 UPCOMING EVENTS

Including: DSPE Conference on Precision Mechatronics.

THE COMPETENCE OF **MANAGING THERMAL EFFECTS** IN MECHATRONIC SYSTEMS



Everybody who ever had to deal with precise position measurements recognises the effect of temperature on the results of their experiments. Thermally induced drift and position accuracy are linked to each other one on one. In the middle of the last century, mainly driven by the requirements set by the manufacturing of optical systems for the American defence programmes, the 'design for thermal stability' competence was pushed enormously. Looking at scientific publications or academic initiatives, it seems like nothing exciting has happened since.

However, quite the opposite is the case in the high-tech industry. The awareness of thermal effects on the performance of high-end systems and the necessity to take these effects into account in the design of such systems has grown enormously over the last decade. In most of the high-tech companies in our region thermal competence groups have been established. It is very clear that thermal effects are one of the main concerns in high-end systems and the industry needs expertise in this field. As such this trend gives an opportunity for our technical universities to re-establish this competence after extinguishing of the Precision Engineering group at Eindhoven University of Technology following the retirement of Prof. P. Schellekens.

Designing high-end systems requires a thorough understanding of thermal effects towards system performance. This clearly not only concerns positioning or dimensional stability. The effects towards life-time and process quality are in some systems even more challenging. For example, getting the dissipated heat out of a high-performance actuator system is a huge challenge and the design of such a system is mainly driven by this. The quality in all kinds of processes is often thermally driven as well, for example the investigation of samples in an electron microscope at cryogenic temperatures. In general a thorough understanding of multiple physical effects in the system and process is necessary, and robust and effective solutions need to be developed.

Different phases in the development process require different kinds of support and yield different levels of detail of information. It appears that existing methods and techniques from other competences, such as structural dynamics and control, can be applied effectively to the thermal domain as well. Different types of mode shapes (not only Eigen-mode shapes of the homogeneous system) can be studied successfully to understand thermal effects and to increase dimensional stability. The same applies to properties like controllability and observability. Dedicated model reduction techniques are necessary and error budgeting becomes less trivial due to the relative slowness of thermal systems. Thermal deformation inherently means internal flexibility and therefore proper thermal actuation and metrology (temperature/deformation measurement) systems are needed. Developing design rules for systems at extreme temperatures, like cryogenic or space applications, is also a typical example with huge challenges.

All together, we are dealing with very exciting subjects involving multiple physical effects. Development of the competence has just been started and is, like lots of other competences, crucial for the success of our business to develop next-generation mechatronic systems in our region.

Theo Ruijl
CTO and senior mechatronic system architect at MI-Partners
t.ruijl@mi-partners.nl

THE TROPOSPHERIC MONITORING INSTRUMENT

Thermal and opto-mechanical design and analysis work has been done on the Tropospheric Monitoring Instrument (TROPOMI), a spectrometer on the Copernicus Sentinel 5 Precursor satellite. To verify compliance with the stringent opto-mechanical stability requirements, detailed thermal and thermo-mechanical simulations were performed to assess the thermo-mechanical deformation of the UVN (Ultraviolet-Visible-Near infrared spectrometer) module. The predicted stability provides confidence that the desired optical performance will be achieved.

MARTIJN TE VOERT, ROB VAN BRAKEL AND GERT WITVOET

1 The Sentinel 5P satellite with the TROPOMI instrument. (Photo courtesy of ESA)

The Tropospheric Monitoring Instrument (TROPOMI) is a spectrometer on the Copernicus Sentinel 5 Precursor satellite (Figure 1), commissioned by the European Space Agency (ESA) and the Netherlands Space Office (NSO). Copernicus is a joint initiative of the European Commission and ESA.

The spectrometer has four spectral channels: ultraviolet (UV), ultraviolet combined with visual (UVIS), near infrared (NIR), short-wave infrared (SWIR). It uses sun-backscattered radiation to study the earth's atmosphere and to monitor air quality, on both global and local scale. Compared with its predecessors, TROPOMI will take a major step forward in spatial resolution ($7 \times 7 \text{ km}^2$) and signal-to-noise ratio. This allows observations of air quality at sub-city level.

The TROPOMI instrument consists of a Telescope Support Structure (TSS) on which the Ultraviolet-Visible-Near infrared (UVN) spectrometer module and the Short Wave InfraRed (SWIR) spectrometer module are mounted (Figure 2). Dutch Space is the prime contractor of TROPOMI. TNO and Dutch Space jointly develop the UVN module in an integrated team. TROPOMI has passed the Critical Design Review and production and integration of the flight hardware is well underway [1] [2]. On 12 May 2014, TNO delivered the UVN module to Dutch Space for



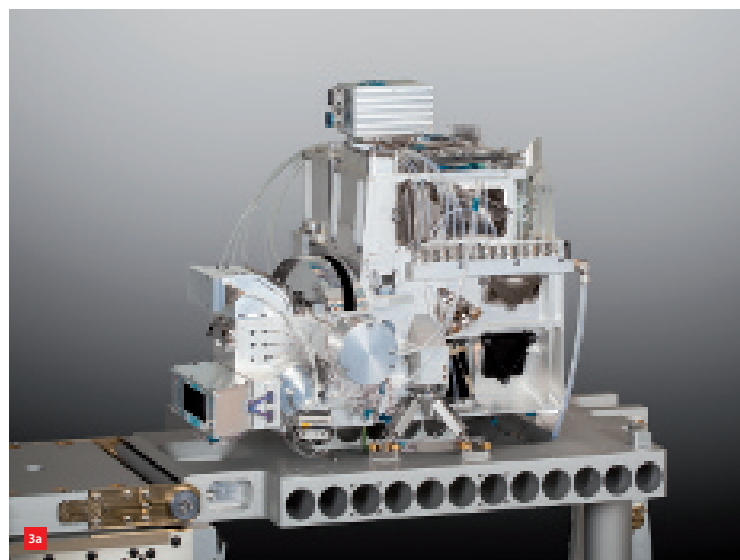
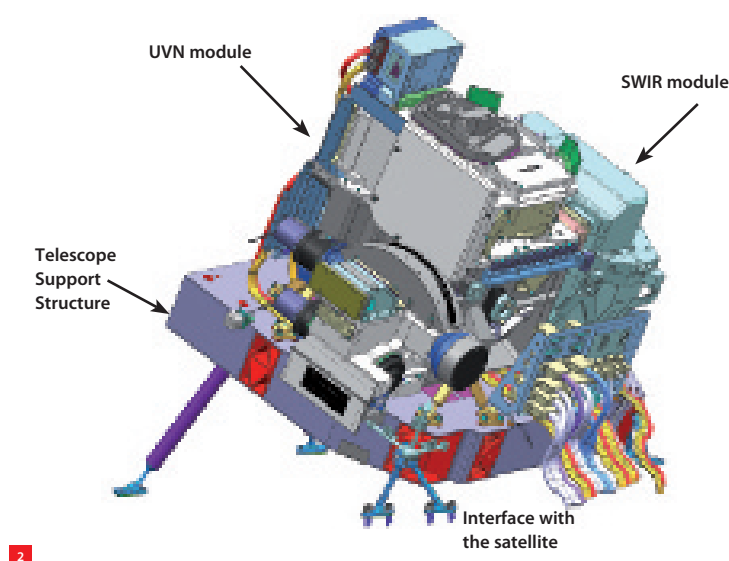
further integration in the instrument (Figure 3a). TROPOMI is scheduled for launch early 2016.

To meet the optical performance requirements, the optical components (such as lenses, gratings and mirrors) inside the modules have to be aligned to very tight tolerances. After alignment, these components have to remain stable

AUTHORS' NOTE

Martijn te Voert is an opto-mechatronic systems designer at TNO Opto-mechatronics in Delft, the Netherlands, working on various space and semicon projects. Rob van Brakel is a thermal control engineer at Dutch Space in Leiden, the Netherlands, working on various instrument and solar array projects. Gert Witvoet is a control specialist at TNO Opto-mechatronics, working on various space and astronomy related projects. He is also part-time Motion Control lecturer at Eindhoven University of Technology, the Netherlands.

martijn.tevoert@tno.nl
www.tno.nl
www.dutchspace.nl



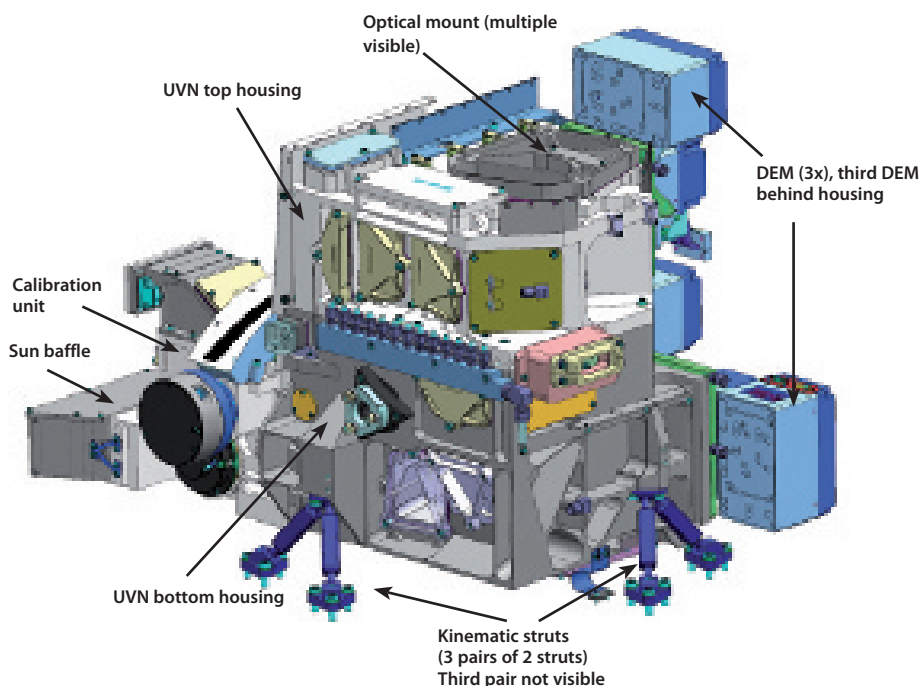
relative to their aligned positions despite environmental disturbances such as gravity changes, launch accelerations and time-varying heat loads. Detailed thermal and thermo-mechanical simulations of the UVN module were performed to verify compliance with the stringent component stability requirements. A high-level overview of the verification activities on the UVN module is given in this article.

UVN module opto-mechanical design

The UVN module has a mass of 80 kg and is about 0.6 m by 0.5 m by 0.5 m in size (Figure 3b). It consists of a Calibration Unit (CU), the main UVN housing with the UV, UVIS and NIR optical channels, and three Detector Modules (DEMs).

The calibration unit contains diffusers, white-light sources, and a mechanism with folding mirrors to reflect sunlight directly into the instrument. This unit is used to monitor and correct the optical performance and to guarantee the accuracy of the measurements. The detector modules contain the CCD detectors and the corresponding readout electronics.

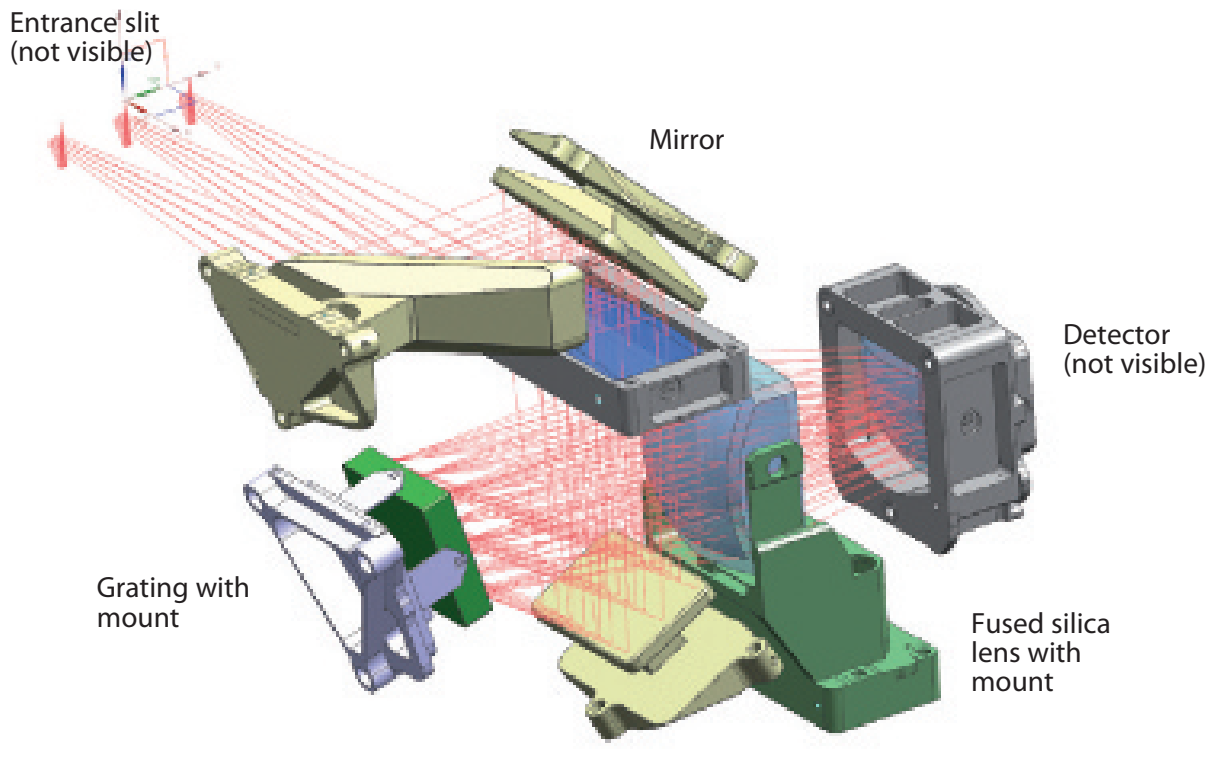
The UVN housing is made from aluminium 6061-T6 and contains the UV, UVIS and NIR spectrometer channels with in total 15 nickel-plated aluminium mirrors and 32 fused silica and silicon lenses which are bonded to high-stability optical mounts [3] [4]. The UVN housing is iso-statically supported by six titanium struts on the TSS and designed to withstand the launch vibrations (equivalent to a quasistatic loading of 250 m/s²) and to survive (non-operational) temperatures between -40 °C to +45 °C.



2 The TROPOMI instrument consists of the UVN module and the SWIR module mounted on the TSS.

3 The UVN module of the TROPOMI instrument.
(a) Mounted on ground support equipment (GSE), as delivered by TNO to Dutch Space on 12 May 2014. (Photo courtesy of TNO/Leo Ploeg)
(b) Schematic.

The optical layout of the UVN module consists of a telescope with freeform optical surfaces, which images light from the earth's atmosphere to the entrance slit of the UV, UVIS and NIR spectrometer channels [5]. Each spectrometer channel contains a grating to separate the light into different wavelengths, multiple (imaging) mirrors and lenses and a CCD detector. The light paths in the UVN module are folded to minimise mass and volume of the instrument. This leads to a complicated optical layout. A rendered animation of the folded light paths inside the UVN module can be found at [6]. As an example, the layout of the NIR channel is shown in Figure 4.



4

4 The NIR channel optical layout from the entrance slit (not visible) to the detector module (not visible). The aluminium mirrors and optical mounts containing the fused silica lenses are included. The light path is folded to minimise the mass and volume of the instrument.

UVN module thermal design

Due to the vacuum in space convection is absent; the only heat transfer mechanisms are conduction and radiation. TROPOMI receives thermal radiation directly from the sun, earth-reflected solar radiation (also called albedo) and earth-emitted thermal radiation. TROPOMI emits thermal radiation towards the cold deep space. The amount of absorbed radiation depends on the season, the position and orientation in orbit (sunlit or in the shadow of the earth) and on the changing properties of the instrument due to degradation in space over its lifetime of seven years.

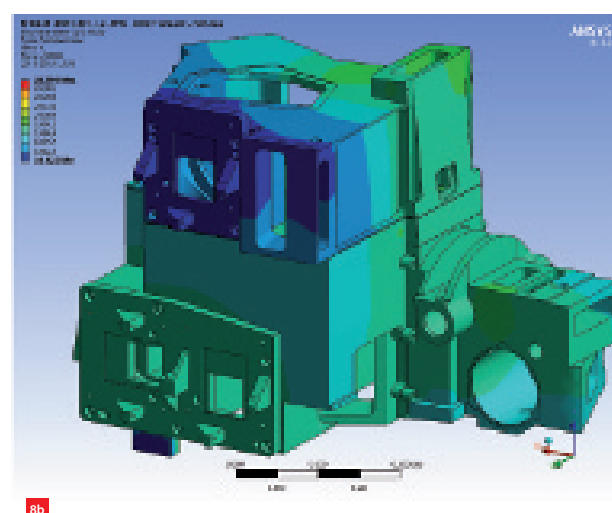
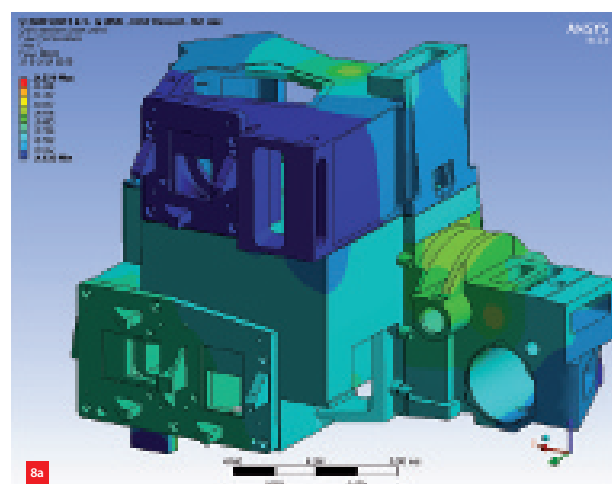
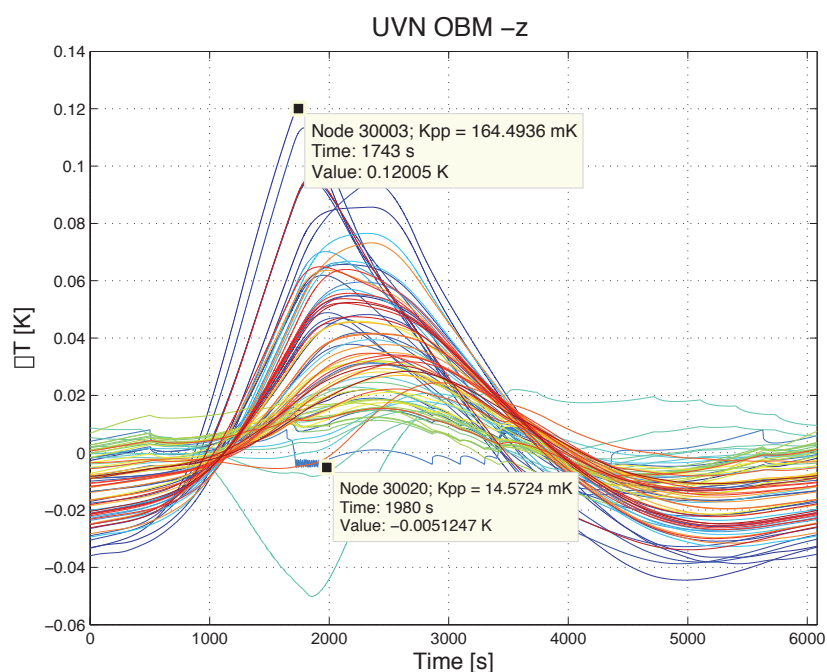
Inside the instrument various temperature levels need to be maintained. The UVN module operates at room temperature (293 K), but the CCD arrays are cooled to 196 K in order to suppress detector dark current. To reduce background noise due to internal thermal emission ('black-body radiation'), the SWIR module is cooled to 205 K. Its detector is cooled to a much lower temperature, 140 K [7]. The temperature of the optical modules and the detectors needs to be stabilised within strict limits in order to maintain the desired radiometric accuracy. For the UVN module detectors and the SWIR detector the temperature variation should not exceed 100 mK and 80 mK, respectively.

To minimise heat transfer to and from space and between the UVN and the SWIR modules, the instrument is

insulated by a Multi-Layer Insulation (MLI) tent. MLI foil is the gold-coloured thermal insulation seen on most spacecraft that acts as a barrier for thermal radiation. Due to the varying heat loads on the instrument the temperatures of the external layer of the MLI tent vary from 194 K to 400 K during each orbit.

The instrument is cooled slightly below the desired temperature levels by a passive radiant cooler (RC) that radiates excessive heat to deep space. Heat pipes transfer the excessive heat from the UVN module to the radiant cooler. The UVN module contains three active heater circuits and a level heater on the UVN main housing and two heaters on the calibration unit to bring the temperature back to the required levels. The temperature is monitored by thermistors and controlled by the Instrument Control Unit (ICU).

The aluminium UVN housing has a high thermal conductivity, which helps to minimise thermal gradients over the structure. The relatively large thermal capacity of the housing minimises temperature variations due to changing heat loads. The heater locations on the housing are chosen such that temperature gradients are further minimised. The UVN module is insulated from the TSS platform by low-conductivity titanium struts. An overview of the thermal design is given in Figure 5.



Here, δT and δu denote deviations with respect to the operating point.

This model is discretised and additional delays are added (which are induced by the Instrument Control Unit), to obtain realistic transfer functions from heater inputs u to thermistor temperatures T .

The model is actually multiple-input-multiple-output (MIMO) because of the multiple heater-thermistor pairs attached to the UVN module. However, the interaction between them is negligible, hence a multiple single-input-single-output (SISO) controller design suffices. For each SISO loop a PI-controller has been optimised for both robustness (the maximum value of the sensitivity is below 1.94 dB) and performance (the I-action is maximised to force maximal bandwidth and low-frequent gain).

A closed-loop simulation result with the obtained controllers is depicted in Figure 7, showing temperature variations over a complete orbit for a part of the UVN module, including various nonlinear effects induced by the ICU. The temperature varies at most 164 mK in this simulation. The temperature fluctuation is periodic, which is a logical result as the disturbances (the radiative heat loads in orbit) are also periodic.

Simulating the thermo-mechanical deformation

The time-dependent heat loads as calculated by ESATAN are included as boundary conditions in an ANSYS finite-

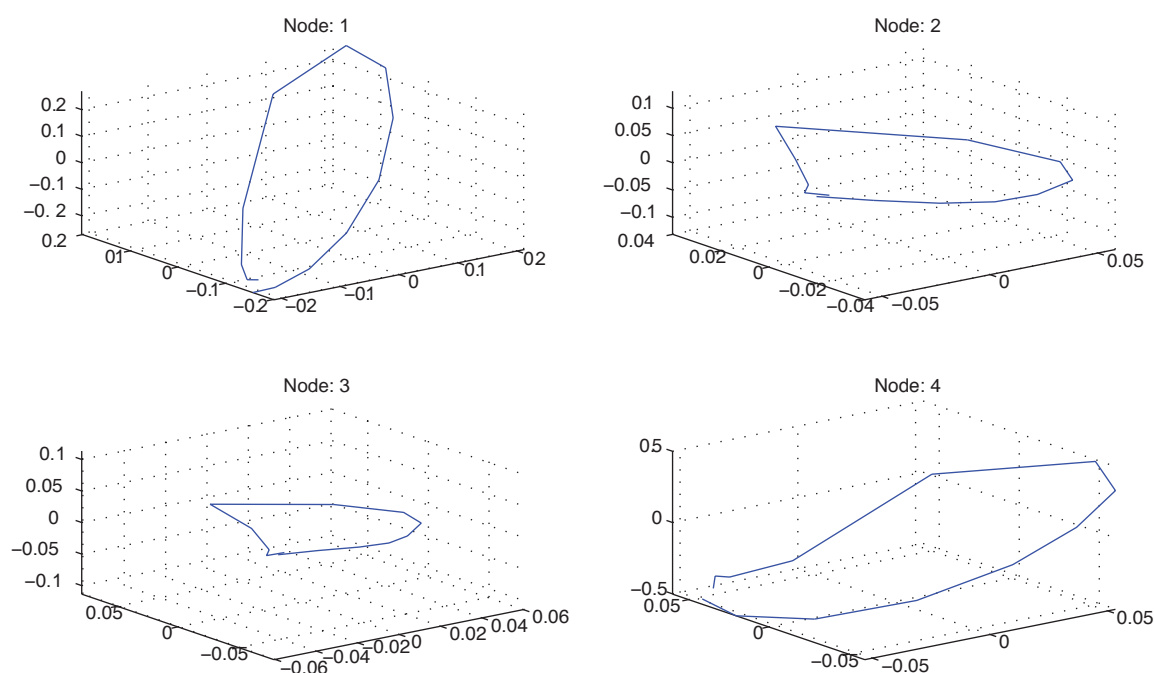
7 Closed-loop simulation result showing temperature variations over a complete orbit for a part of the UVN module.

8 The temperature distribution of the UVN module.
(a) At the start of an orbit.
(b) Halfway an orbit.

element method (FEM) model of the UVN. The positions of critical optical elements are represented by point nodes in the FEM. The deformations of these nodes due to transient heat loads relative to their position under steady-state heat loads are used to evaluate the stability of the component.

In ANSYS, steady-state and transient thermal analysis has been performed to simulate the temperature distribution of the UVN while in orbit. Figure 8 shows the temperature distribution of the UVN at the start of an orbit and halfway, as determined by the transient thermal analysis.

From these temperature fields the time-dependent thermo-mechanical deformation of the UVN over an orbit is determined by a coupled structural analysis. The displacements of the nodes representing the optical components are extracted from the FEM. Figure 9 shows the time-dependent displacements of four nodes (representing the mirrors and lenses inside the UVN



9

module) over one orbit. Because the heat input is periodic, the nodes return to their original position at the end of each orbit.

The overall predicted stability of the lenses and mirrors in the UVN over an orbit is $0.3 \mu\text{m}$ on translation and $1.3 \mu\text{rad}$ on rotation during operation in orbit. As these numbers are within the requirements of $5 \mu\text{rad}$ on rotation and $0.5 \mu\text{m}$ on translation, the optical performance of the instrument will be met.

Conclusions and outlook

This article presents an overview of some of the thermal and opto-mechanical design and analysis work on the TROPOMI instrument. To verify compliance with the stringent opto-mechanical stability requirements, detailed thermal and thermo-mechanical simulations were performed to assess the thermo-mechanical deformation of the UVN module. The predicted stability provides confidence that the desired optical performance will be achieved. This will be further confirmed during the test campaign at instrument level. In the end, final validation will occur during operation in orbit.

The requirements on this type of instruments will only get more stringent in the future. Therefore, TNO is continuously investigating methods to more accurately predict the performance of optical systems by integrating the optical and thermo-mechanical models. This will allow fast and accurate performance assessment of optical

systems under heat loads by coupled opto-thermo-mechanical analysis.

Acknowledgements

TROPOMI is being developed for launch on the Copernicus Sentinel 5 Precursor satellite commissioned by the European Space Agency (ESA) and the Netherlands Space Office (NSO). Copernicus is a joint initiative of the European Commission and ESA.

Dutch Space is the prime contractor of TROPOMI. TNO and Dutch Space jointly develop the UVN module in an integrated team in which the complementary engineering disciplines of both partners are represented.

This document has been produced with the financial assistance of the European Union. The views expressed herein can in no way be taken to reflect the official opinion of the European Union and/or ESA. ■

9 The time-dependent displacement of four nodes (representing the mirrors and lenses inside the UVN module) over one orbit. Because the heat input is periodic, the nodes return to their original position at the end of each orbit. The axis unit is μm .

REFERENCES

- [1] www.tropomi.nl
- [2] R. Voors et al., "The TROPOMI instrument: first H/W results".
- [3] J. Nijenhuis, "Aluminium, de kampioen van het compromis", *Mikroniek* Vol. 47 (6), pp. 34-37, 2007.
- [4] J. Pijnenburg, M. te Voert, J. de Vreugd, A. Vosteen, W. van Werkhoven, J. Mekking and B. Nijland, "Ultrastable bonded optical mounts for harsh environments", *Mikroniek* Vol. 52 (5), pp. 11-19, 2012.
- [5] "The TROPOMI Telescope: Design, fabrication and test of a freeform optical system", *Proceedings ICSSO*, 2012.
- [6] www.tropomi.nl/over-tropomi/zo-werkt-tropomi/?lang=nl
- [7] P. Zevenbergen et al., "Thermal Design of the Sentinel 5 precursor TROPOMI Instrument", *42nd ICES conference*, 2012, AIAA 2012-3580.

DESIGN OF AN AM FOR EUV LITHOGRAPHY

The high absorption of extreme ultraviolet (EUV) light causes thermal deformation of the mirrors in an EUV lithography machine, which in turn distorts the wavefront. This distortion deteriorates the imaging process in lithography. An adaptive optics correction strategy for counteracting these wavefront errors with sub-nm precision is studied. To achieve this precision, an active mirror (AM) is designed and validated in an experimental set-up. A comparison is presented between modelling and experimental results, as well as a feasibility experiment for PI control of the AM.

RUDOLF SAATHOF, JO SPRONCK AND ROB MUNNIG SCHMIDT

Thermal issues in EUV lithography

The cost of integrated circuits can be reduced by miniaturising the size of their functional features and increasing the throughput of their production line. This miniaturisation is achieved by improving the resolution of lithography machines by decreasing the wavelength to an EUV of 13.5 nm and by using image enhancement techniques such as dipole illumination [1]. The throughput is increased, amongst other means, by more powerful light sources.

Since EUV light is highly absorptive, the projection optics of EUV lithography machines have mirrors instead of lenses [2]. Nonetheless, these mirrors heat up and therefore deform. This results in a wavefront error that is greater than

AUTHORS' NOTE

Rudolf Saathof did his Ph.D. work student in the research group Mechatronic System Design at the Department of Precision and Microsystems Engineering, Delft University of Technology, the Netherlands, with associate professor Jo Spronck and professor Rob Munnig Schmidt. Rudolf Saathof now works as a post-doc researcher at the Automation and Control Institute, Vienna University of Technology, Austria.

saathof@acin.tuwien.ac.at
www.acin.tuwien.ac.at
www.pme.tudelft.nl

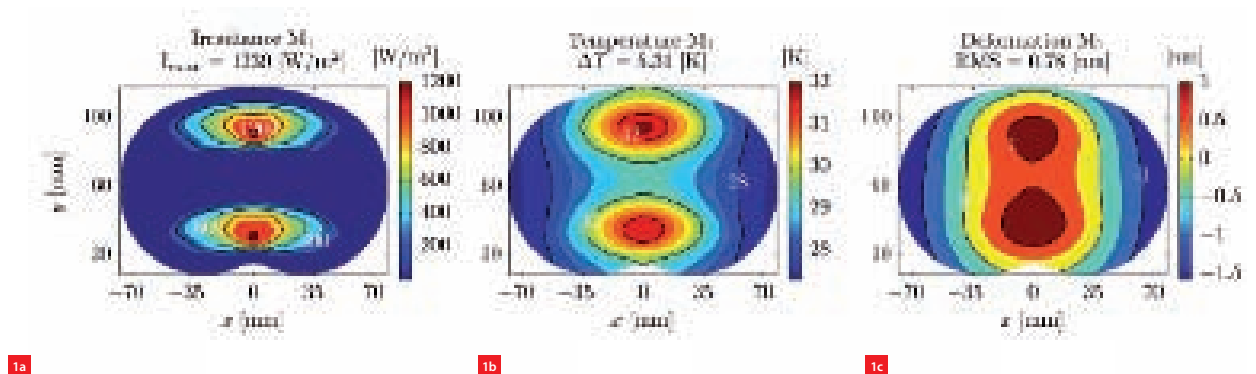
the 0.33 nm RMS allowed [1]. A typical mirror deformation is shown in Figure 1. Exceeding this limit of 0.33 nm critically degrades the image, which in turn can lead to defective integrative circuits.

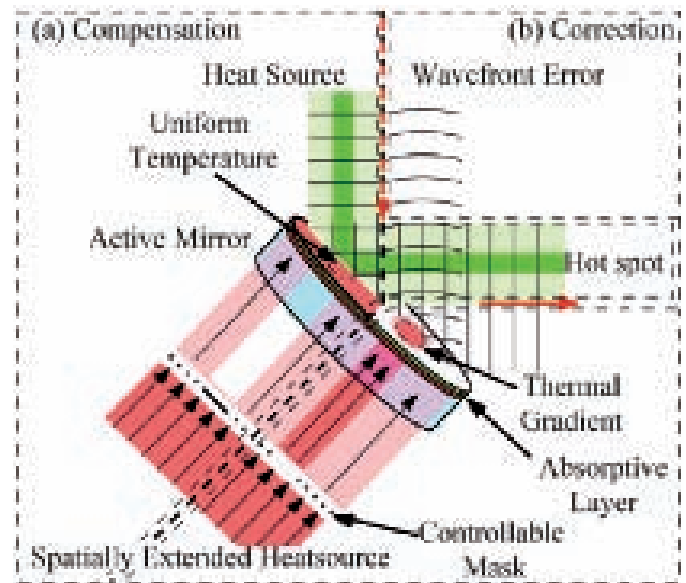
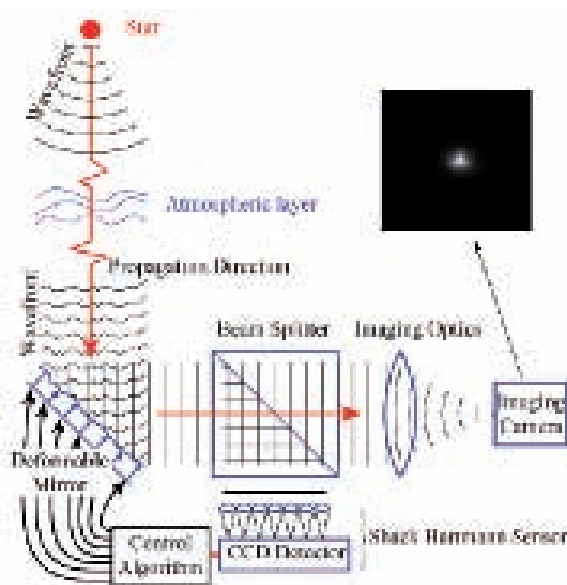
Current corrective methods

To prevent thermal aberrations, EUV lithography machines are equipped with mirrors made of low-thermal-expansion material. This material has zero thermal expansion for one specific temperature, i.e. the zero crossing temperature (ZCT), which is optimised to the lithographic process [3]. Furthermore, the mirrors have active positioning capabilities. To correct wavefront aberrations using these, the wavefront error is measured and minimised using a sensitivity matrix. This sensitivity matrix contains the

1 Simulation results of the first mirror (M1) in the projection optical system. The simulation assumed a dipole illumination setting and a mask with horizontal dense lines and spaces.

(a) Irradiance.
(b) Temperature profile.
(c) Deformation profile.





2 The working principle of an adaptive optics system; see text for explanation.

3 Active mirror design; see text for explanation.

sensitivity between the displacement of the mirrors and the aberration coefficients, which are the amplitudes of orthogonal polynomials, which can be Zernike polynomials. As a result, the ideal placement of the mirrors can be determined [4].

Unfortunately, the variability of the imaging process does not allow the temperature of the mirrors to maintain the exact ZCT, and the computer-aided alignment procedure mainly corrects for defocus and spherical aberration, while dipole illumination for instance causes other aberrations as shown in Figure 1.

Adaptive optics system

To counteract the residual wavefront errors, an adaptive optics (AO) system is proposed. This system, which is known from its application in astronomy and microscopy [5], can be used to improve image quality as shown in Figure 2. The wavefront of light from a star is disrupted by turbulence in atmospheric layers, and corrected by the deformable mirror (DM). In order to do so, light is separated from the beam using a beam splitter and exposed to a Shack-Hartmann wavefront sensor consisting of a lenslet array and a CCD detector. The sensor signal is subjected to a control algorithm that obtains the necessary control signals for the DM. When the wavefront is properly corrected, the image on the imaging camera reveals the universe at the diffraction limit.

Unlike these AO systems, it is not possible to measure the wavefront in real time in an EUV lithography machine, i.e. during the illumination of wafers. It would decrease the available light for the lithographic process, which is not

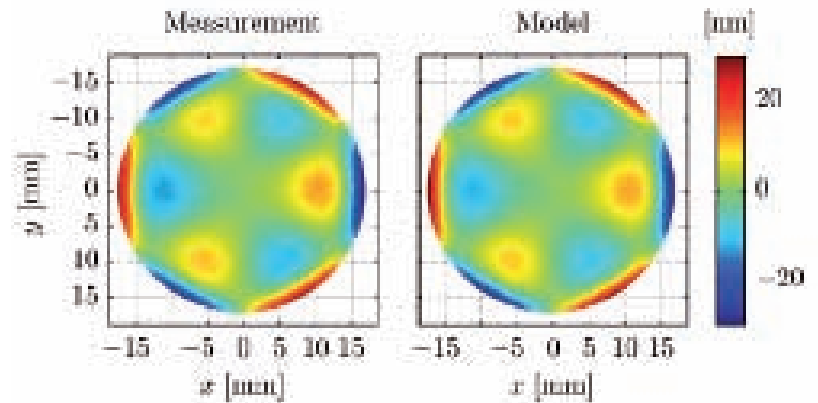
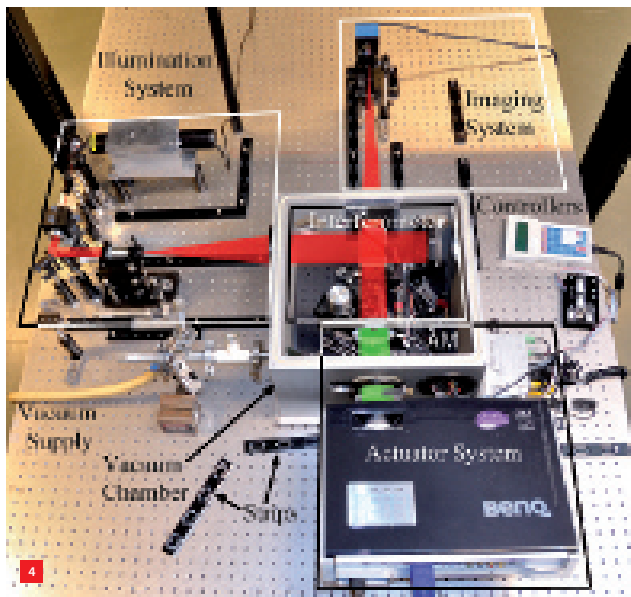
allowed. In addition, the required precision is 2-3 orders of magnitude better.

To anticipate these differences, an adapted compensation approach is proposed. A wavefront sensor measures the wavefront during the wafer exchange procedure, which is every 30 seconds. A control algorithm computes the actuator signal for the DM based on a real-time model predicting the thermal and deformation profile with support of the measurement signal. Instead of a conventional DM, which has a discretised actuation structure, an active mirror (AM) counteracts the predicted wavefront error. This AM needs sufficient stability to bridge the time gap between two individual measurements.

Active mirror (AM) design and realisation

This AM's design is based on the following obvious statement and is depicted in Figure 3. A mirror with a uniform temperature has no thermal gradients that are related to local mirror deformations. Hence, the temperature distribution is modified to achieve a uniform temperature to maintain an undistorted shape of the reflective surface. This is achieved by exposing this AM to a (radiative) heat source instead of using mechanical actuators.

This idea is composed of the following (see Figure 3): an absorptive layer absorbs radiation from a spatially controllable heat source. The *compensation* aspect of this actuation concept involves the exposure to an actuation profile opposite to the predicted irradiance profile, resulting in a net uniform irradiance profile. The *correction* aspect is based on the principle of thermal expansion; thermally



induced deformations correct the wavefront error caused by other components in the optical system. These aspects are used simultaneously. Since this concept is significantly different compared to conventional deformable mirrors, we refer to this concept as AM.

A demonstrator AM is created by depositing an absorbing optical coating, which has an optical quality, on a mirror substrate. A normal reflective (aluminium) coating is deposited on this absorbing coating. The mirror substrate material is BK7, which is a conventional material for optics. This material also offers significantly more thermal expansion than the low-thermal-expansion materials, which makes the experimental procedure considerably easier with respect to measuring the deformation. Obviously, the difference in thermal expansion must be taken into account in the analyses of the experimental results. The spatially adjustable heat source for demonstration is provided by a commercial video projector with a relatively powerful lamp (BENQ 5000 ANSI Lumens).

Experimental set-up

Figure 4 shows the experimental set-up. The main parts are the interferometer and the illumination, the imaging and the actuator system. The photograph also shows the vacuum chamber and supply, strips for mounting the shielding against turbulence and the controllers, which are used for aligning the AM and shutters to block the reference and measurement for calibration purposes.

The set-up has to be sufficiently accurate, which is not an easy task given the required sub-nanometer precision.

Instead of using a Shack-Hartmann wavefront sensor, which is the simplest choice for AO systems, a Michelson (surface) interferometer is built. Usually, surface interferometry uses a phase-stepping method, in which subsequent interferograms are recorded to extract the surface shape.

Instead, the built interferometer uses one interferogram for one measurement to facilitate the possibilities of closed-loop feedback control. This interferometer has a tilted reference mirror to create an interferogram consisting of (almost) straight interference fringes, which are demodulated using the Fourier transfer method [6], to obtain the phase difference between the reference and measurement beam.

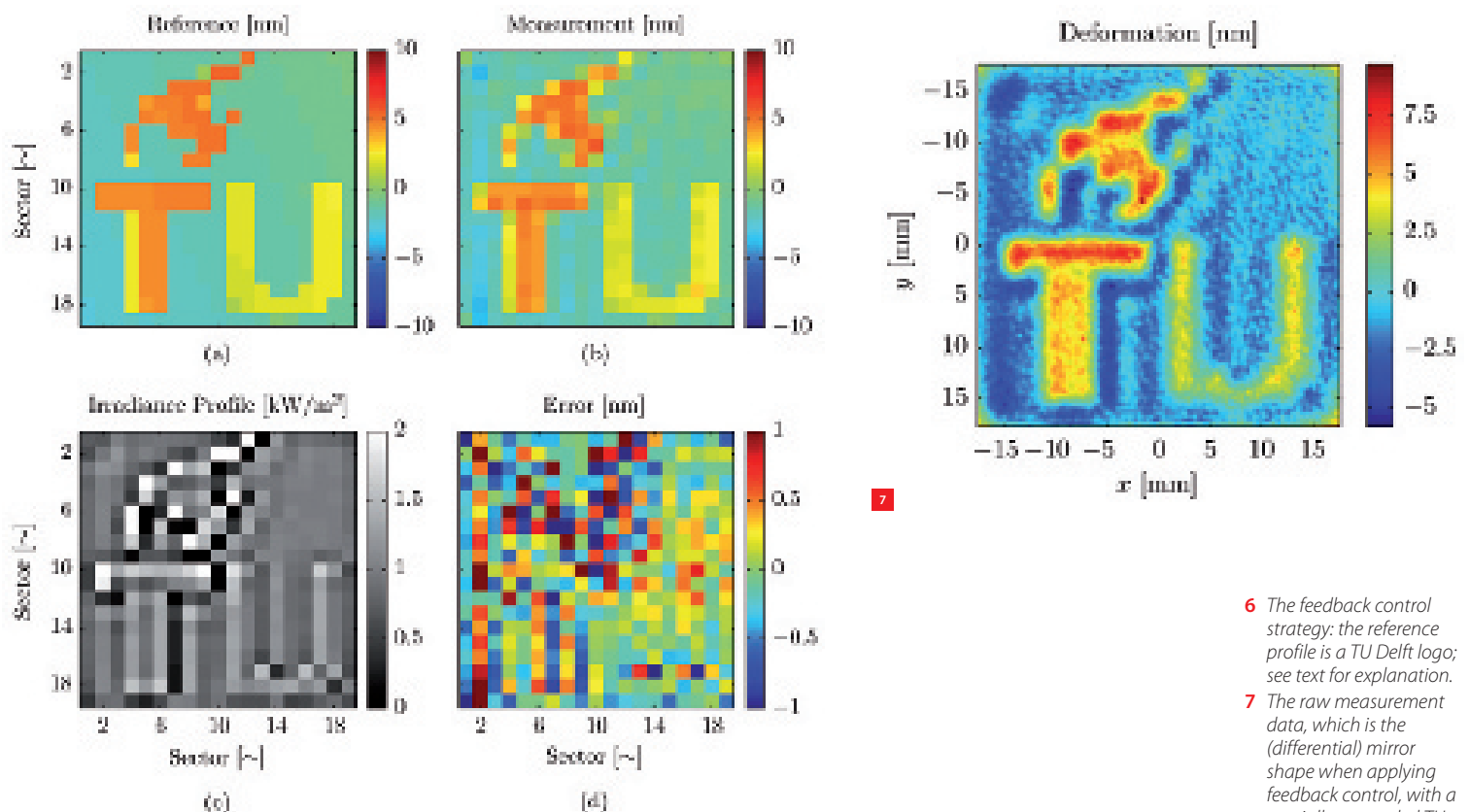
Experimental results

Our research demonstrated that this AM fulfils the requirements, even though they were 2-3 orders of magnitude more strict than conventional systems. In addition, other functional aspects were investigated and carried out, such as the active control of the AM. Here, the results of predetermined actuation profiles using active feedback control are presented.

Predetermined actuation profiles

Wavefront correction is often done by decomposing the wavefront error into orthogonal shapes. To correct the error requires knowledge of the actuation signals to create these orthogonal shapes and superimposing them according to the decomposed wavefront error. Using the FEM (finite element method) package COMSOL Multiphysics, actuation profiles are determined. The approach is an optimisation procedure with the actuation profile as the

- 4 The experimental set-up; see text for explanation.
5 Exposure of the AM to an actuation profile.
(a) Experimental set-up.
(b) Model; a curvature with a peak-to-valley (P-V) amplitude of 2.5 nm is subtracted.



6 The feedback control strategy: the reference profile is a TU Delft logo; see text for explanation.

7 The raw measurement data, which is the (differential) mirror shape when applying feedback control, with a spatially resampled TU Delft logo as reference.

input variable and the squared error between desired shape and obtained shape as the minimisation criterion. Using the video projector, the demonstrator AM has been exposed to these profiles. The modelling and experimental results are shown in Figure 5; these results show no significant differences.

Active mirror control

To check feasibility for control, PI feedback is applied to the AM. To this end, the AM is partitioned in 19x19 sections, which are all independently controlled with the PI feedback controller. Before the control action is applied, a reference shape is obtained that is subtracted from all successive measurement samples to remove the nominal mirror shape. The control strategy is shown in Figure 6 and consists of a TU Delft logo as a reference profile (setpoint), a measurement that is partitioned and an error map with the difference between the measurement and the reference. The control action, which is exposing the AM to an irradiance profile, is derived from the error map. This results in a (differential) mirror shape as shown in Figure 7, clearly displaying nanometer precision.

Conclusions

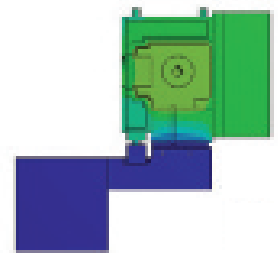
In EUV lithography, the absorption of EUV light could lead to thermally induced wavefront errors that degrade the image quality. This article presents the development and verification of an AM concept that can be used in EUV lithography. Experimental results show that predetermined actuation profiles result in mirror shapes that resemble the expected shape. Furthermore, the results show that feedback control can be applied to obtain mirror shapes with high spatial fidelity. Both experiments show that sub-nm precision can be achieved using an AM. ■

REFERENCES

- [1] V. Bakshi, *EUV lithography*, SPIE, John Wiley & Sons, Inc., 2008.
- [2] Y. Li, K. Ota, K. Murakami, L. Yanqiu, O. Kazuya and M. Katsuhiko, "Thermal and structural deformation and its impact on optical performance of projection optics for extreme ultraviolet lithography," *J. Vac. Sci. Technol. B*, Vol. 21, no. 1, pp. 127-129, 2003.
- [3] J. W. Berthold III and S. F. Jacobs, "Ultraprecise thermal expansion measurements of seven low expansion materials," *Appl. Opt.*, Vol. 15, no. 10, pp. 2,344-2,347, Oct. 1976.
- [4] H. N. Chapman and D. W. Sweeney, "Rigorous method for compensation selection and alignment of microlithographic optical systems," in *Proceedings of SPIE*, 1998, Vol. 3,331, pp. 102-113.
- [5] R. K. Tyson and P. L. Wizinowich, *Principles of adapt. opt.*, Vol. 45, Academic Press, 1992, p. 100.
- [6] M. Takeda, "Spatial-carrier fringe-pattern analysis and its applications to precision interferometry and profilometry: An overview," *Ind. Metrol.*, Vol. 1, no. 2, pp. 79-99, 1990.

PCMs FOR IMPROVING MEASUREMENT AND MANUFACTURING PRECISION

Many technological processes require well-defined and stable thermal conditions. However, inhomogeneous temperature fields can be caused by heat sources like drives, light sources (lasers) or electronics. Thermal stabilisation by means of phase changes may provide a solution. The concept was demonstrated using a special application. In general, the validated approach could be applied to various cooling tasks.



MARC SCHALLES

Introduction

Processes in the field of micromachining, precision manufacturing, optical technologies and precision measurement require well-defined and stable thermal conditions. Homogenous and static temperature fields in the set-ups are ideally required to ensure reproducible and dimensional precise manufacturing or measurements. Inhomogeneous temperature fields can be caused by heat sources like drives, light sources (lasers) or electronics. These temperature fields can cause creeping, dimensional drifts or deformations in these partly complex set-ups. This happens particularly if materials with different coefficients of expansion, joints and non-symmetric machine designs are used.

To reduce thermal effects, heat sources could be controlled, the used equipment could be cooled or its design could be optimised to achieve a reduced thermal sensitivity of the equipment. In many cases, the design of the equipment is quite fixed or the dissipated heat cannot be varied.

In general, there are two approaches to remove heat from hot components, namely active and passive cooling. Typical examples of active cooling methods are liquid cooling, air cooling or Peltier cooling. Compared to passive cooling methods, active cooling methods can deliver a higher

cooling capacity due to the better heat transport resulting from forced convection, high flow rates or low temperatures of the working fluid. The resulting temperature fields can be controlled so that they become quasi-static or less time-varying. In this case, the drawbacks of the methods are mechanical vibrations due to the circulating fluids. These vibrations can influence mechanically sensitive equipment and may disturb measurements or manufacturing.

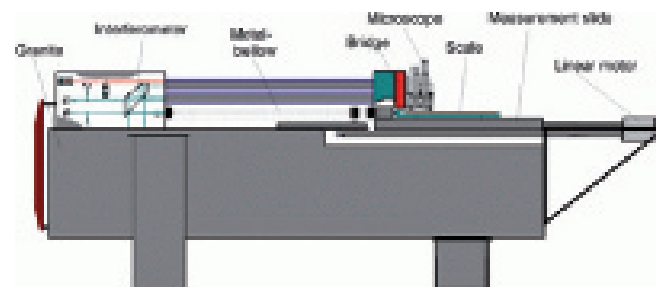
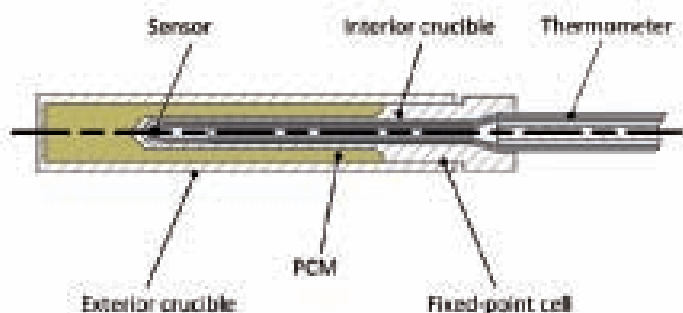
When mechanical vibrations are an important issue, as is the case with dimensional measurements in the nanometer scale, passive cooling approaches without moving fluids have to be selected. Here, thermal conduction, free convection or radiation is used to conduct parasitic heat to thermally insensitive parts of the equipment or to the environment. In this case, the cooling capacity depends on the temperature difference between the hot parts and the heatsinks, the cooling elements and the environment. Since this temperature difference may vary over time, especially when the dissipated parasitic heat is changing, the resulting temperature fields are transient and cannot be stabilised by passive cooling.

To still achieve thermal stabilisation, a passive cooling approach can be enhanced by including a phase change

AUTHOR'S NOTE

Marc Schalles is head of the research group for temperature measurement, Institute of Process Measurement and Sensor Technology, Technische Universität Ilmenau, Germany. The group's focus is on research and development in the field of thermometers and thermometer calibration equipment, and on thermal modelling and thermal optimisation of precision measuring instruments.

marc.schalles@tu-ilmenau.de
www.tu-ilmenau.de



1 Schematics of a thermometer that is calibrated in a PCM-filled fixed-point cell [4].

2 Sketch of the Nanometer Comparator at PTB [5].

material (PCM). Here, the PCM's latent heat of melting can be used as a heat sink.

Solid-liquid phase changes

When materials change from a solid to a liquid constitution, the order of their atoms or molecules decreases and the internal energy of the material increases. To initiate this, energy must be fed into the material. This energy, which is called latent heat of melting, causes the material to break existing bonds and to reorganise in the less ordered molten state. During this melting process, the material remains at a certain material-specific temperature, T_{ph} , until the phase change is finished.

Depending on the material, the melting procedure develops in very different ways. For pure metals and metal eutectics, melting typically takes place in a small temperature range between a tenth of a mK to a few mK. The phase transition is reversible and the corresponding freezing occurs at the same temperature. Contrary to that, most organic or multi-component materials change their phase in a broader temperature range up to a few K. Their phase transition

temperature is not distinctly determined, and segregation, demixing or hysteresis of T_{ph} can be observed.

A selection of materials with melting temperatures around ambient temperature is shown in Table 1.

Depending on their individual thermo-physical properties, PCMs are used in thermal energy stores like solar power plants or for thermal stabilisation in buildings for instance. When the melting temperature of a PCM is very reproducible and well known, T_{ph} can be used as a temperature reference to calibrate thermometers. In this application, special cells are filled with a PCM that is used to accurately stabilise a thermometer to T_{ph} . These cells are called fixed-point cells. Figure 1 shows an example of a thermometer calibrated using a fixed-point cell.

In this example, a fixed-point cell consisting of an exterior and interior crucible is filled with a typically pure metal. A thermometer is inserted into the cell in such a way that the sensor is completely surrounded by the PCM. When the fixed-point cell is heated up by an external heat source, the PCM starts to melt and the temperature within the fixed-point cell, including the thermometer, stabilises at T_{ph} . The thermometer reading can be compared with the well-known temperature T_{ph} and the thermometer can be calibrated.

Thermal shielding set-up

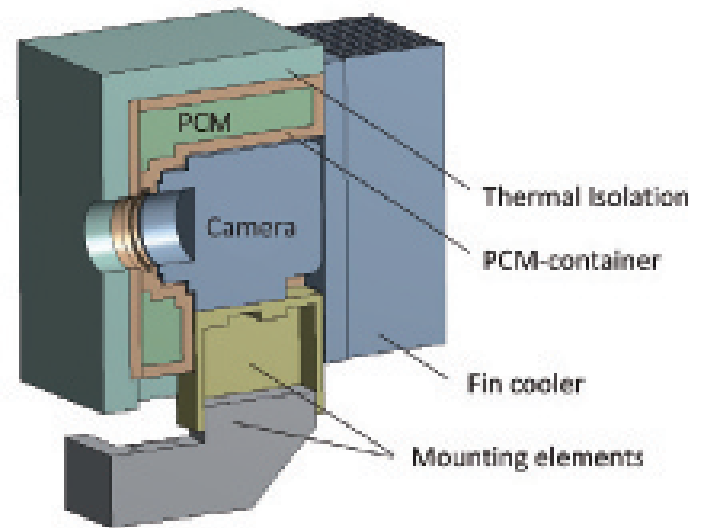
In fixed-point cells, the conversion of heat from the external heat source into latent heat is used to stabilise and homogenise the temperature field in the interior of the cell. The inverse mechanism can be used to cool or shield heat sources in precision equipment or to thermally stabilise temperature fields. Here, heat sources can be encased by a PCM that absorbs parasitic heat and shields the surrounding thermally sensitive parts from the heat source.

One example of this type of precision equipment is the Nanometer Comparator at Physikalisch Technische

Table 1 Selection of materials with melting temperatures around ambient temperature and their latent heat [1-3].

Group	Material ^a	Melting temperature [°C]	Latent heat [kJ·kg ⁻¹]
Inorganic substances	Water	0	333
	Gallium	29.7646	80
	Caesium	28.4	15
	Ga-In (18 %wt In)	15.66	n/a
	Ga-Sn (13.8 %wt Sn)	20.48	n/a
	Ga-Zn (3.7 %wt Zn)	25.19	n/a
Organic substances	CaCl ₂ ·6H ₂ O (salt hydrate)	29...30	170...192
	n-Heptadecane (paraffin)	22	215
	Glycerin	17.9	199
	Butyl stearate (fatty acid)	19	140

^a %wt = weight percent.



Bundesanstalt in Braunschweig, Germany (Figure 2). This piece of equipment is used for precision dimensional measurements of incremental length measurement systems (e.g. linear encoders, line scales) with nanometer uncertainty. Although the measurement principle is interferometric, a microscope with a UV camera is used to observe the stripes of the scales. Joule heating causes this camera to heat up when it is switched on, and its temperature increases significantly above the ambient temperature of 20 °C during a measurement (Figure 3).

This temperature change may lead to variations in the local temperature field close to the measuring microscope and scale. As a result, time-dependent dilatations in the set-up may occur which will lead to deviations in the dimensional measurement. To reduce the temperature changes of the local temperature field without adding mechanical vibrations to the set-up, a passive thermal shielding of the UV camera such as a PCM can be used.

The proof of principle of the PCM shielding was achieved using a demonstration model (Figure 4) which was designed and developed using thermal finite-element analysis (FEA). In this model, the camera is surrounded by a container made of polyethylene (Figure 4, orange) that is filled with PCM (green). The container shields the camera from four sides. A fin cooler is mounted at the back of the camera, which cools down the camera further. The camera itself is mounted on elements of Zerodur (yellow) and Invar (grey). For testing purposes, the whole assembly is mounted on a block (Figure 5).

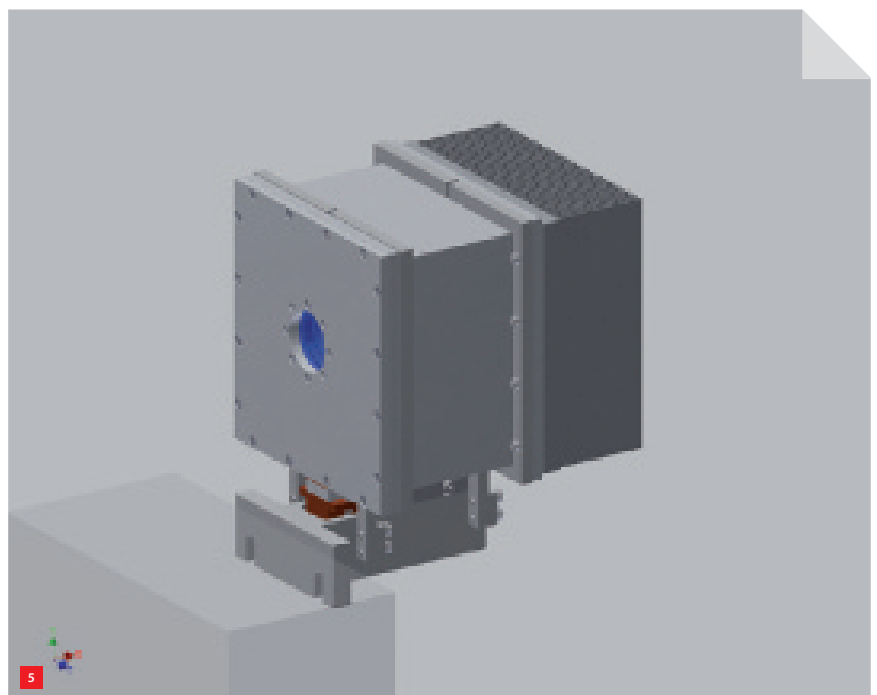
To keep the temperature of the shield as close as possible to ambient temperature, a PCM with a melting temperature above 20 °C had to be chosen. Best suited is a eutectic alloy of gallium and tin (13.8 %wt Sn) with a melting temperature of $T_{ph} \approx 20.5$ °C (s. tab. 1). This was preferable to other materials because it has a melting temperature very close to 20 °C, a narrow melting range and a sufficient reversible behaviour of melting and freezing.

- 3 Infrared picture of UV camera around 38 °C; blue colours indicate high temperatures.
- 4 Schematic of a demonstration model with camera and PCM container.
- 5 Design of measuring set-up without isolation.

The heat flow into the measuring set-up of the Nanometer Comparator is also reduced by using mounting elements with low thermal conductivity (Zerodur and Invar) and small dimensions. Furthermore, the camera temperature is kept low by directing some parts of the generated heat to the environment using the fin cooler. This also helps to elongate the duration of the PCM melting.

Simulation

The theoretical behaviour of the set-up was investigated in thermal calculations using FEA. In these dynamic

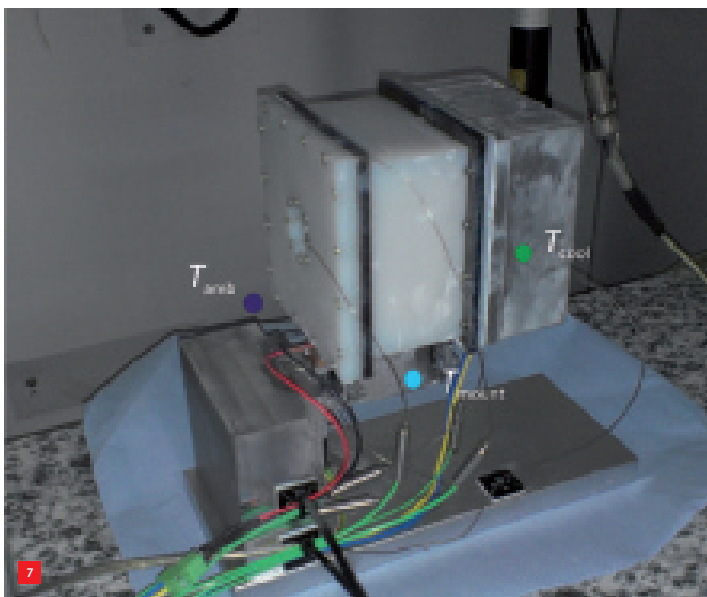
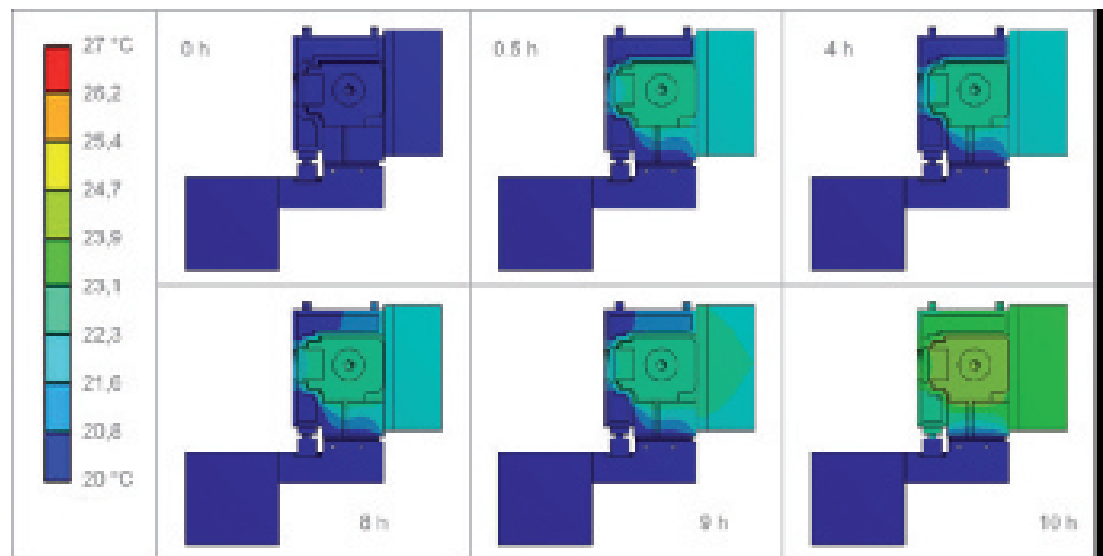


6 Temperature field in the demonstration model calculated by means of FEA.

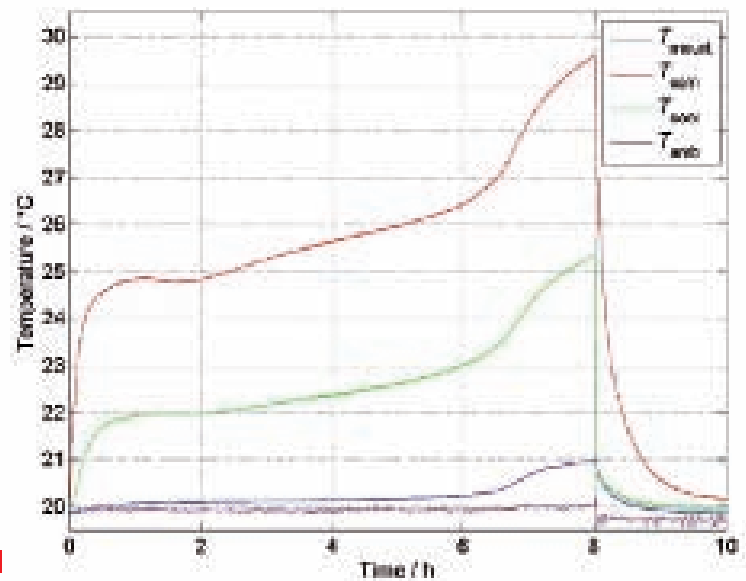
7 Set-up in climatic chamber and monitoring points of temperature curves shown in Figure 8.

8 Results of a measurement in a climatic chamber; locations of the temperature monitoring points are indicated in Figure 7.

6



7



8

simulations, where the camera was switched on at time $t = 0$ s, the time dependence of the temperature field was estimated. Results of this simulation are shown in Figure 6. It can be seen that for $t = 0$ s no heat sources influence the set-up and therefore the temperature is homogeneous at $T = 20$ °C.

When the heating power of approximately 4.5 W at $t > 0$ s is applied to the camera, the camera and the fin cooler start to heat up ($t = 0.5$ h). However, because the PCM absorbs the parasitic heat, the exterior walls and mounting elements remain cold for several hours. After approximately 7-9 hours, the PCM is already molten in some areas and the quality of the thermal shielding decreases. After approximately 10 hours, all of the PCM has been melted by the camera's parasitic heat.

The calculations show that it is possible to provide a thermal shield, a cold exterior surface and stable thermal conditions at the mounting for up to 8 hours. In this time span, a measurement with the camera could be performed. After that, the PCM must be refreshed or solidified again.

Measurement results

To prove the calculation results, a demonstration model was built. It was placed in a climatic chamber (Figure 7) for the measurements and was measured at the same conditions assumed for the calculation. The temperature at certain points was monitored by means of thermocouples (Figure 8). In the graph, three typical periods of the phase change can be observed. In period 1 from $t = 0$ h to $t = 1$ h, the set-up heats up and thermally stabilises. There are quite

stable thermal conditions present between $t = 1$ h and $t = 7$ h. In period 3, after approximately 7 hours, the PCM is nearly molten and the temperature starts to increase significantly.

The measurements are pretty much in line with the calculations. They show that the temperature T_{mount} at the mounting position (Figure 8, blue curve) remains stable for 7 hours, although the temperature of the camera T_{cam} is significantly higher. As such, it can be concluded that the PCM's thermal stabilisation of the demonstration model is successful, the surface of the demonstration model remains cold and heat flow into the mounting is minimised.

Conclusions

The concept of thermal stabilisation by means of phase changes was demonstrated using a special application. Here, the positive results achieved with the demonstration model suggest an improvement of the thermal conditions at the Nanometer Comparator and the measuring microscope. In general, the validated approach could be applied to various cooling tasks. Then, different PCMs could be

chosen depending on the cooling capacity required and the application-specific temperatures.

This new concept of PCM cooling was investigated in the context of the JRP-IND13 research project of the European Metrology Research Programme (EMRP) [6]. The author gratefully acknowledges the joint funding provided by the EMRP-participating countries within EURAMET and the European Union. ■

REFERENCES

- [1] Preston-Thomas, H., "The International Temperature Scale of 1990 (ITS-90)", *Metrologia*, 1990, 27: p. 3-10.
- [2] Sharma, S.D., and Sagara, K., "Latent Heat Storage Materials and Systems: A Review", *Int'l J. Green Energy*, 2005, 2(1): p. 1-56.
- [3] Burdakin, A., et al., "Melting points of gallium and of binary eutectics with gallium realized in small cells", *Metrologia*, 2008, 45(1): p. 75.
- [4] Krapf, G., and Schalles, M., "Comparison of Different Methods of Fixed-Point Evaluation", in *XIX IMEKO World Congress*, 2009, Lisbon, Portugal.
- [5] PTB, Working Group 5.21, *Sketch of Nanometer Comparator at PTB*, www.ptb.de/cms/en/fachabteilungen/abt5/fb-52/ag-521/messgeraete521.html
- [6] EMRP, T3D, *Thermal Design and Dimensional Drift Project*, projects.npl.co.uk/T3D

Skipping a lap lets you get to the finish more quickly

The NTS-Group develops, makes and improves opto-mechatronic systems and modules. We work for leading machine builders (OEMs) all over the world. Our methods enable our clients to innovate and respond to their customers' demands more quickly and radically shorten the time to market for new products. Do you want to move over to the fast lane? We would be pleased to make an appointment to become acquainted. www.nts-group.nl

The NTS-Group is a chain of companies in the Netherlands, the Czech Republic, Singapore and China specialised in developing and building opto-mechatronic systems and modules.



Accelerating your business

WWW.DSPE.NL/KNOWLEDGE-BASE/THERMOMECHANICS

If this would be a digital newsletter, you would already have clicked on this link and would be reading our interesting new website on thermo-mechanics. As this is a magazine, let us give an overview of the information you can find on our website.

PIETER KAPPELHOF, ERIK DE JONG, MARTIN LEMMEN, ROLAND LAMERS, EVERT HOOJKAMP, JASPER WINTERS AND PETER GIESEN

In our high-tech industry, everything has to be positioned with great precision or to stand still with even greater stability. Whether an interferometer with sub-nanometer precision in a conditioned room or a heavily thermally loaded sensor module in space, all high-precision systems are invariably subject to either expansion or shrink because of temperature fluctuations: the thermo-mechanical behaviour of these systems.

As a group of 'fellow engineers' working at different companies, but sharing the same passion and insights on this increasingly important discipline, we started off small over two years ago with the development of a website on thermo-mechanics. The website was set up with two things in mind: DSPE's traditional objective that, as a technology-driven association, it aims to encourage knowledge sharing among colleagues, and the modern fact that the internet has become the largest reference work for polytechnics ever.

Today's engineers can find everything on the internet – an unparalleled revolution that brings engineers from different disciplines closer together than ever before. As an association, this is a trend that we applaud, as also reflected by our own, well-visited website where some 2,000 technical articles and a great many Mikroniek issues can be consulted and searched.

The thermo-mechanics site contains about 50 pages of practical content and features a number of calculators. It is divided into the following sections:

- Basics of thermomechanics starts with the fundamentals, like materials characteristics such as heat capacity or conductivity. There is an overview of such thermo-couplings as conductions, radiation or convection. The essentials and formulas, which most of you learned about at school but many have forgotten, are summarised and elucidated with examples. A valuable page is certainly the one on thermo-mechanical beam equations. See also the article on the subject in this issue of Mikroniek.
- In depth goes beyond the basics. Aspects and insights you won't easily find on the internet

but mostly only in thick books for specialists are presented here clearly and compactly.

- Thermomechanical design makes this a website about thermo-mechanics and tells about the mechanical design aspects. Thermo-mechanics is not about temperature but about thermal drift or, essentially, inaccuracy of your system. Topics addressed include: How to compensate passively or actively? Use of static design principles. How to realise a thermal centre?
- Thermomechanical modelling goes again in depth into the modelling aspects, such as network analyses or the importance and use of transient analyses. We go further than any "Wikipedia on thermomechanics". This paragraph certainly demonstrates this statement.



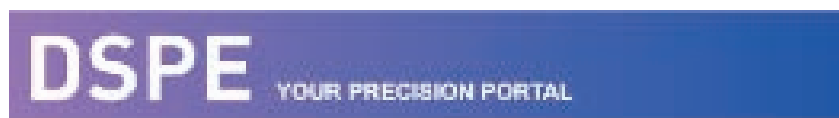
**SPECIAL INTEREST GROUP
THERMOMECHANICS**

- Sensors is about the pros and cons of various sensor principles and how to carry out a successful and reliable measurement. After creating a system you have to verify whether it fulfils its performance. For thermo-mechanics this means mostly temperature measurement on your system.
- Calculators, last but not least, presents the calculators that can be found throughout the website. Ranging from simple linear calculations to complex 6-nodal network calculations, this overview is enough to keep you visiting this website time and time again.

The website was developed by Erik de Jong of Mapper Lithography, Evert Hooijkamp of Delft University of Technology, Ronald Lamers of MI-Partners, Martin Lemmen of TNO and DSPE webmasters Peter Giesen and Jasper Winters, both of TNO.

Besides the pleasure we had in working together on creating this website, we realised the importance of collaborating on such an important discipline and started the Special Interest Group Thermo-mechanics. One of the results is this special issue of Mikroniek.

Furthermore, we will team up with Mikrocentrum to help them organise their next Thermo-mechanics theme day. Of course, the site is not yet finished and we plan to expand it. Everyone interested is invited to sign up, contribute and come up with new ideas. ■



Transient temperature calculator

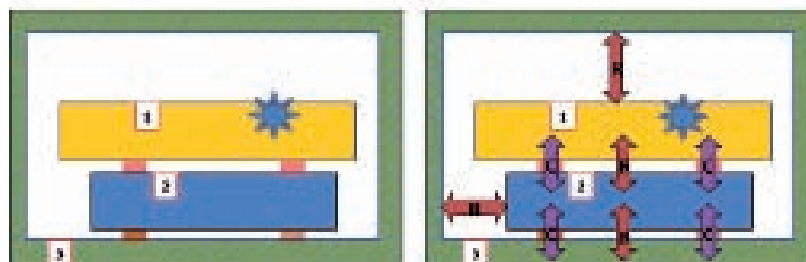
In this calculator you can calculate the steady state temperatures of a network. As well as the temperatures as function of time. Follow the steps, and if you are ready press the button calculate and evaluate the results in the graph.

In a lumped capacity model, a thermal system is divided in to:

- Heat Capacities
- Thermal Couplings

The heat capacities are called Nodes, and it is assumed that the temperature in one node is uniform. Heat capacities can be:

- Large parts
- Thermally conductive parts
- Multiple parts with good thermal conduction between them
- Parts with "important" temperatures



In the image above, a three node system is shown. Part 1 is in contact with body 2 by a few convection points. Body 2 is in contact with body 3, which is a large and surrounds the other parts.

In the picture to the right, the conductive couplings and radiation couplings identified. Body 1 has a heat source.

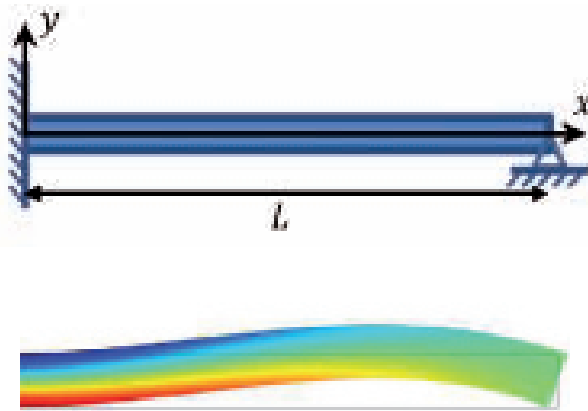
Use the calculation tool to calculate the temperatures as function of time.

• Step 1 Input system size

BACK-OF-THE-ENVELOPE THERMO-MECHANICS

Engineers regularly use back-of-the-envelope calculations to get a rough idea of how a system behaves. In mechanics, beam equations are commonly used to approximate the displacement of a structure under a mechanical load. Surprisingly, similar expressions for loads introduced by temperature fluctuations are hard to find. After some historical perspective, the thermo-mechanical beam equations are derived and their limitations discussed. Finally, the beam equations under thermal load for a beam with a rectangular cross section are presented on a practical handout.

EVERT HOOJKAMP



da Vinci already mentioned the stress distribution in a bending beam in his “Codex Madrid I” (1493), Bernoulli and Euler had to recalculate the approximations, as Da Vinci’s codex was lost until the 20th century. Euler published the beam equations in 1750, but their results were not widely applied until large steel structures such as the Eiffel Tower were built in the second half of the 19th century.

The history of thermal stresses starts with the first paper by Duhamel in 1835, which was published just after the theory of heat was published by Fourier in 1822. Many publications on thermo-elasticity followed, but it took until 1956 before the thermo-elastic beam equations were presented by Boley [2]. These expressions were never as widely used as the beam equations in mechanics, however. Prompted by the precision industry’s growing interest in thermo-mechanical analysis [3], DSPE now provides a thermo-mechanics database including thermo-mechanical beam equations.

Derivation

Beam equations are relatively simple expressions used to compute the deflection and rotation of a single beam. Each equation corresponds to a set of boundary conditions and a single load (see e.g. [4] [5]). Given that the equations are linear, the expressions for combined loads can be obtained by superposition. Here, we limit ourselves to mechanical

History

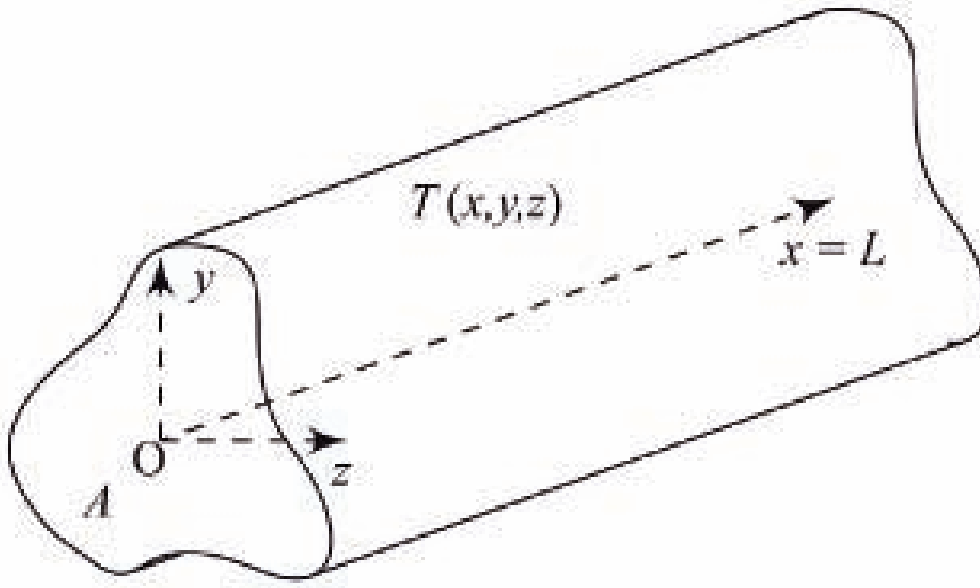
The first engineering rule concerning beams was published by Galileo Galilei in 1638. His rule provided a rough estimate of the bending strength of a beam. Although this rule was completely incorrect, engineers used it for over 300 years [1]. They did so primarily because of Galileo’s reputation and the clear-cut formulation of his rule. Leibniz corrected Galileo’s rule in 1677, but his result was not recognised until the 20th century.

The beam equations used by engineers today were developed in the 18th century by several members of the Bernoulli family and Leonhard Euler. Although Leonardo

AUTHOR’S NOTE

Evert Hooijkamp is finishing his Ph.D. on thermo-mechanical system design in the Structural Optimization and Mechanics (SOM) group, embedded in the Precision and Microsystem Engineering Department of Delft University of Technology, the Netherlands.

e.c.hooijkamp@tudelft.nl
www.3me.tudelft.nl/som



1

loads caused by a known temperature distribution in the beam. Therefore, an extra term is added to the stress, which contains the effect of thermal expansion. We then present the steps required to derive a beam equation subjected to a combination of thermal stresses and mechanical loads.

Let us consider a single beam based on the Bernoulli-Euler hypothesis. It is L long, has a cross-sectional area A and known boundary conditions at both ends of the beam ($x = 0$ and $x = L$); see Figure 1. The beam is subjected to known applied loads and a known temperature distribution $T(x, y, z)$. This will result in axial displacements $u(x)$ and deflections $w(x)$.

Limitations

The beam equations are used a lot, and unfortunately also misused a lot by crossing the limits of the Bernoulli-Euler beam theory. Practical limits to the theory are (see e.g. [5]):

- The material properties are assumed to be linear elastic, isotropic, homogeneous and temperature-independent.
- The beam is straight with a uniform cross section, of which the geometry (ratio) is limited by $L/H > 8$ and $W/H < 2$, where L , W and H denote the length, width and height of the beam, respectively.
- The stiffness changes due to stress are not taken into account, like pre-stress or buckling.

Governing equations

Following the Duhamel-Neumann law, the axial stress component in the beam is written as a combination of the mechanical stress and thermal stress:

$$\sigma_{xx}(x, y, z) = E(\varepsilon_m(x, y) - \varepsilon_T(x, y, z)) \quad (1)$$

Here, E denotes the Young's modulus.

The mechanical strain is estimated as:

$$\varepsilon_m(x, y) = \gamma(x) + \kappa(x) y \quad (2)$$

Here, γ is the axial strain and κ the curvature at the neutral plane of the beam. The linear axial strain is written as:

$$\gamma(x) = \frac{du(x)}{dx} \quad (3)$$

The curvature of the beam is approximated as:

$$\kappa(x) = -\frac{d^2 w(x)}{dx^2} \quad (4)$$

The axial displacements $u(x)$ and deflections $w(x)$ are to be determined. The thermal strain for an arbitrary temperature distribution is defined as:

$$\varepsilon_T(x, y, z) = \alpha (T(x, y, z) - T_0) = \alpha \Delta T(x, y, z) \quad (5)$$

Here, T_0 denotes the temperature of the undeformed beam and α denotes the linear coefficient of thermal expansion.

Finally, the equilibrium equations relate to the known external axial forces and moments due to the internal axial forces and moments due to stress:

$$N(x) = \int_A \sigma_{xx}(x, y, z) dA \quad (6)$$

$$M(x) = \int_A \sigma_{xx}(x, y, z) y dA \quad (7)$$

1 Definition of the single beam under consideration.

Note that the external axial forces and moments include both applied loads and reactions at the two ends.

Combining Equation 1 to 7 and the boundary conditions results in two equations for the two unknowns: the axial displacement and the deflection. Consequently, the analytical expressions for both the axial displacement and deflection can be found. The analytical expressions of some common cases are shown on the practical cut-out page. For additional information on the solution in three dimensions, the reader is referred to [6], and for the solutions of composite or pre-curved beams, solutions are presented in [7].

Common cases

Here, we derive the beam equations for the common cases presented on the practical cut-out page step by step. First, we substitute Equation 1 to 5 into Equation 6 and 7 to obtain the relations between the loads, mechanical and thermal, and displacements:

$$N(x) = \int_A \left\{ E \left(\frac{du(x)}{dx} - \frac{d^2w(x)}{dx^2} y - \alpha \Delta T \right) \right\} dA \quad (8)$$

$$M(x) = \int_A \left\{ E \left(\frac{du(x)}{dx} - \frac{d^2w(x)}{dx^2} y - \alpha \Delta T \right) y \right\} dA \quad (9)$$

These relations can be rearranged and separated into three terms:

$$N(x) = E \frac{du(x)}{dx} \int_A \{ \} dA - E \frac{d^2w(x)}{dx^2} \int_A \{ y \} dA - \alpha E \int_A \{ \Delta T \} dA,$$

$$M(x) = E \frac{du(x)}{dx} \int_A \{ y \} dA - E \frac{d^2w(x)}{dx^2} \int_A \{ y^2 \} dA - \alpha E \int_A \{ \Delta T y \} dA$$

The two first terms of each equation include known integrals:

$$\int_A \{ \} dA = A, \quad \int_A \{ y \} dA = 0, \quad \int_A \{ y^2 \} dA = I$$

Here, I denotes the moment of inertia about the z axis. After substitution, Equation 8 and 9 can be written as:

$$EA \frac{du(x)}{dx} = N(x) + \alpha E \int_A \{ \Delta T \} dA \quad (10)$$

$$-EI \frac{d^2w(x)}{dx^2} = M(x) + \alpha E \int_A \{ \Delta T y \} dA \quad (11)$$

The common cases presented here are free from applied loads. Hence, the external axial forces and moments can only contain effects due to the reactions at the boundaries:

$$N(x) = N_0 \quad (12)$$

$$M(x) = M_0 + M_0 \quad (13)$$

Here, N_0 , M_0 and D_0 denote the unknown axial force, moment and shear force at the ends $x = 0$, respectively. Integrating Equations 10 and 11, after substitution of Equations 12 and 13, results in the analytical expressions of the axial displacement and the deflection:

$$u(x) = u_0 + \frac{N_0}{EA} x + \int_0^x \left(\frac{\alpha}{A} \int_A \{ \Delta T(x_1, y, z) \} dA \right) dx_1 \quad (14)$$


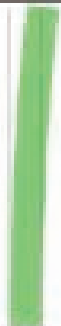
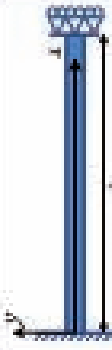

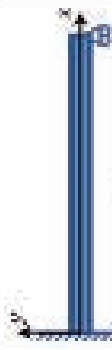

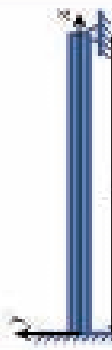





$$w(x) = c_0 + c_1 x - \frac{M_0}{2EI} x^2 - \frac{D_0}{6EI} x^3 - \int_0^x \int_0^{x_2} \left(\frac{\alpha}{I} \int_A \{ \Delta T(x_1, y, z) y \} dA \right) dx_1 dx_2 \quad (15)$$

Here, u_0 indicates the axial displacement at $x = 0$ and c_0 and c_1 denote the unknown integration constants. The final step is to determine the unknowns by the boundary conditions and the known temperature distribution. Finally, the stress field can be determined by Equation 1. ■

REFERENCES

- [1] Truesdell, C., "History of Classical Mechanics - Part 1", *Die Naturwissenschaften* 63 (2): pp. 53-62, 1976. doi:10.1007/BF00622403.
- [2] Boley, B.A., "The Calculation of Thermoelastic Beam Deflections by the Principle of Virtual Work", *J. Aeronautical Sci.* 24 (2), pp. 139-141, 1957.
- [3] Lamers, R., "Keep your cool in precision machine design", *Mikroniek* 51 (3): pp. 27-33, 2011.
- [4] Leijendekkers, P.H.H., et al., *Polytechnisch zakboek*, Vol. 49, Elsevier, 2002.
- [5] Pope, E.J., et al., *Rules of thumb for mechanical engineers: a manual of quick, accurate solutions to everyday mechanical engineering problems*, Gulf Publishing Company, 1997.
- [6] Copper, C. D., and Pilkey, W.D., "Thermoelasticity Solutions for Straight Beams", *J. Appl. Mech.* 69 (3): pp. 224-229, 2002. doi:10.1115/1.1427340.
- [7] Hetnarski, R.B., and Reza Eslami, M., *Thermal Stresses – Advanced Theory and Applications: Advanced Theory and Applications*, Vol. 158, Springer, 2008.

Beam equations under thermal load

Beam type \mathbb{D}	Thermal load case A: $\Delta T(x, y, z) = \Delta T^0$ Equations $\{u(x) = 0\}$	Thermal load case B: $\Delta T(x, y, z) = \Delta T^0 \frac{y}{L}$ Equations $\{u(x) = 0\}$	Thermal load case C: $\Delta T(x, y, z) = \Delta T^0 \frac{y}{H}$ Deformed shape and stress field \mathbb{E}	Equations $\{u(x) = 0\}$
	$u(x) = u \Delta T^0 x$ $\sigma_{xx}(x, y, z) = -\alpha E \Delta T^0 z$	$u(x) = \frac{\alpha \Delta T^0 x^2}{2} \frac{y}{L}$ $\sigma_{xx}(x, y, z) = 0$		$w(x) = -\frac{\alpha}{2H} \Delta T^0 x^2$ $\sigma_{xx}(x, y, z) = 0$ $\sigma_{yy, max} = 0$ $\sigma_{zz, max} = 0$
	$u(x) = 0$ $\sigma_{xx}(x, y, z) = -\alpha E \Delta T^0 z$	$u(x) = 0$ $\sigma_{xx}(x, y, z) = -\alpha E \Delta T^0 \frac{y}{L}$		$w(x) = 0$ $\sigma_{xx}(x, y, z) = -\frac{\alpha E \Delta T^0}{H} y$ $\sigma_{yy, max} = 0$ $\sigma_{zz, max} = -\frac{\alpha E \Delta T^0}{2}$
	$u(x) = u \Delta T^0 x$ $\sigma_{xx}(x, y, z) = 0$	$u(x) = \frac{\alpha \Delta T^0 x^2}{2} \frac{y}{L}$ $\sigma_{xx}(x, y, z) = 0$		$w(x) = -\frac{\alpha}{2H} \Delta T^0 x^2 \left(\frac{y^2}{L} - \frac{y^2}{2} \right)$ $\sigma_{xx}(x, y, z) = \frac{\alpha E \Delta T^0}{2} \frac{y}{H} \left(\frac{y^2}{L} - \frac{y^2}{2} \right)$ $\sigma_{yy, max} = \frac{\alpha E \Delta T^0}{4}$ $\sigma_{zz, max} = \frac{\alpha E \Delta T^0}{4}$
	$u(x) = 0$ $\sigma_{xx}(x, y, z) = -\alpha E \Delta T^0 z$	$u(x) = 0$ $\sigma_{xx}(x, y, z) = -\alpha E \Delta T^0 \frac{y}{L}$		$w(x) = -\frac{\alpha}{2H} \Delta T^0 x^2 \left(\frac{y^2}{L} - \frac{y^2}{2} \right)$ $\sigma_{xx}(x, y, z) = \frac{\alpha E \Delta T^0}{2} \frac{y}{H} \left(\frac{y^2}{L} - \frac{y^2}{2} \right)$ $\sigma_{yy, max} = \frac{\alpha E \Delta T^0}{4}$ $\sigma_{zz, max} = \frac{\alpha E \Delta T^0}{4}$
	$u(x) = u \Delta T^0 x$ $\sigma_{xx}(x, y, z) = 0$	$u(x) = \frac{\alpha \Delta T^0 x^2}{2} \frac{y}{L}$ $\sigma_{xx}(x, y, z) = 0$		$w(x) = -\frac{\alpha}{2H} \Delta T^0 x^2 (x^2 - Lx)$ $\sigma_{xx}(x, y, z) = 0$ $\sigma_{yy, max} = 0$ $\sigma_{zz, max} = 0$
	$u(x) = 0$ $\sigma_{xx}(x, y, z) = -\alpha E \Delta T^0 z$	$u(x) = 0$ $\sigma_{xx}(x, y, z) = -\alpha E \Delta T^0 \frac{y}{L}$		$w(x) = -\frac{\alpha}{2H} \Delta T^0 x^2 (x^2 - Lx)$ $\sigma_{xx}(x, y, z) = 0$ $\sigma_{yy, max} = \frac{\alpha E \Delta T^0}{4}$ $\sigma_{zz, max} = 0$

- 10 The cross-section is rectangular of which $L/H > 8$ and $M/H < 2$, where L , M and H denote the length, width and height of the beam, respectively.
11 The colours represent the stress field (green is zero, red is positive and blue is negative).
12 Note that buckling is not included in this model.

8

CPE COURSE CALENDAR

COURSE (content partner)	CPE points	Provider	Starting date (location, if not Eindhoven)
-----------------------------	------------	----------	---

BASIC

Mechatronic System Design - part 1 (MA)	5	HTI	29 September 2014
Mechatronic System Design - part 2 (MA)	5	HTI	25 Augustus 2014
Construction Principles	3	MC	18 November 2014 28 October 2014 (Utrecht)
System Architecting (Sioux)	5	HTI	10 November 2014
Design Principles Basic (SSvA)	5	HTI	2 July 2014
Motion Control Tuning (MA)	6	HTI	19 November 2014

DEEPENING

Metrology and Calibration of Mechatronic Systems (MA)	3	HTI	1 December 2014
Actuation and Power Electronics (MA)	3	HTI	22 September 2014
Thermal Effects in Mechatronic Systems (MA)	3	HTI	5 November 2014
Summer school Opto-Mechatronics (DSPE/MA)	5	HTI	to be planned
Dynamics and Modelling (MA)	3	HTI	28 October 2014
Summer School Manufacturability	5	LiS	25 August 2014

SPECIFIC

Applied Optics (T2Prof)	6.5	HTI	28 October 2014
Applied Optics	6.5	MC	11 September 2014
Machine Vision for Mechatronic Systems (MA)	2	HTI	25 September 2014
Electronics for Non-Electronic Engineers (T2Prof)	10	HTI	13 January 2015
Modern Optics for Optical Designers (T2Prof)	10	HTI	12 September 2014
Tribology	4	MC	21 April 2015 28 October 2014 (Utrecht)
Introduction in Ultra High and Ultra Clean Vacuum (SSvA)	4	HTI	27 October 2014
Experimental Techniques in Mechatronics (MA)	3	HTI	to be planned
Design for Ultra High and Ultra Clean Vacuum (SSvA)	3	HTI	to be planned
Advanced Motion Control (MA)	5	HTI	6 October 2014
Iterative Learning Control (MA)	2	HTI	3 November 2014
Advanced Mechatronic System Design (MA)	6	HTI	to be planned
Finite Element Method	5	ENG	30 October 2014

DSPE Certification Program

Precision engineers with a Bachelor's or Master's degree and with 2-10 years of work experience can earn certification points by following selected courses. Once participants have earned a total of 45 points (one point per course day) within a period of five years, they will be certified. The CPE certificate (Certified Precision Engineer) is an industrial standard for professional recognition and acknowledgement of precision engineering-related knowledge and skills. The certificate holder's details will be entered into the international Register of Certified Precision Engineers.

WWW.DSPEREGISTRATION.NL/LIST-OF-CERTIFIED-COURSES

Course providers

- Engenia (ENG)
WWW.ENGENIA.NL
- The High Tech Institute (HTI)
WWW.HIGHTECHINSTITUTE.NL
- Mikrocentrum (MC)
WWW.MIKROCENTRUM.NL
- LiS Academy (LiS)
WWW.LISACADEMY.NL

Content Partners

- Dutch Society for Precision Engineering (DSPE)
WWW.DSPE.NL
- Mechatronics Academy (MA)
WWW.MECHATRONICS-ACADEMY.NL
- Settels Savenije van Amelsvoort (SSvA)
WWW.STTSL.NL
- Sioux
WWW.SIOUX.EU
- Technical Training for Professionals (T2Prof)
WWW.T2PROF.NL

REPORT ON SIG MEETING IN ZURICH

Research groups and industries are working on simulating thermal effects in order to compensate for thermally induced errors, and on developing new concepts to reduce these kinds of errors. The ongoing work in this area has led euspen (European Society for Precision Engineering and Nanotechnology) to bring together an international Special Interest Group (SIG) on Thermal Issues. On 19 and 20 March 2014, euspen organised a SIG meeting in Zurich, Switzerland.

RONALD LAMERS

Thermal effects are regarded as a major contributor to errors on machine tools, measuring equipment and workpieces. Measuring thermal effects is becoming even more important as workpiece tolerances decrease, given that thermal effects not only take up a larger part of the tolerances, but also influence repeatability and long-term stability of machine tools and measuring equipment. Consequently, several research groups and industries are working on simulating thermal effects in order to compensate for thermally induced errors, and on developing new concepts to reduce these errors. Progress in this field was discussed during the meeting of the euspen Special Interest Group in Zurich on 19 and 20 March 2014.

AUTHOR'S NOTE

Ronald Lamers works as a senior designer and project manager for MI-Partners, based in Eindhoven, the Netherlands. He especially likes to work at the interface of the mechanical and thermal domain. As such, he contributed to this special issue of Mikroniek and the thermo-mechanics website of DSPE.

r.lamers@mi-partners.nl
www.mi-partners.nl

evolution of motor bikes over the years, which have become smaller in size and mass, and have more speed and power. The motor bikes have evolved from air cooling to liquid cooling and are increasingly equipped with temperature sensors. In addition to this simple example, two grinding machines were examined. The first machine from 1988 weighed 120 tonnes, dissipated 1.5 kW and was equipped with two temperature control channels and four temperature sensors. The second machine from 2006 weighed 17 tonnes, dissipated 15 kW and was equipped with four temperature control channels and fourteen temperature sensors.

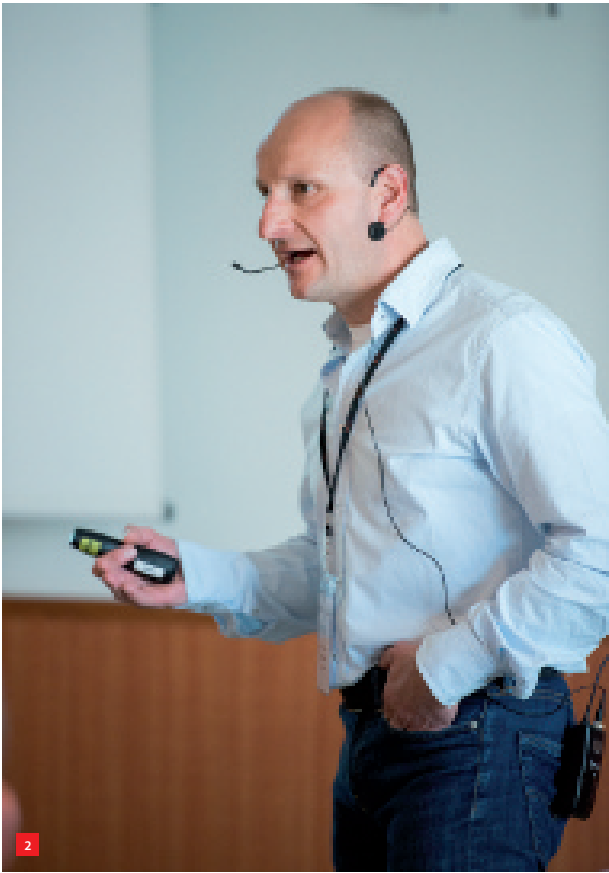
The welcome and opening address was given by Wolfgang Knapp, who works at the Institute of Machine Tools and Manufacturing (INSPIRE / IWF) at ETH Zurich and is currently the euspen president (see Figure 1). ETH Zurich brings together 25,000 people from 80 nations. INSPIRE / IWF, which is the Swiss competence centre for production technology, was the host for this conference. IWF (93 employees, www.inspire.ethz.ch) is a university institute, whereas INSPIRE is a knowledge transfer institute, similar to the German Fraunhofer Institute.

Past and present

The first keynote was given by Professor Paul Shore from the Precision Engineering Institute of Cranfield University, UK. In his presentation, past and present thermal issues were discussed. A simple example was given on the

1 Wolfgang Knapp during his opening address. (Unless otherwise indicated, photos courtesy of euspen; photographer: www.rgbphoto.ch)





2 Theo Ruijl during his presentation on transient thermal validation techniques in mechatronic systems.

3 Conference dinner at 'Zunftthaus zur Schmiden', an old guild house.

The following techniques to reduce thermal effects were explained:

- improved and more sophisticated temperature control;
- designs that are less susceptible (immune) to temperature differences (e.g. gridiron pendulum principle, materials with low coefficient of thermal expansion);
- designs that isolate heat, directing it to 'low-sensitive' regions;
- operations that are repeatable, and components being repeatable, re-gaining dimensional equilibrium after machining, measuring, re-measuring and use.

The final conclusion was that in principle, all thermal error sources (environment, process, machine tool, workpiece) are deterministic and systematic, and can therefore be considered to be measured, understood and described.

Semiconductors

In session 1, "Thermal Error Reduction in Metrology & Control for Semi-Conductors", Jens Flügge from PTB started off with a status overview of results and work at national measurement institutes, such as PTB (Germany), NPL (UK) and VSL (the Netherlands). Marc Schalles from TU Ilmenau presented an interesting application of passive cooling of precision measuring equipment by means of

phase change materials. Rudolf Saathof from TU Delft and TU Wien presented a summary of his Ph.D. work concerning the counteracting of thermal issues in EUV lithography using adaptive optics.

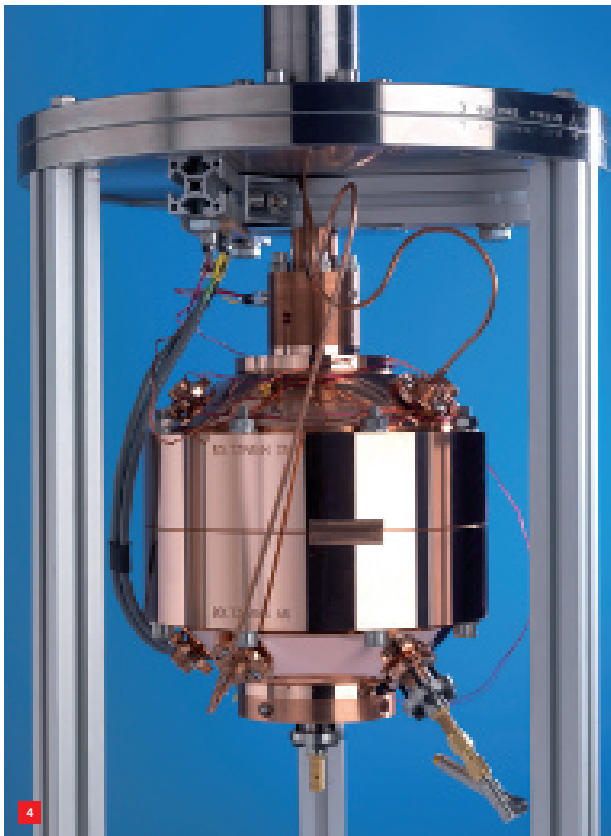
Theo Ruijl from MI-Partners presented the benefit of transient thermal validation techniques in mechatronic systems (see Figure 2). Transient measurements give much more insight into a system than steady-state validation only. Commonly applied techniques in structural dynamics (such as Singular Value Decomposition) have been successfully applied to thermo-elastic systems.

Henny Spaan from IBS Precision Engineering presented a newly formed (primarily Dutch) consortium for industrial research in the field of advanced thermal control of high-precision systems. The main goal is to advance the theoretical and applied approaches to design, simulation, measurement and compensation techniques. The consortium will focus on the following subjects:

- thermal design and optimisation;
- advanced identification and control for thermal systems;
- next-generation model reduction techniques.

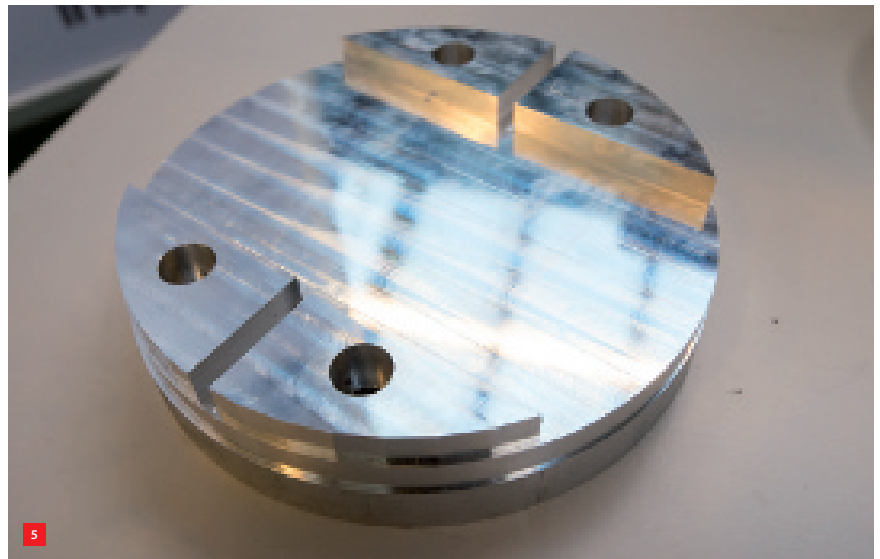
Evert Hooijkamp from TU Delft presented a novel thermal error reduction method by topology optimisation. In many cases, topology optimisation is used for static applications. In his presentation, he showed that topology optimisation can be used for transient thermal error reduction. Timo Laufer from Zeiss SMT presented a thermal fluid-structure analysis of an optical device. Unfortunately, not much information could be shared because of secrecy reasons.





4 The NPL – Cranfield acoustic resonator to accurately measure the Boltzmann constant. (Photo courtesy of NPL)

5 Test piece to visualise the thermally induced deformations on a five-axis machine tool.



Several of the aforementioned presenters have published an article in this Mikroniek issue.

The first day was concluded with a conference dinner (see Figure 3).

The Boltzmann constant

The second keynote, “The Boltzmann constant: accurate measurements for the new Kelvin”, was given by Robin Underwood of the National Physical Laboratory (NPL). Founded in 1900, NPL is the United Kingdom’s National Measurement Institute. The main statement was that the definition of the SI unit of temperature, the Kelvin, is about to change. The Kelvin, the unit of thermodynamic temperature, is the fraction $1/273.16$ of the thermodynamic temperature of the triple point of water, which is chosen so that $1 \text{ Kelvin} \approx 1 \text{ degree centigrade}$. The new definition will be based on fundamental physics: the Boltzmann constant, k_B . The Boltzmann constant, named after Ludwig Boltzmann, is a physical constant relating energy at the individual particle level with temperature. The accepted value in SI units is $1.3806488(13) \cdot 10^{-23} \text{ J/K}$. NPL has measured the value of k_B with the lowest uncertainty in publication (0.7 ppm). Precision engineering by Cranfield University was a significant factor in this success. Figure 4 shows the the set-up, which includes a 62 mm triaxial

ellipsoid resonator chamber, manufactured with an uncertainty of 30 nanometers. The diameters are: $a_x = 62.000 \text{ mm}$, $a_y = 62.031 \text{ mm}$ and $a_z = 62.062 \text{ mm}$

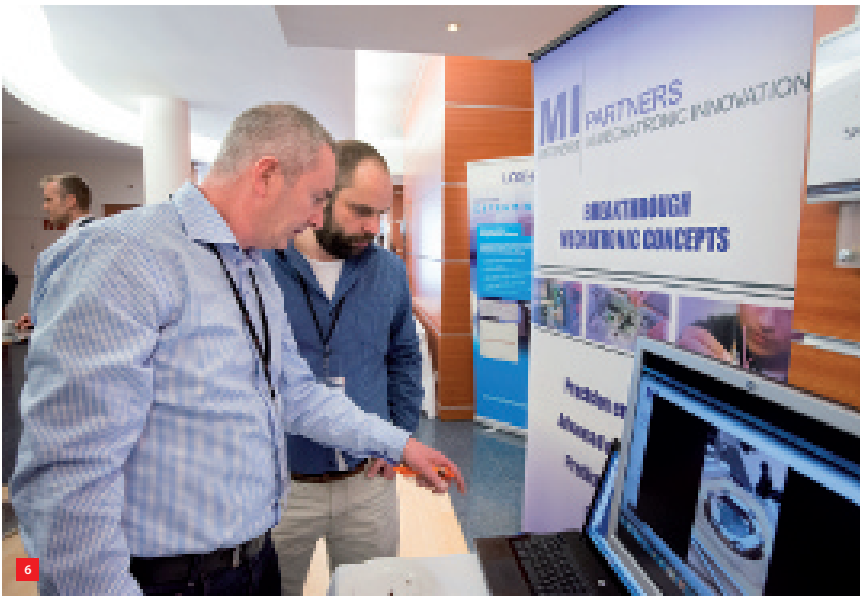
Machine tools

In session 2, “Thermal Control on Machine Tools”, Ralf Bernhardt from Zeiss Industrial Metrology presented some examples of thermo-mechanical design principles applied to measurement machines, such as proper material selection and combining materials with different coefficients of thermal expansion to compensate for (static) temperature variations. Jan Hornych from the Czech TU in Prague presented the influence of the cutting process on the thermal deformation of machine tools. Moritz Wiessner from ETH Zurich presented a method to visualise and measure the thermally induced deformations on a five-axis machine tool with a specially designed test piece (see Figure 5).

Martin Peterek from Fraunhofer IPT presented the measurement uncertainty evaluation of machine tools in a controlled climate surrounding. Large machines are placed inside a climate chamber to investigate such factors as the effect of thermal memory. In his second presentation, Paul Shore presented some thermal control measurements of the $\mu 4$ machine, which mainly included a water-cooled heat shield to prevent heat from the electrical cabinet to flow to the machine, and water-cooling the amplifiers.

Error compensation

In session 3, “Thermal Error Compensation”, Philip Blaser from ETH presented a method to measure the thermal deformation online on a machine tool while machining a workpiece. Otaker Horejs and Martin Mares, both from



6 Impression of the exhibition at the meeting: the small stand of MI-Partners; on the right the author.

Czech TU in Prague, presented thermal error compensation models of several machines based on transfer functions. The latter presented an approach to compensate machine tool angular thermal errors using controlled internal heat sinks and sources.

Makoto Fujishima from DMG MORI presented design improvements of a CNC lathe to reduce thermal displacements. With respect to the ambient temperature variations, the thermal displacements can be reduced by making the bed temperature saturation time shorter and by applying symmetry (thermal and mechanical) to the headstock. For heat generated by the cutting process, thermal compensation is necessary because it is difficult to balance the thermal displacement between bed and turret. Another conclusion was that it is important to conduct analyses and measurements at the design stage.

Gorka Aguirre from Tekniker presented thermal error compensation techniques for large heavy-duty milling-boring machines. His main considerations were to focus on dominant errors and to keep the compensation model simple by using a minimum number of sensors. Matthias Wennemer from Fraunhofer IPT presented a method for volumetric compensation of thermal machine tool errors by using a laser tracer. Simon Fletcher from Huddersfield University presented a method for optimising temperature sensor placement for machine tool thermal error compensation. His method includes IR camera measurements and FEM modelling to find the most sensitive sensor locations, and has been applied to several machines.

Besides an exhibition (see Figure 6), there were two lab tours: one on micro-machining and the other on thermal issues with machine tools. In the latter, the test facilities at ETH were shown, as well as the measurement set-ups from the two contributors from ETH to this conference (see Figure 5).

Conclusion

This SIG meeting on thermal issues covered very diverse aspects of thermal issues in precision systems, ranging from very accurate measurements to material selection and design principles, to thermal control and error compensation, to topology optimisation. The next SIG meeting will be held in 2016 in Prague in the Czech Republic. ■

euspen

With a vision for leading industrialists and academics to come together and form a networking community, euspen (European Society for Precision Engineering and Nanotechnology) has set the standards for innovation in the field of precision, micro- and nano-engineering since 1998. euspen events offer a platform for leading organisations to raise their profile on a world-wide scale embracing its unique target audience of industry and academia. euspen Special Interest Group meetings bring together individuals with other like-minded professionals across the world. They address emerging challenges to industry, discuss common technical issues and galvanise leading activity.

WWW.EUSPEN.EU



YOUR PRECISION PORTAL

DUTCH SOCIETY FOR PRECISION ENGINEERING

DSPE Conference 2014

Conference on Precision Mechatronics



Conference Hotel De Ruwenberg, Sint Michielsgestel
2-3 september 2014

Presentations

Posters and demonstrations

Discussions and networking

Share ideas and experiences

Meet peers in precision mechatronics

Conference by and for technologists, designers and architects in precision mechatronics. This conference is targeted at companies and professionals that are member of:

- Dutch Society for Precision Engineering
- Brainport Industries
- Mechatronics contact groups MCG and MSKE
- Selected companies/academia

The DSPE Conference on Precision Mechatronics creates a forum for discussion and gives the opportunity to share ideas and experiences in order to enhance successful application of systems, control and precision engineering techniques in products, production and manufacturing equipment.

Conference partner:



Brainport
Industries

CONFERENCE CONTRIBUTION:

ADINSYDE
ALTEN MECHATRONICS
ASML
ASTRON
BOSCH REXROTH
BRAINPORT INDUSTRIES
DELFT UNIVERSITY OF TECHNOLOGY
DEMCON
EINDHOVEN UNIVERSITY OF TECHNOLOGY
EMCMCC
FEI COMPANY

FRENCKEN EUROPE
HOLLAND INNOVATIVE
IBS PRECISION ENGINEERING
JANSSEN PRECISION ENGINEERING
MECHATRONICS ACADEMY
MECHATRONICS CONTACT GROUP
MECHATRONICS SYSTEM KNOWLEDGE EXCHANGE
MICE
NIKHEF
NOBLEO TECHNOLOGY
NTS GROUP
NXP SEMICONDUCTORS

OCÉ-TECHNOLOGIES
PHILIPS HEALTH CARE
PHILIPS INNOVATION SERVICES
SEGULA TECHNOLOGIES
SKF ENGINEERING AND RESEARCH CENTRE
TMC
TNO
TU DELFT
VDL ENABLING TECHNOLOGY GROUP
VSL
WITTYWORKX
XPRESS

More information about content and costs: www.dspe-conference.nl

FROM SIGNAL ANALYSIS TO SYSTEM ANALYSIS

AUTHORS' NOTE

Pieter Nuij, senior system architect, and David Rijlaarsdam, group leader, both work at NTS Systems Development in Eindhoven, the Netherlands.

pieter.nuij@nts-group.nl
www.nts-group.nl

Following the previous article on signal analysis, this article focuses on system analysis, specifically on the Frequency Response Function (FRF) as a tool to describe the frequency-dependent behaviour of linear time-invariant systems. This article will outline the move from signal analysis to system analysis and then explain the concept of the cross-spectrum, the FRF and the coherence function. Finally, it will address the specific problems that arise in the identification of closed-loop systems, paying special attention to the practical aspects of FRF measurements.

PIETER NUIJ AND DAVID RIJLAARSDAM

Input-output relationship

In the time domain, the input-output relationship of a causal, linear, time-invariant system is described using a differential equation (DE). Figure 1 shows a mass-spring-damper system with input force $f(t)$ and output displacement $x(t)$.

The DE describes the input-output relationship:

$$f(t) = m\ddot{x}(t) + d\dot{x}(t) + cx(t)$$

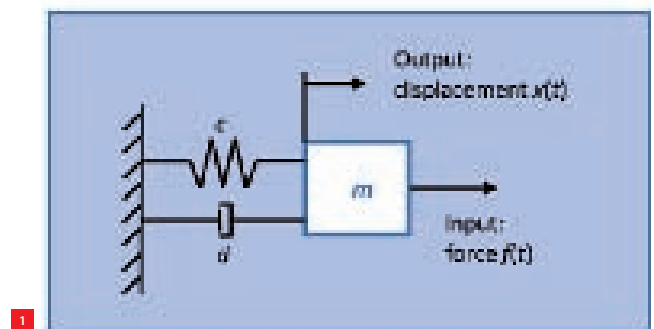
with m representing the mass, d the damping coefficient and c the stiffness. Although this equation describes the dynamics of the system completely, it requires solving for $x(t)$ to explicitly relate the displacement to the excitation force. For more complex systems, solving the DE is often a tedious job. An alternative to solving the DE in the time domain is to transform the DE to the Laplace domain using the Laplace transform $L\{f(t)\}$ is defined as:

$$F(s) = \int_0^{\infty} e^{-st} f(t) dt$$

with complex parameter $s = \sigma + j\omega$. As a result of this transformation, $f'(t) = \frac{d}{dt}f(t)$ in the time domain becomes a multiplication with 's' in the Laplace domain:

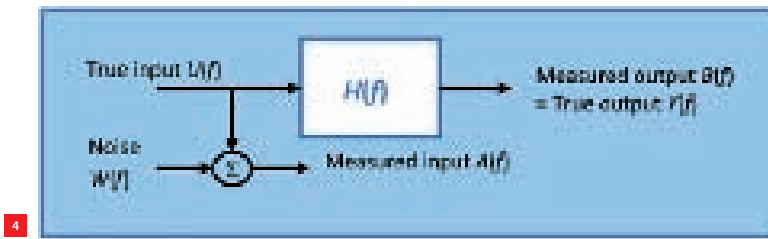
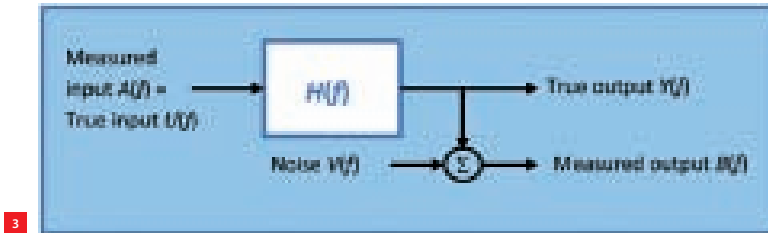
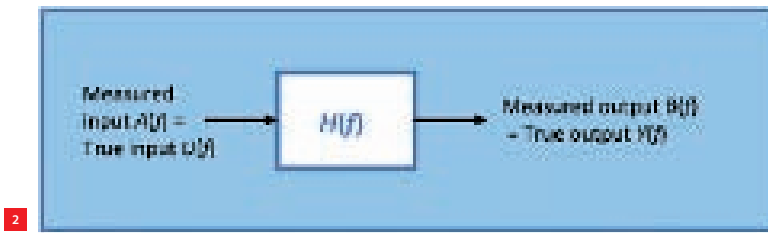
$$L\{f'(t)\} = sF(s) - f(0)$$

1 Mass-spring-damper system loaded with excitation force $f(t)$ responds with displacement $x(t)$.



Three articles

In a series of three articles on Frequency Response Function (FRF) measurements, this second article introduces the FRF, explaining the choice of test signals in relation to the coherence function and the measurement of the FRF in open- and closed-loop systems. The first article, which was published in the previous issue of Mikroniek, covered the steps necessary to convert a time-continuous signal into a discrete spectrum. Potential errors caused by aliasing and leakage were explained and solutions were presented. An overview of several types of test signals was presented. The third article will focus on the extension of frequency-domain methods towards nonlinear systems and the application of such methods to define and optimise the performance of such systems. Each article is illustrated with examples.



Bias errors in FRF estimates

As discussed in the previous section, the FRF can be calculated from the Fourier transforms of the input and output signals of the system to be described. In the ideal situation as shown in Figure 2, the FRF calculation will yield an unbiased estimate:

$$\frac{B(f)}{A(f)} = \frac{Y(f)}{U(f)} = H(f)$$

It is clear that the signal $U(f)$ must contain power in the frequency lines of interest to generate proper results. Without a proper excitation, no estimate is possible. In practice, the measured signals will always include a certain amount of noise. In the situation with noise $V(f)$ in the output signal, as shown in Figure 3, the FRF estimate will be biased:

$$\frac{B(f)}{A(f)} = H(f) + \frac{V(f)}{A(f)}$$

Moreover, noise in the input signal, as shown in Figure 4, will also result in a biased FRF estimate:

$$\frac{B(f)}{A(f)} = H(f) \left[1 - \frac{W(f)}{A(f)} \right]$$

Since noise is always present in realistic measurements, the calculation of the FRF from the Fourier-transformed time signal $A(t)$ and $B(t)$ will always be biased. A significant improvement in the estimation of the FRF can be achieved by using the cross-spectrum. This will be introduced in the next section.

The auto-spectrum and the cross-spectrum

The Fourier transform of a time signal $a(t)$ is defined as:

$$A(f) = F\{a(t)\} = \int_{-\infty}^{+\infty} a(t) e^{-j2\pi ft} dt$$

Applying this transformation to the DE results in:

$$F(s) = ms^2 X(s) + dsX(s) + cX(s)$$

assuming $f'(0) = f(0) = 0$

From this expression, the input-output relationship becomes a polynomial expression with variable s :

$$\frac{X(s)}{F(s)} = \frac{1}{ms^2 + ds + c}$$

which is called the transfer function. Next, substituting $s = j\omega = j2\pi f$ in the transfer function results in the FRF:

$$\frac{X(f)}{F(f)} = \frac{1}{(j2\pi f)^2 m + j2\pi fd + c}$$

$X(f)$ and $F(f)$ are the Fourier transforms of $x(t)$ and $f(t)$, so the FRF of a dynamic system can be determined from its input excitation signal and the resulting output response time signal using a fast Fourier transform (FFT) analyser. This is correct from a theoretical point of view, but the estimate will be biased if the influence of measurement noise is not taken into account, as will be discussed in the next section.

- 2 Ideal, noise-free situation.
- 3 Noise in the output signal.
- 4 Noise in the input signal.

Certified Precision Engineer competencies

The content of this series of three articles is in part covered in the "Experimental Techniques in Mechatronics" course, provided by The High Tech Institute (HTI). This course has been selected for the DSPE Certification Program (see page 26).



WWW.DSPEREGISTRATION.NL WWW.HIGHTECHINSTITUTE.NL

and results in a complex spectrum $A(f)$ with magnitude and phase information describing the cosine components that approximate the time signal $a(t)$. The auto-spectrum of $a(t)$ is defined as:

$$S_{AA}(f) = A^*(f) \cdot A(f)$$

where $*$ indicates the complex conjugate. Since the FFT routine only uses a finite-length time record of length T of the signal $a(t)$, the result is an estimate $\hat{A}_i(f)$ of the true Fourier transform $A(f)$ at the frequencies $k \cdot \Delta f = k/T$. From these individual estimates, the true auto-spectrum of $a(t)$ can be calculated by averaging over n measurement records:

$$S_{AA}(f) = \lim_{n \rightarrow \infty} \frac{1}{n} \sum_{i=1}^n \hat{A}_i^*(f) \cdot \hat{A}_i(f)$$

Unlike the complex spectrum $A(f)$, the auto-spectrum $S_{AA}(f)$ is real and describes the power distribution as a function of frequency.

The cross-spectrum $S_{AB}(f)$ between the time signals $a(t)$ and $b(t)$ is defined by:

$$S_{AB}(f) = A^*(f) \cdot B(f)$$

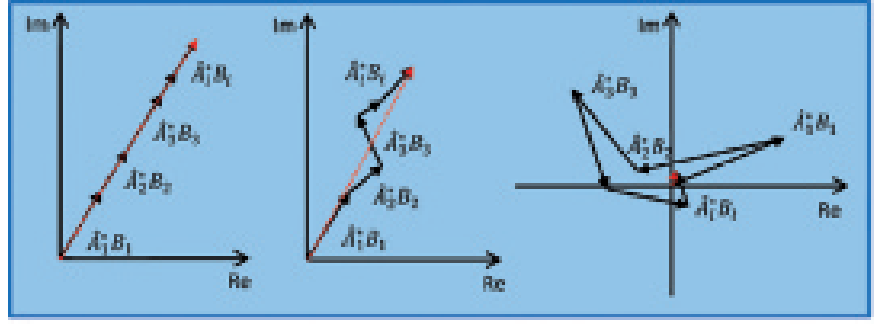
and can be calculated using the FFT by averaging the individual cross-spectra estimates:

$$S_{AB}(f) = \lim_{n \rightarrow \infty} \frac{1}{n} \sum_{i=1}^n \hat{A}_i^*(f) \cdot \hat{B}_i(f)$$

Unlike the auto-spectrum $S_{AA}(f)$, the cross-spectrum $S_{AB}(f)$ is complex valued. The magnitude of each individual cross-spectrum estimate is the product of the magnitudes of the two individual signal components with frequency f_k . The phase of the cross-spectrum is the phase difference $\Delta\phi(f_k)$ between the corresponding frequency components $\hat{A}(f_k)$ and $\hat{B}(f_k)$.

Since the averaging operation is done on complex values, the magnitude of the averaged cross-spectrum will also depend on the variation of $\Delta\phi(f_k)$ over the measurement records as can be seen in Figure 5. If two signals are uncorrelated, the phase difference $\Delta\phi(f_k)$ will be random and the magnitude of the averaged cross-spectrum will be zero (see Figure 5c).

The cross-spectrum emphasises common frequency components in both signals, with a consistent phase relationship. This characteristic will be used in all practical measurements where noise is always present. In the second part of this paper, the variables in all derivations are assumed to be a function of frequency and the notation ' f ' is left out in the formulae for clarity.



5a

5b

5c

5 Averaging of cross-spectrum estimates for increasing variation in $\Delta\phi(f_k)$.

- (a) No phase variation and fully correlated.
- (b) Some phase variation but still correlated.
- (c) Fully uncorrelated.

The H_1 and H_2 frequency response function estimators

The previous section explained that the averaged cross-spectrum of two uncorrelated signals is zero. This property will be used to determine a better estimate of the FRF in the case of noise in the input and output measurements as depicted in Figures 3 and 4. For noise in the output measurement (see Figure 3), the following relationships hold:

$$B = H \cdot A + V$$

$$A^* \cdot B = H \cdot A^* \cdot A + A^* \cdot V$$

$$\frac{A^* \cdot B}{A^* \cdot A} = H + \frac{A^* \cdot V}{A^* \cdot A}$$

$$H_1(f) = \frac{S_{AB}(f)}{S_{AA}(f)} \quad \text{if } S_{AV}(f) = 0$$

$$[v(t), a(t) \text{ uncorrelated}]$$

Likewise for the situation of noise in the input measurement, as shown in Figure 4, the unbiased estimate for the FRF can be calculated using:

$$H_2(f) = \frac{S_{BB}(f)}{S_{BA}(f)} \quad \text{if } S_{BW}(f) = 0$$

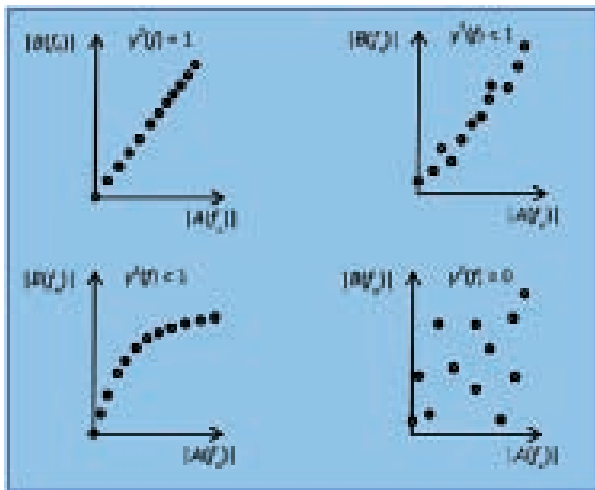
$$[w(t), b(t) \text{ uncorrelated}]$$

In both cases, the excitation signal is expected to be uncorrelated with the noise components in the measured input and output signals. This is always the case if the excitation signal is a random signal.

The coherence function

In system analysis, it is important to quantify the degree of linear relationship between the input and output signals. In statistics, this relationship is indicated by the correlation coefficient, while in the frequency domain, it is indicated by the coherence function $\gamma^2(f)$:

$$\gamma^2(f) = \frac{|S_{AB}(f)|^2}{S_{AA}(f) \cdot S_{BB}(f)} \quad 0 \leq \gamma^2(f) \leq 1$$



6

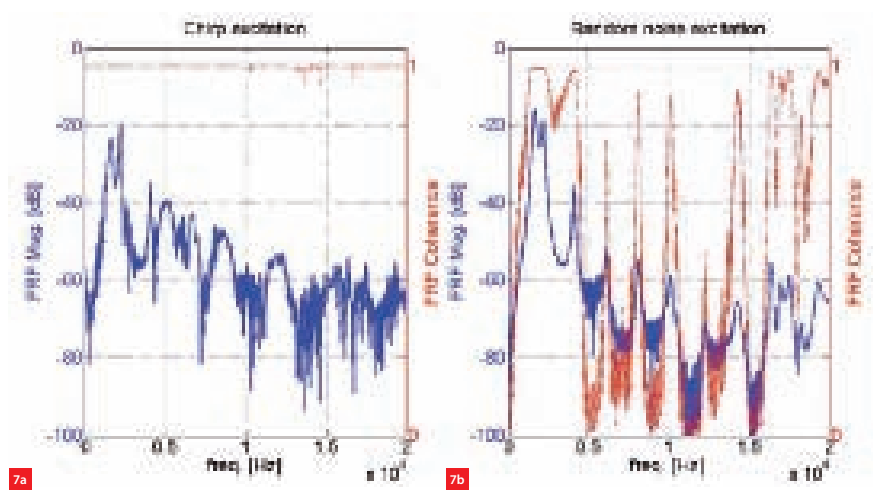
Figure 6 shows the relationship between the frequency components at frequency f_n of signal $A(f)$, which is the measured input of a system, and $B(f)$, which is measured at the output. Figure 6a clearly shows that the input-output relationship is linear and the coherence is equal to one. The input-output relationship in Figure 6b is no longer a straight line through the origin, but varies due to noise in either or both the measurement signals. Consequently, the coherence is less than one. Figure 6c shows a perfect, noise-free, non-linear relationship between the input and output signals and again the coherence is less than one. Figure 6d shows the situation where input and output signals are not related, resulting in a coherence equal to zero.

A coherence value less than one can be caused by:

- Nonlinear system behaviour.
- Noise in the measurements of $a(t)$ and/or $b(t)$.
- Leakage in the FFT.
- Time-variant system behaviour.

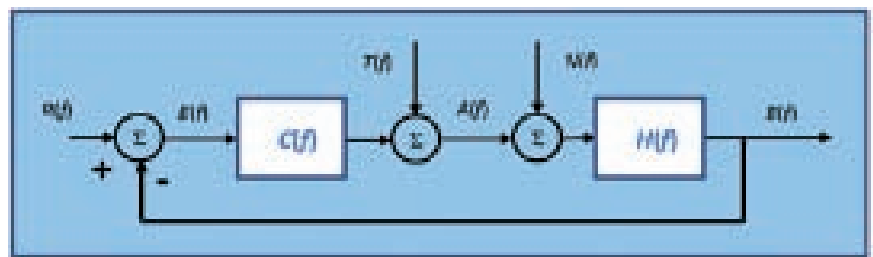
It is a common misunderstanding that a measurement with a coherence equal to one is proof of linear system behaviour. If the measurement is based on only one data block, i.e. without averaging across additional data blocks, coherence will always be equal to one even in the case of nonlinear system behaviour. Even if the coherence is determined using averaging, all deterministic test signals will yield a coherence value close to one if there is minimal measurement noise compared to the test signal. Examples of these types of test signals are the multi-sine and the hammer impact if all impacts are equally strong.

Figure 7a shows the FRF and coherence of a measurement of a nonlinear system using chirp excitation. The coherence is clearly one over most of the frequency range, which



7a

7b



8

contradicts the fact that the system is known to be nonlinear. Figure 7b shows the results for the same system, this time, however, measured with a random noise signal with the same RMS value used in the chirp excitation. The random noise excitation yields a coherence which is clearly less than one over most of the frequency range, as is to be expected for a nonlinear system.

FRF estimation in closed-loop systems

Unlike open-loop systems, closed-loop systems include a feedback path between output and input. This feedback can cause unexpected problems in the FRF identification. Figure 8 is a model of a closed-loop system with controller $C(f)$ and plant $H(f)$ with setpoint $R(f)$, test signal $T(f)$ and external noise $N(f)$ acting on the system.

Any attempt to determine $H(f)$ directly from the measured input signal $A(f)$ and the measured output signal $B(f)$ will fail because of the correlation between $N(f)$ and $A(f)$ and $R(f)$ and $A(f)$:

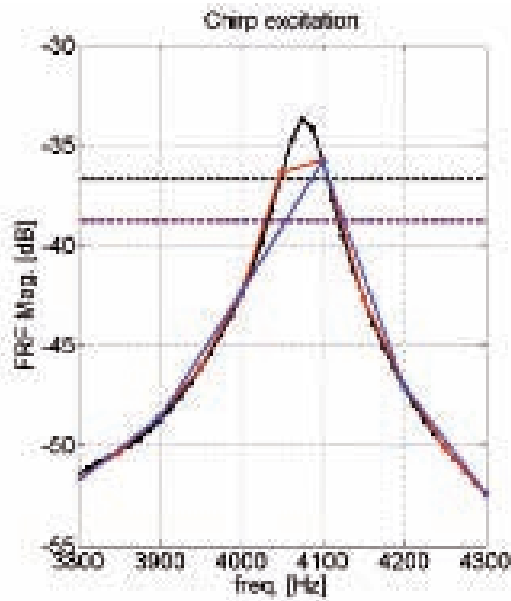
$$\begin{aligned} B &= H(N + T + CR - CB) \rightarrow B(1 + CH) = H(N + T + CR) \\ A &= T + C(R - H(N + A)) \rightarrow A(1 + CH) = T + C(R - HN) \\ \frac{B}{A} &= H \frac{N + T + CR}{T + C(R - HN)} \rightarrow \frac{S_{AB}}{S_{AA}} = H \cdot \frac{S_{AN} + S_{AT} + CS_{AR}}{S_{AT} + C(S_{AR} - HS_{AN})} \end{aligned}$$

6 The coherence function quantifies the amount of linearity between input signal component $A(f_n)$ and output signal component $B(f_n)$.

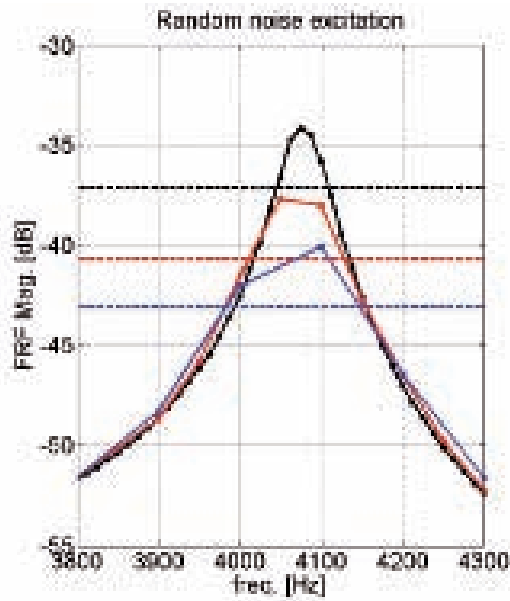
7 FRF (in blue) and coherence (in red) of a nonlinear system. (a) Determined with a chirp, a deterministic signal.

(b) Measured with a random noise excitation.

8 Closed-loop system with $R(f)$ setpoint, $T(f)$ test signal and $N(f)$ external noise source acting on the system. $A(f)$ is the measured input signal, $B(f)$ is the measured output signal.



9a



9b

9 FRF of a resonance. The horizontal lines indicate the -3dB magnitude levels of the respective resonances.
(a) Measured with a chirp.
(9) Measured with white noise.

Even if the setpoint signal $R(f)$ is equal to zero, the estimate of $H(f)$ will remain biased:

$$\frac{S_{AB}(f)}{S_{AA}(f)} = H(f) \cdot \frac{S_{AN}(f) + S_{AT}(f)}{S_{AT}(f) - C(f)H(f)S_{AN}(f)}$$

Depending on the signal-to-noise ratios in the loop, the estimate of the FRF of the plant may vary between $H(f)$ and $-1/C(f)$.

A robust alternative to determine the plant FRF $H(f)$ in a closed-loop system is the three-point method in which the sensitivity $S(f)$ and the process sensitivity $PS(f)$ are determined:

$$S(f) = \frac{S_{TA}}{S_{TT}} = \frac{1}{1+CH} + \frac{C}{1+CH} \left(\frac{S_{TR} - HS_{TN}}{S_{TT}} \right) = \frac{1}{1+C(f)H(f)}$$

$$PS(f) = -\frac{S_{TE}}{S_{TT}} = \frac{H}{1+CH} - \frac{1}{1+CH} \left(\frac{S_{TR} - HS_{TN}}{S_{TT}} \right) = \frac{H(f)}{1+C(f)H(f)}$$

$$H(f) = \frac{PS(f)}{S(f)}$$

if $R(f)$, $T(f)$ and $N(f)$ are uncorrelated, and averaged spectra and cross-spectra are used.

Tips for measuring an FRF in practice

Although a thorough understanding of the theory behind the FRF helps, it does not guarantee good measurement results. Experience with experimentation is also required for good results. This section focuses on some practical measurement aspects.

Choose the proper input and output signals

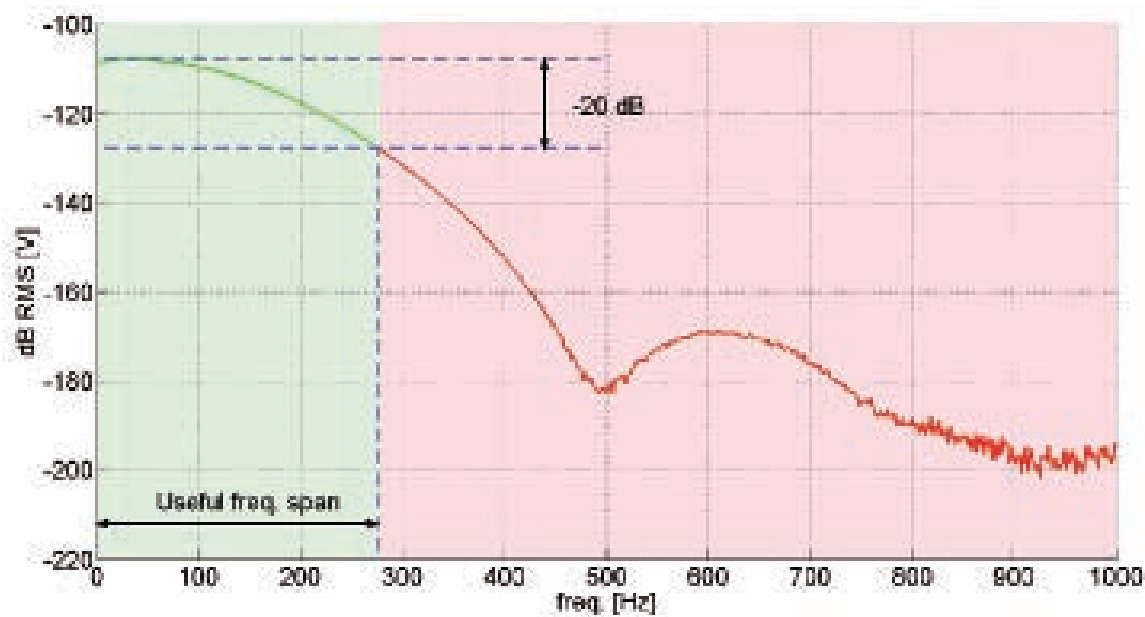
The choice of input and output signal is often determined by the accessibility of the signals. Measuring torque is often

difficult, but the torque signal can be calculated from a simple motor current measurement if the motor constant is known. Measuring small displacements at high frequencies with a good signal-to-noise ratio is often difficult, while measuring accelerations at high frequencies is simple because of the increase in sensitivity with $(j2\pi f)^2$. The corresponding FRF can be calculated by dividing the FRF by $(j2\pi f)^2$. Time spent on optimising the signal-to-noise ratio of the measurement signals is time well spent.

Choice of frequency range and frequency resolution

Take a broad frequency range for the first measurement to get a good general overview of the region of interest. In the subsequent measurements, however, limit the frequency range to the region of interest so as not to excite system dynamics outside that range. The required frequency resolution of the measurement depends on the damping at the resonances or antiresonances. Too coarse a resolution will underestimate the magnitude at the resonance frequency because of the 'picket fence effect'. A very narrow resolution will not result in any additional quality improvement; it will only result in unnecessary measurement time.

Figure 9a shows the measurements of a resonance at three different frequency resolutions with a chirp test signal under leakage-free conditions. The estimate of the resonance magnitude depends on the frequency resolution used and shows a 2.2dB variation. As a rule, a resonance is estimated correctly if the frequency interval between the -3dB magnitude frequencies is covered by at least five frequency lines. Figure 9b shows the measurement results of the same system but with a random noise test signal.



10

Apart from the 'picket fence effect', leakage errors are also evident. These errors show up as a difference in the magnitude values for the same frequency line as a function of the resolution. Even using a Hanning weighting function, these differences amount to approximately 4 dB at 4,100 Hz.

Hammer or shaker excitation for modal analysis?

The choice of excitation is often dictated by practical considerations like the accessibility of the test object, the ease of mounting a shaker and the required frequency range of excitation. In the case of impact excitation, the tip of the hammer determines the width of the excitation spectrum. The useful frequency range starts at 0 Hz and is limited to that frequency at which the magnitude is 20 dB less than the low-frequency magnitude, as can be seen in Figure 10.

When testing very sensitive equipment, shaker excitation is often preferred over impact excitation. A band-limited white noise test signal in combination with a Hanning weighting function is a good starting point because the total signal power is evenly distributed over the frequency range of interest. This reduces the risk of over-driving resonances, which can happen with a sinusoidal excitation signal. Moreover, because random noise is not a deterministic signal, the information from the coherence function can be used to assess the linearity of the measurement.

Optimise the signal-to-noise ratio of the signals

A dip in the coherence function often coincides with a low value in the excitation and/or response spectra. If the magnitude at the anti-resonance frequency is relevant, increasing the signal-to-noise ratio by increasing the input

10 The -20dB rule to determine the useful frequency range in the case of impact excitation.

power in this frequency range is an option. Other options are zoom measurements in that limited frequency range. This will allow the signal conditioning to be optimised to reduce the quantisation noise.

Reduce unnecessary nonlinear behaviour as much as possible

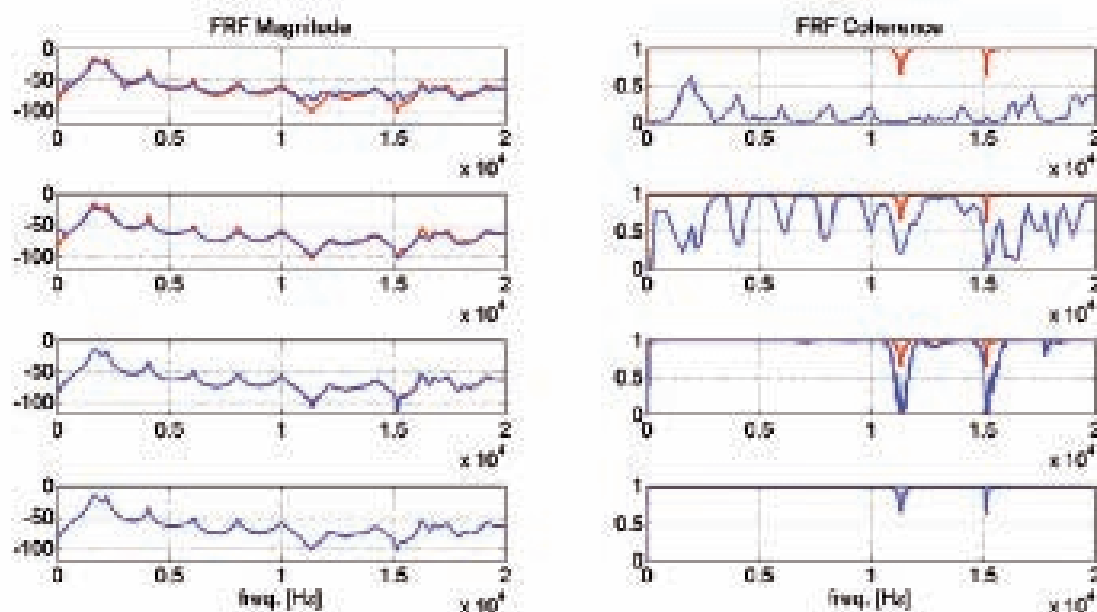
All real systems are in essence nonlinear, but for many systems, under normal operating conditions, the nonlinear behaviour can be ignored if the measurements are carried out carefully. Do not over-drive the system, check for saturating power amplifiers and overloaded sensors. Listen for rattles in coverings, check for strong 50/60Hz harmonics. Optimise the sensor signal-to-noise ratio and choose proper ADC input ranging. Prevent aliasing and reduce leakage.

Do the FRF measurements under the proper operating conditions

Friction in positioning systems often induces stick-slip behaviour. The stick phase system dynamics are very different from the dynamics in the slip phase. For FRF measurements in the stick phase, only very small excitations are allowed in the 100 nm range. The slip phase dynamics can be measured reliably by jogging the system.

Be critical about the measurement results

Figure 11 shows a typical evolution in the quality of an FRF measurement. The excitation signal is band-limited white noise. The left column shows the magnitudes of the FRF measurements, while the right column shows the corresponding coherence plots. In both columns, the red curves represent the final results. In the upper row in blue, a



11

frequency resolution of 200 Hz was used with a rectangular weighting function. Both large leakage errors and picket fence errors are present.

The second row shows the results for a measurement with equal excitation signal level and frequency resolution but with a Hanning weighting function. The increase in coherence is caused by a significant reduction in leakage error. The picket fence error is not reduced. The coherence function still shows ranges with low values, however. These ranges coincide with the resonances and antiresonances. There are different reasons for the low coherence values of the resonances and antiresonances. In the case of the resonances the low coherence is due to leakage, while in the case of the antiresonances the low coherence is caused by low signal-to-noise ratios, as will become evident from the subsequent measurements.

With the same excitation signal level and weighting function as in row two, the measurement in the third row is done with a frequency resolution of 6.25 Hz. Once again, the leakage error is reduced as indicated by the increased value of the coherence function. The picket fence error is also reduced. The remaining minima in the coherence function coincide with the antiresonances. The bottom row shows the final results. In this measurement, the RMS value of the excitation signal is increased by a factor of 10, which results in an increased signal-to-noise ratio of the output signal. This results in a better coherence for the antiresonances. One should be careful about increasing the excitation signal any further, as this may over-drive the system resulting in a lower coherence value due to the induced nonlinearity. ■

11 FRF estimates for various weighting functions, frequency resolutions and excitation levels.

Coming up in Part 3

Part 3 will introduce frequency domain methods to use in practice to model and optimise the performance of nonlinear systems. The article provides a brief overview and experimental examples of existing modelling techniques and a novel method to assess and optimise the performance of nonlinear systems using frequency domain-based tooling.

LITERATURE

- P. Nuij, D. Rijlaarsdam, "Introduction to Frequency Response Function Measurements (Part 1)", *Mikroniek*, Vol. 54 (2), pp. 8-13, 2014.
- J.S. Bendat, A.G. Piersol, *Engineering applications of Correlation and Spectral Analysis*, Chichester: Wiley-Interscience, 1993, ISBN: 0-471-57055-9.
- H. Herlufsen, "Dual Channel FFT Analysis (Part 1)", *Brüel & Kjær Technical Review*, No. 1, 1984.

THERMAL POSITION STABILITY IN MECHATRONIC SYSTEMS

Validating the thermal position stability of complex systems requires a combination of thorough modelling and dedicated experimental identification. Three examples are given of model-supported validation of mechatronic systems. Measurements are performed in a transient mode, as this gives much more insight into the system than steady-state validation only. Techniques commonly used in structural dynamics have been applied successfully to these thermo-elastic systems.

THEO RUIJL, RONALD LAMERS, DAAN TIMMERS AND JACK VAN DER SANDEN

Validation of the thermal position stability of complex systems is often very difficult. Establishing an absolute reference (metrology reference) not affected by thermally induced deformations cannot be achieved in practice.

Validating the entire system and isolating only the thermally induced influence from a specific error source is often also not feasible.

A practically feasible method is to validate a model describing the thermal system performance rather than trying to validate the final system performance. In such a model, the desired ideal situation can be simulated to quantify the actual performance of the system. The validation of the actual system can then be reduced to quantifying or validating the critical parameters of the model to guarantee reliable simulation results.

Three examples are described in this paper. The first example considers the sample position stability in a TEM (Transmission Electron Microscope). The goal is to quantify the sensitivity to the main thermal error sources. The second example deals with the sample position stability in a SEM (Scanning Electron Microscope). The goal is to quantify the contribution of the SEM vacuum chamber to the sample position stability. In the last example the position stability of a hexapod structure is validated. The

goal is to guarantee the position stability of the optical system supported by the hexapod.

TEM: Frequency domain analysis

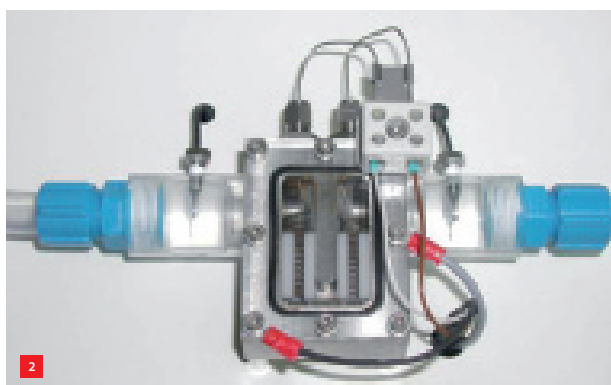
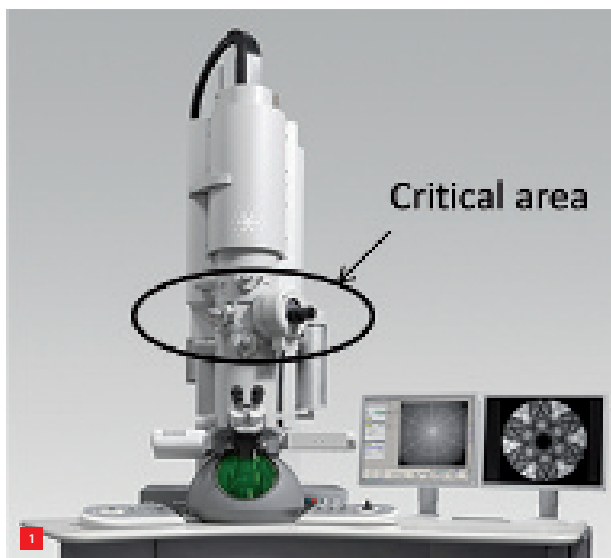
In common high-end TEMs, analyses are made at the atomic level. Accordingly, high sample position stability is required to guarantee a blur-free image. Typically, thermally induced sample position drift should not exceed the sub-nanometer level for the duration of the investigation. To improve thermal stability, a thorough understanding of the system's sensitivity to the main thermal error sources is necessary. In addition, the coupling mechanisms from the error sources to the sample drift need to be understood to improve the system for future requirements.

A thermo-elastic model (lumped-mass model) has been created to describe the most important part of the TEM; a structural loop between the last pole tip and sample manipulation system (see Figure 1). Besides internal heat loads, e.g. from electro-magnetic lenses, the main external error sources are the conditioning water temperature fluctuations and room air temperature fluctuations. The latter influences the system by means of the column and the sample manipulator.

AUTHORS' NOTE

Theo Ruijl is CTO and senior mechatronics system architect at MI-Partners, based in Eindhoven, the Netherlands. Ronald Lamers and Daan Timmers work at MI-Partners as senior designer/project manager and mechatronics designer respectively. Jack van der Sanden works as senior technologist at Philips Innovation Services (PInS), Eindhoven.

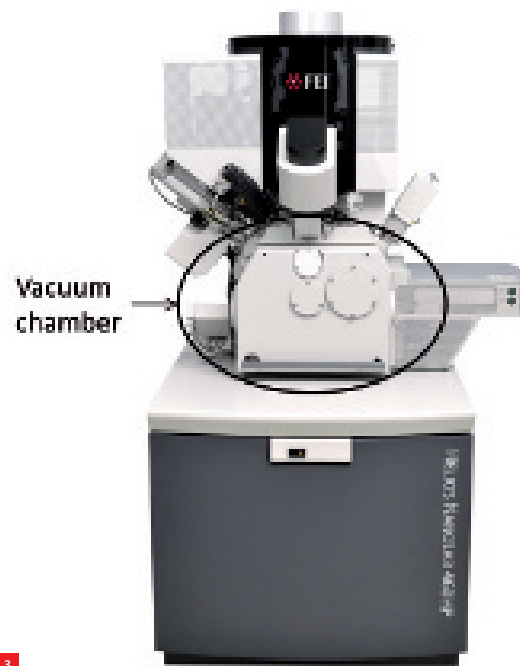
t.ruijl@mi-partners.nl
www.mi-partners.nl
www.innovationservices.philips.com



- 1 TEM and critical area for sample stability. (Source: FEI)
- 2 Local fluid heater. (Source: PInS)
- 3 Example SEM system. (Source: FEI)

With the lumped-mass model, the critical parameters can be identified. To validate and quantify some of these critical parameters, the conditioning water could be used as an excitation source. By means of a dedicated local fluid heater, the water temperature can be controlled down to mK level (see Figure 2). By exciting the conditioning water (e.g. single sinusoidal excitation), frequency responses to several outputs (temperatures as well as sample drift) can be measured. Irrespective of the presence of other heat sources, such as room temperature fluctuations, the sinusoidal excitations enable a well-correlated measurement.

By means of the lumped-mass model, updated by the measured critical parameters, the sensitivities of the sample position stability towards the main heat sources have been simulated. The results are presented as transfer functions, depicting the sensitivities as a function of the (disturbance) frequency.



SEM: Singular Value Decomposition

The position stability of a sample in a SEM microscope is strongly influenced by the stability of the electron column, the sample manipulation stage and the vacuum chamber. The vacuum chamber is the structural part between the column and the sample manipulation system. Measuring the position drift of the sample by analysing the drift of the SEM image means that all three contributors (column, stage and chamber) are involved. To quantify the contribution of the chamber only, a thermo-elastic finite-element (FE) model has been created. The chamber is a cast structure that can be analysed effectively by an FE model. The main problem is to quantify the boundary conditions as present in real use cases.

In this particular case, predicting the actual heat loads to the chamber appears to be very difficult. The main heat loads are coming from room temperature fluctuations, often driven by air flow from air conditioning systems in the ceiling above the microscope. Heat loads from operators around the machine or control cabinets (electrical cabinets, also from surrounding systems) are also dominant. To avoid having to do a very tedious study to quantify these heat loads, the chamber has been equipped with temperature sensors (NTCs) to measure the temperature while operating the microscope in normal realistic conditions (see Figure 3). The measured temperature fields have been applied directly as a temperature boundary condition to the FE model to establish the corresponding thermo-elastic deformation of the chamber.

The problem however, is the huge number of measured temperature fields (transient behaviour, every 30 seconds, during several days of operation) and how to translate them into transient thermo-elastic deformations to simulate the transient sample drift. Computing the thermo-elastic deformation corresponding to each measured temperature field would require unacceptable computation time. To overcome this problem, the temperature data has been reduced.

All the measured temperature fields ($1 \dots m$), can be ranked in a matrix \mathbf{T} . Each column i of \mathbf{T} represents a temperature field measured at instance t_i . Where \mathbf{T} has the dimensions $k \times m$ (k : number of temperature sensors, m : number of temperature fields measured over time). The column vectors, representing the temperature fields, can be considered as vectors in a vector space with dimension k . By means of a POD (Proper Orthogonal Decomposition), also known as SVD (Singular Value Decomposition), the sub-space spanned by all the temperature field vectors can be found. By means of the decomposition, an orthogonal basis \mathbf{U} is found defining the sub-space. By means of the POD (or SVD) we can rewrite \mathbf{T} to:

$$\mathbf{T} = \mathbf{U}\Sigma\mathbf{V} \quad (1)$$

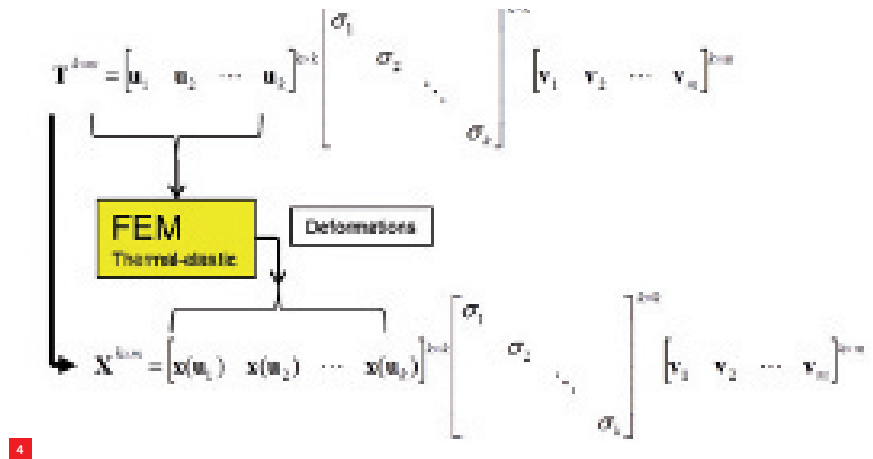
Note that the sub-space (with orthogonal basis \mathbf{U}) has only dimension p ($p \leq k$). In our case, the sub-space dimension was equal to the number of sensors k . Hence, instead of analysing the huge number of temperature fields m in the FE model to find the thermo-elastic deformations \mathbf{X} , only the small number of independent temperature fields need to be analysed (see Figure 4). The corresponding thermo-elastic deformations of all the temperature fields are accordingly obtained from:

$$\mathbf{X}(\mathbf{T}) = \mathbf{X}(\mathbf{U})\Sigma\mathbf{V} \quad (2)$$

Hexapod structure: Position stability

To align an optical module in a production tool and hold it stable in position over time, a hexapod structure has been developed. The system consists of six adjustable spindles. To place the system in the right perspective: the weight of the optical module is several tons and the size including the hexapod is about $2 \times 2 \times 2 \text{ m}^3$. To achieve the required position stability over time, the spindles are equipped with a water circuit to stabilise the temperature of the spindles. Existing commercial spindles are used and as such only a separate temperature conditioning ring can be attached at the left end of the spindle (see Figure 5).

It was not possible to analyse the thermal drift of the entire set-up in order to prove that the position stability of the system is met. Such a measurement of the entire system



would require a stable reference, which is not feasible. Creating realistic load cases (according to the worst-case specifications) would require a more or less real system environment, which is also not practically feasible. The design of the hexapod structure has been supported by thorough modelling, showing that the main thermal distortions are coming from temperature fluctuations of the air around the system. Hence, the position stability of the

4 Only the independent temperature fields \mathbf{u}_i obtained from the POD are analysed in the FE model to find all the thermo-elastic deformations \mathbf{X} .

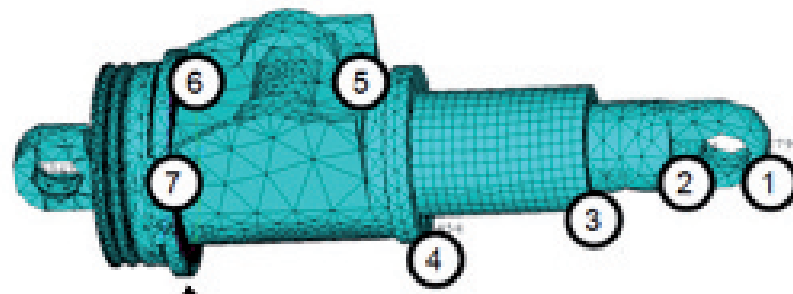
Certified Precision Engineer competencies

Two of the authors (Th.R. and J. v/d S.) are the teachers of the "Thermal Effects in Mechatronic Systems" course from Mechatronics Academy (MA), offered to the market by The High Tech Institute (HTI). This course has been selected for the DSPE Certification Program (see page 26). It features many of the topics discussed in this special Mikroniek issue.



The course focuses on the various aspects related to thermal effects that impact the performance (accuracy, life time or process quality) of precision modules/systems. Participants will acquire theoretical and practical background on design, simulation, measurement and compensation techniques that are essential in the development of precision modules/systems that are subject to internal or external thermal loads. After three succesful editions, it was decided to increase the duration from two to three days (and hence the CPE points from 2 to 3), to accommodate for an additional topic, thermal control, and for more time for exercises.

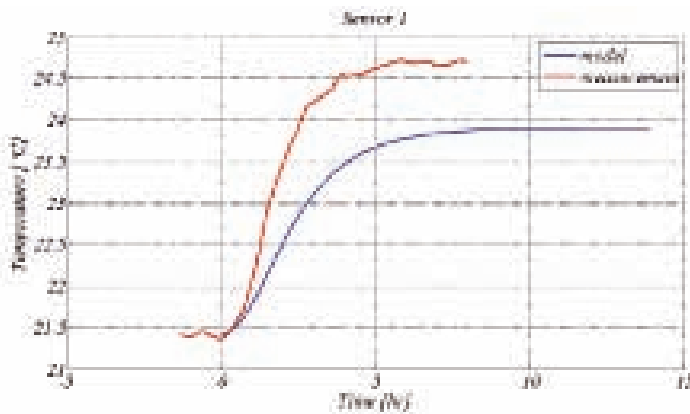
WWW.DSPEREGISTRATION.NL WWW.HIGHTECHINSTITUTE.NL WWW.MECHATRONICS-ACADEMY.NL



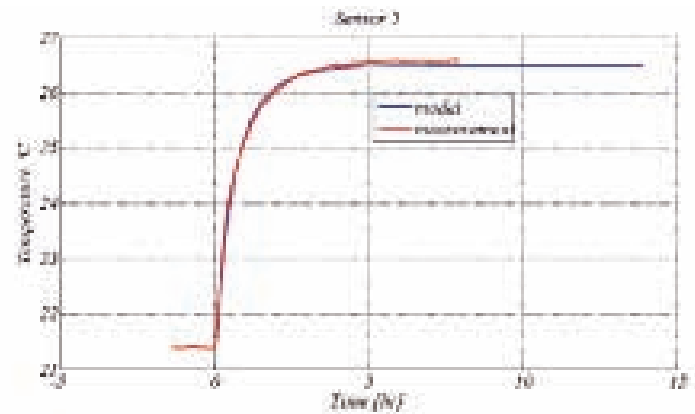
Conditioning ring

5

- 5 Spindle test set-up and temperature measurement points.
6 Measured and modelled temperature responses.
(a) Sensor 1.
(b) Sensor 5.



6a



6b

system is determined by the ability of the conditioning water to stabilise the temperature of the spindles.

Knowledge about the spindle to develop the thermo-elastic model is limited; especially the assumptions about the internal thermal resistances (contacts in bearing and spindle-to-nut, material properties, etc.) are not accurate enough. However, based on the model assumptions the conditioning performance of the ring at the left end of the spindle was sufficient to guarantee the stability of the whole spindle.

Hence, instead of trying to measure the actual position stability of the whole system, the validation has been reduced to quantifying only the conditioning performance of the water in relation to the spindle temperature. Based on the thermal model, step responses of temperatures along the spindle to the conditioning water temperature can be analysed. If the actual (measured) responses are quicker (smaller time constant), the actual conditioning ability will also be better than predicted by the model. It should be noted that a smaller time constant means that the spindle has a stronger thermal coupling to the conditioning water.

The time responses of several positions of the spindle have been measured by means of a stepwise change in the temperature of the conditioning water (e.g. from 21.5 to 28 °C). The measurement set-up and two of the temperature responses are shown in Figure 5 and 6. The measurements show that the actual time constants are smaller and the steady-state temperatures are higher. Hence the temperature stability will be better than assumed in the model, which means that the required position stability will be met.

Conclusion

Validating the thermal position stability of complex systems is often difficult. Establishing an absolute stable reference, not suffering from thermally induced deformations, is generally not practically feasible. Boundary conditions are often complex and identifying and separating various error sources is often not possible. This paper shows three examples where, based on modelling and transient thermal measurements, systems have been validated and identified successfully. Techniques commonly used in structural dynamics have been applied successfully to these thermo-elastic systems. ■

WHERE **NO MOVEMENT** IS POSSIBLE

AUTHORS' NOTE

The authors work at Janssen Precision Engineering (JPE) in Maastricht, the Netherlands. Maurice Teuwen is a systems engineer and Maarten Dekker is a mechanical engineer.

maurice.teuwen@jpe.nl
www.jpe.nl

Experimenting in cryogenic environments poses special positioning challenges. JPE has developed and realised piezo- and voice-coil-based actuation principles to overcome these challenges in different ways for various applications, such as a linear actuator with μm resolution and infinite stroke, a fast 3-DoF chopping mirror device and JPE's Piezo-Knob Actuation. The latter consists of stick-slip-inertia actuators that are built in several translational and rotational stages with nanometer resolution and sub-nanometer stability proven to operate down to 1 K.

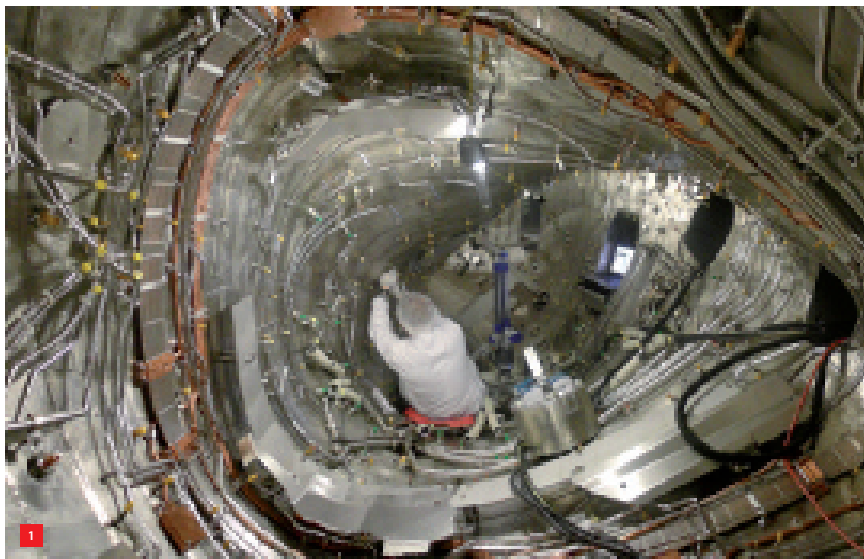
MAURICE TEUWEN AND MAARTEN DEKKER

Some types of dedicated research, such as space and quantum physics, often involves experiments in cryogenic environments, i.e. environments with temperatures below -150°C and sometimes even very close to the absolute zero (μK range). To maintain these temperatures, the 'cryostats' are as small as possible with an internal vacuum to prevent convection. On top of this, several other phenomena, such as cold-welding, dissipation, thermal expansion, superconductivity, etc. can compromise trivial solutions for mechanisms to be used for experiments.

Cryogenics

The definition of cryogenics is as follows: the science and technology of temperatures below 120 K [1]. These temperatures do not occur on earth naturally; the lowest natural temperature recorded is 184 K [2] at the Vostok station in Antarctica in 1983.

Lower temperatures are created artificially using refrigerators. The simplest cooling method is to use compressed gases such as liquid helium. With liquid helium, a temperature of 4.2 K can be reached. Using oxygen or nitrogen, a temperature of 90 K or 77 K respectively can be reached. Absolute zero, at which entropy is zero, cannot be reached by thermodynamic means only because the temperature of the matter being cooled reaches the temperature of the coolant asymptotically. To reach temperatures below 4 K, other methods like evaporative cooling (4K to 300 mK), dilution



1 Cross section of the experimental nuclear fusion Wendelstein 7-X stellarator. (Source: de.wikipedia.org/wiki/Wendelstein_7-X)

refrigeration (600 mK to 2 mK) and adiabatic demagnetisation refrigeration (below 10 mK) can be used. The world record is $1 \cdot 10^{-10}$ K or 100 pK, reached with nuclear demagnetisation [3].

Applications

Cryogenics has many applications. A frequent example is electrical conductivity; the electrical conductivity of most metals increases as temperatures decrease. Some of these metals even become hyper-conductive below a certain temperature, implying zero electrical resistance. This effect combined with electromagnets can produce extremely high



44 MIKRONIEK nr 3 2014

thereby destroying the adjustment (e.g. 400 micron drift for a 100 mm piece of aluminium).

Furthermore, it should be considered that relatively small differences in CTE at room temperature can result in significant dimensional differences at cryogenic temperatures. For example, a clearance fit of 20h7/G7 at room temperature of a stainless steel part in an aluminium housing will turn into an effective transition fit of 20d7/Y7 at 4 K. Similarly, a bolted connection can fail (become loose, or break) due to contraction differences between the clamped part and the bolt material.

In most cases, these issues can be overcome by applying common precision engineering design principles, like the use of kinematically constrained, monolithic structures and the implementation of thermal compensation parts which cancel out integrated CTE differences, etc.

Cryogenic environments and vacuum also imply the following construction challenges:

- Vacuum introduces adhesive wear, deteriorating material contact. At worst, this can get completely stuck.
- Through outgassing of materials, implying the scattering of molecules through the experimental volume, the vacuum level decreases (and this is even worse for quantum physics, affecting the experiment due to the impact of these molecules).
- A small volume is helpful when maintaining cryogenic temperatures and vacuum. This volume limits the size of components.
- Touching objects under a certain load that are made from the same material tend to cold-weld in cryogenic environments.
- Superconductivity and superconductive magnets.
- Dissipation of actuators, which affects temperature (stability).
- Conventional DC/stepper motors often cannot be used due to stringent (non-magnetic) material requirements related to the experiment or the environment, and failures related to the dimensional changes during cryogenic cycling which introduces play or makes the actuators get stuck.

JPE has developed and realised several actuation principles to overcome all these challenges in different ways for all sorts of applications. A number of these actuation principles are described in the following paragraphs.

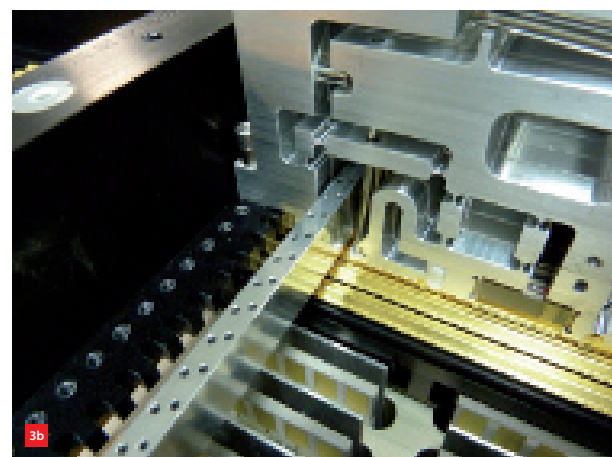
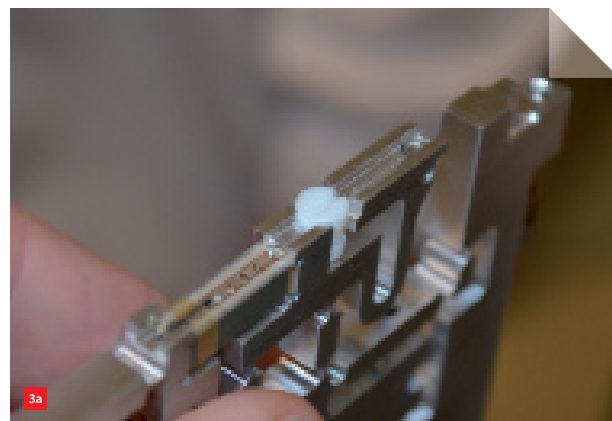
Infinite-stroke linear actuation

A cryogenic linear actuator with 'infinite' stroke has been developed by JPE as part of the configurable slit unit (CSU) [7]. The CSU is one of the key sub-modules within the

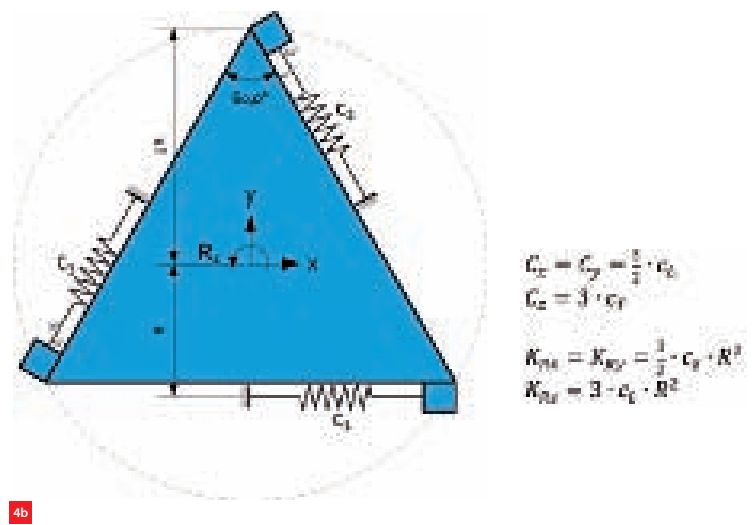
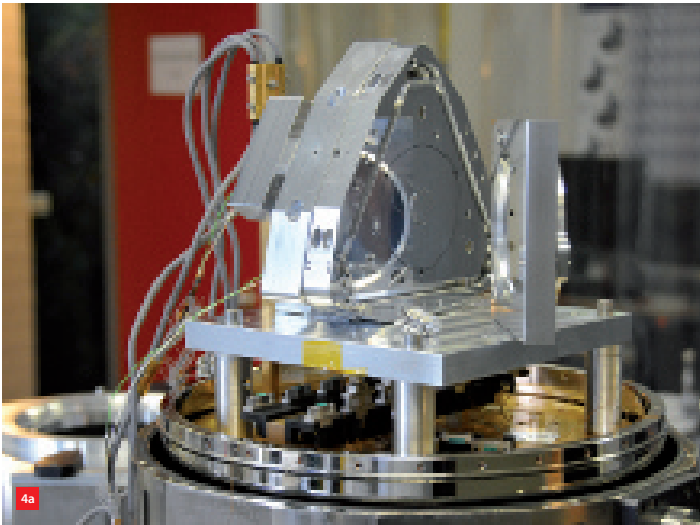
infrared multi-object spectrograph EMIR. This unit will shortly be fitted to the world's largest telescope, the Gran Telescopio de Canarias (GTC) on La Palma (Canary Islands).

The actuator in the CSU is based on a piezo drive. Piezo elements are widely used in cryogenic positioning applications because of their relatively small volume, limited dissipation, high stiffness and sub-micron resolution. Nevertheless, a big drawback is the significant reduction of piezo stroke at cryogenic temperatures. This means that the performance of widely used 'walking' piezo actuators (in ambient conditions) decreases as the piezo motion is reduced to the same order of magnitude as the contact deformation, thereby undermining the 'walking' principle.

Therefore, an elementary stick-slip concept is chosen, as this is less sensitive to piezo performance deterioration compared to other piezo actuators. By choosing a completely monolithic structure, which is under defined pretension against the positioned element, the actuator is intrinsically robust in terms of cryogenic cycles. A depiction of the actuator can be seen in Figure 3.



3 The actuator.
(a) Close-up picture.
(b) Integrated in mechanism.



The performance features of the actuator are listed in Table 1.

Table 1 Realised cryogenic linear actuation performance at 77 K.

Description	Requirement
Stroke	Infinite
Maximum speed	2.0 mm/s
Typical stepping frequency	150 Hz
Typical step size	12 µm
Minimum step size	< 1.0 µm
Typical operating environment	77 K, 10 ⁻⁶ mbar
Dissipation at standstill	0 W (powerless)
Typical drive force	3 N

For closed-loop positioning, a measurement system is required. Given the cryogenic conditions, the relatively limited envelope and the large number of actuators (110), a custom sensor including electronics read-out has been developed based on a capacity measurement. This technology is now available for generic, long-stroke movements in cryogenic or vacuum environments. The technology is based on changing the common area between two capacitor plates, where one plate is part of the static sensor and the other is part of the moving object. The sensor has proven to be very reproducible. By calibrating it, a relative accuracy in the order of a few microns over a nearly 400 mm stroke has been achieved. Table 2 summarises the characteristics of the measurement system.

Table 2 Realised cryogenic displacement sensor performance at 77 K.

Description	Requirement
Stroke	Infinite
Resolution	< 1 µm
Accuracy (after calibration)	< 5 µm
Sample rate	500 Hz

4 METIS Cold Chopper.
(a) Prototype in opened cryostat.
(b) Concept design sketch [9].

Fast tip-tilt actuation

The Mid-infrared E-ELT Imager and Spectrograph (METIS) is the third instrument for the planned European Extremely Large Telescope (E-ELT). A key part of METIS is the Cold Chopper (MCC). This is an extremely fast tip-tilt mirror which switches (chops) the optical beam between the target and a nearby reference sky during observation to eliminate the fluctuating IR background signal in post-processing. Table 3 lists the MCC requirements.

Figure 4 is a depiction of the mechanical hardware of the chopper [8] mounted on the base platform of the opened cryostat. Meanwhile, the chopper has been tested and the feasibility of the requirements was successfully confirmed. The following key implementations have contributed to the success of this cryogenic instrument:

- Monolithic, thermally symmetric triangular structure with integrated flexure-based guiding with an integrated 6-DoF kinematically supported mirror to isolate it from deformations induced by drive force (DoF = degree of freedom). Both are common construction principles for ambient applications. Nevertheless, it is these principles

Table 3 Main METIS cold chopper requirements.

Category	Description	Requirement
Positioning and chopping	Stability and repeatability	≤ 1.7 µrad 3σ
	Accuracy	≤ 85 µrad
	2D chop stroke	≥ 13.6 mrad
	Chop frequency	0.1...10 Hz
	Switch time	≤ 5 msec
Environment and interface	Operational temperature	40 K
	Operational pressure	10 ⁻¹⁰ mbar
	Power dissipation	< 1 W
Reliability	Lifetime	> 10 ⁸ cycles

that make the design suitable for cryogenic use, as it is by nature robust against dimensional changes.

- Custom-designed, moving-magnet voice-coil actuators to ensure an extreme minimisation of the thermal load on the moving structure. This is achieved by affixing the coil to the base. Unlike conventional voice-coil actuators, the back iron is not directly attached to the permanent magnet assembly, but instead to the coil so as to minimise the moving mass.
- Fibre-based interferometer displacement measurement system (30 nm (3 σ) noise level @ > 10 kHz) which is used with retro-reflectors to maintain signal quality during tip-tilt motions.

Cryogenic linear actuator technology

The cryogenic linear actuator (CLA), also called the PiezoKnob actuator, has been developed for positioning applications at extremely low temperatures, even < 1 K. It is a piezo stepping actuator with nanometer level resolution, combining a high drive and holding force with unpowered sub-nanometer stability.

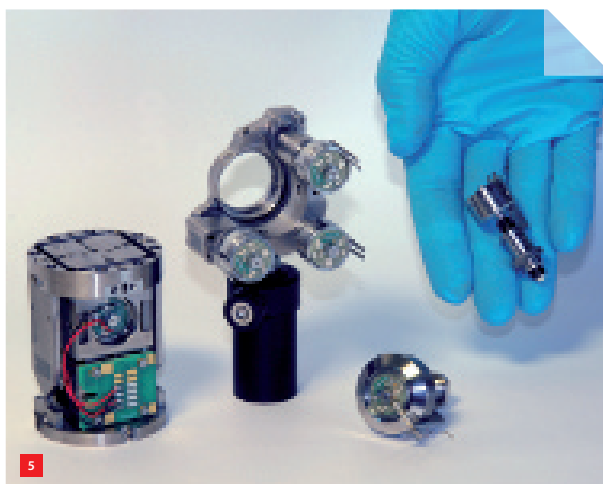
The CLA is commonly used in fundamental physics research applications, where samples or laser beams need to be positioned at micrometer accuracy and with stability at nanometer level for experiments at absolute milli-Kelvin temperatures or even lower. Given the large thermal deformations during cryogenic cycling, the set-ups are typically coarsely adjusted at room temperature, and later set to near working conditions (e.g. 4 K, helium boiling point) tuned to the exact position. As is generally known, all matter tends to come to a standstill at these temperatures, but the CLA has proven to still move in quite a robust fashion. This is because of its unique and patented piezo drive concept, which makes JPE one of the very few global suppliers in this market.

Table 4 lists the elementary features of the CLA[10].

Table 4 CLA features.

Description	Performance
Travel range	12 mm
Resolution @4K	1...5 nm
Stepping frequency	1...600 Hz
Max velocity @4K	3 μ m/s
Max load capacity	50 N

The CLA actuator is compatible with typical manipulator knobs of commercially available spindle mechanisms for optical benches, such as linear stages or tip-tilt lens holders like those depicted in Figure 5. Other configurations could also be considered, such as the 2-DoF translation stage



which is depicted as well. This stage can even be configured with an additional module to create a 3-DoF (XYZ) stage. There are also more specific solutions available, like a high-resonance (> 1 kHz) XY stage and even a high-resonance (> 1 kHz) 6-DoF hexapod stage.

5 Elementary CLA actuator (right), optical mount with 3 CLAs (centre), 2D translation stage with integrated CLA actuator (left).

To conclude

Semiconductor processes moving into vacuum environments has greatly accelerated the implementation of positioning mechanisms in vacuum. Although JPE was one of the first companies to provide engineering and specific positioning solutions in this field, the current demand for semiconductor equipment has boosted the availability of a broad range of suppliers for this field of engineering. The design and implementation of mechanisms in cryogenic environments is still concentrated in dedicated fields of research, which means that less knowledge and products are available on the market. This makes JPE one of a handful of global suppliers with broad experience and a wide range of positioning solutions for different applications in cryogenic environments. ■

REFERENCES

- [1] Ph. Lebrun, "An introduction to cryogenics", CERN, Accelerator Technology Department, CH - 1211 Geneva 23, Switzerland, 18 January 2007.
- [2] "World: Lowest Temperature", Arizona State University, World Weather / Climate Extremes Archive, wmo.asu.edu/world-lowest-temperature.
- [3] "World record in low temperatures", Aalto University, School of Science, ltl.tkk.fi/wiki/LTL/World_record_in_low_temperatures.
- [4] G. Hechenblaikner, F. Hufgard, J. Burkhardt, N. Kiesel, U. Johann, M. Aspelmeier, and R. Kaltenbaek, "How cold can you get in space? Quantum Physics at cryogenic temperatures in space", Cornell University Library, 12 September 2013.
- [5] E.D. Marquardt, J.P. Le, and R. Radebaugh, "Cryogenic Material Properties Database", National Institute of Standards and Technology.
- [6] JPE Precision Point, "Cryogenic (4K...293K) material properties", www.jpe.nl/precisionpoint.
- [7] JPE website, "Configurable Slit Unit", www.jpe.nl/projects/configurable-slit-unit.
- [8] JPE website, "Cryogenic chopper", www.jpe.nl/projects/cryogenic-chopper.
- [9] JPE Precision Point, "Triangular body supported by tangential struts", www.jpe.nl/precisionpoint.
- [10] JPE website, "Cryo Linear Actuator 'PiezoKnob'", www.jpe.nl/products/cryo-linear-actuator-piezoknob.

UPGRADING TO PEM

Electrochemical machining – a non-conventional metalworking process – is on the up. In a bid to raise standards, several companies introduced new industrial ECM machinery at the EMO Hannover last year. The general focus has shifted to the more advanced precision electrochemical machining (PEM) technology, the upgraded, ultra-geometric and surface quality variant of traditional ECM. Micromachining the hardest parts is now within reach. The Franco-German company PEMTec has shown impressive advances in (modular) machine tool building.

AUTHOR'S NOTE

Jan Wijers is a freelance technical writer who lives in Eindhoven, the Netherlands. He is specialised in a wide variety of conventional and non-conventional production technologies.

JAN WIJERS

The frontrunners in certain industrial sectors such as aerospace, defence, automotive, energy and medical – typically the ones not hampered in any way by the current crisis – are highly reliant on the 3D machining of corrosion-resistant, high-temperature superalloys such as Ni alloys, titanium and molybdenum, as well as hardened, sintered and high-tensile-strength steel. These high-tech materials are extremely hard to machine conventionally, if at all, or can only be 'EDM-ed' (EDM stands for electrical discharge machining), ground or hard-turned/milled to the toughest quality requirements that can be met today. What's more,

increasingly complex and precise applications with a high degree of design freedom, ever-increasing functionality and the miniaturisation trend have seen the main focus shift to non-traditional machining.

Evolution

The high-current density electrochemical machining process – first patented in 1963 by Excellor USA – can handle several of these industrial demands in a 'pretty cool', highly efficient and stable manner. In the past, setting up, optimising and testing was very time-consuming, even when some kind of simulation based on metal removal modelling was used. In most cases, a number of tests had to be done under practical conditions before production could be launched. Compared to standard 'chipping', this process was also insufficiently accurate.

Table 1. Comparison of conventional and precision ECM.

	Conventional ECM	Precision ECM
Power supply	DC	pulsed
Gap	large (> 0.1 mm range)	small (6-10 µm)
	side gap wider than the frontal one	almost identical
Tool feed	constant feed rate 0.1-1.2 mm/min	superimposed oscillation (25-50 Hz / 200-400 µm) 0.1 - 3.0 mm/min
Rinsing	forced	forced tool (+ electrode) vibration
Quality	low (200-400 µm)	high (2-5 µm)
Max amperage	< 2,000 A	1,000+ A
Voltage	7-15 V	15 V
Process fluid	NaCl (20%)	8% NaNO ₃ (different concentrations)
Flushing	continuous	controlled
Applications	deburring large surfaces, drilling	precision components 1:1 copy
Multi-processing	possible	possible

Over the years, EC machining has gradually become easier to handle, and more predictable and reliable (VDI 3401). By integrating a large set of technology parameters in the CNC unit, today's pulsed and oscillating Precision ECM cycle is a lot faster, and is now within the range of conventional machining speeds. In PEM a process-specific optimising system has been incorporated, ensuring that most jobs are completed right the first time, even those with complicated shapes. Since then, both large volumes and small batches or one-of-a-kind precision products can be machined, provided that the material and the geometry within the range of products are largely identical. Table 1 presents a comparison of conventional and precision ECM.



1

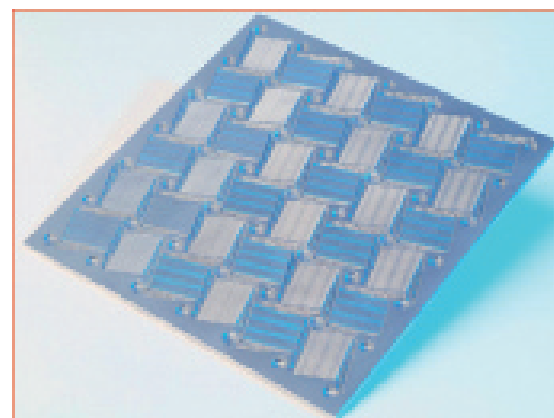
Competitive precision

Nowadays, the use of established PEM procedures as an innovative breakthrough is in direct competition with spark erosion (EDM) and laser beam machining (LBM), both of which are thermo-physical processes. It presents the industry with a fitting 'cold' machining solution to meet critical tolerances and surface quality requirements. In general, the modern developments that have led up to advanced PEM technology have encouraged metalworking companies to use this particular electrochemical version, which closes the gap between traditional and non-conventional machining. A large spectrum of electrically conductive materials can be 'PEM-ed' at an economical speed, irrespective of mechanical properties such as hardness, with no heat input induced and no mechanical forces (i.e. no negative impact on the part such as fissures or internal stresses).

There is a striking similarity with basic EDM in terms of contactless metal removal, machining fluid, pulse generator, working gap and a set of (tool and part) electrodes. In metal removal, the tool is traditionally the hardest one. In EDM and PEM, however, that situation is reversed. 'PEM-ing' – which features a higher metal removal rate on an atomic or molecular scale over the full geometrical surface as well as improved accuracy – produces incomparably rapid one-of-a-kind, precise parts in workshops, as well as in mass production.

There are several dedicated ECM techniques that are active machining processes but in different guises, for instance EC drilling, deburring, sinking, engraving and structuring, polishing and micro-structuring (see Figure 1 and 2). All of

- 1 ECM application samples.
- 2 Precision ECM-ed heat exchanger.



2

them are part of a niche market all their own. For example, STEM (shaped tube electrochemical machining) and ECJ drilling (electrochemical jetting) excel in extreme length-over-diameter (L/D) ratios and miniature bores respectively. Furthermore, combined hybrid process types such as ECG (EC grinding) and ELID (electrolytic in-process dressing) are used frequently. These techniques feature ultra-fine grinding up to a surface roughness of $30 \text{ nm } R_a$.

Technical market leader

A key player in the ECM field is the Franco-German company PEMTec, which is represented in the Netherlands by Encoma, based in Weert. PEMTec has expanded so much over the last five years that it has had to move its head office to brand new premises. During an eye-opening visit to Forbach in the French Saarland region, general manager Hans Kuhn showed us the company's main activities and



3 New PEMTec machine tools.
(a) The PEM 400, which has been specially engineered for SMEs, has a small footprint.
(b) The larger PEM 800, latest design of ECM machine tool configuration.

also shared with us the in-depth technical expertise and experience available in all disciplines from R&D and machine tool building to industrial project solutions. In recent years, this young technical market leader has successfully switched from traditional ECM to the highly advanced PEM. With its definitive competitive advantages, PEM really makes a world of difference.

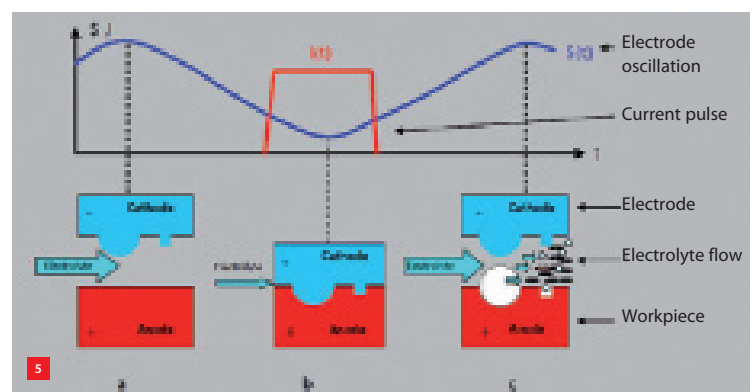
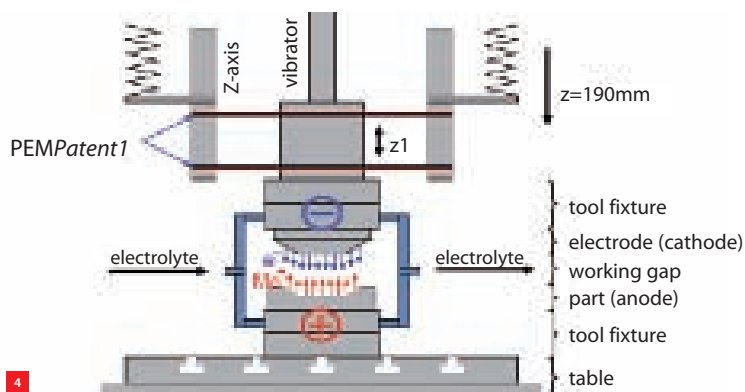
Looking to the future, PEMTec invested in a strong partnership with Kennametal Extrude Hone and set up regional PACs, i.e. PEM application centres, across Europe for consulting, carrying out feasibility studies, producing samples to demonstrate process capabilities and for sharing expertise. Since then, PEMTec has been producing a range of standardised and customer- or product-specific modern machine tools and fixtures at the new facilities. Over 500 machine tools have been manufactured and delivered all over the world, including USA and Japan.

Last year, two completely new state-of-the-art types of modern design were unveiled to visitors to EMO, the international machine tool exhibition in Hannover, Germany. There, visitors were introduced to the new PEM 400 (Figure 3a, smallest footprint) and PEM 800 (Figure 3b), which run on their own company-specific software with an industrial PC-based control.

Fundamentals

Based on Faraday's law, the underlying basic process does not seem to be complex, but it certainly is, because of the complex set of process parameters. The technique under discussion is 'simply' high-capacity, controlled metal removal by way of area-based electrolytic dissolution of the plus-polarity metal workpiece (anode) in a special saline electrolyte solution, which does the actual 'chipping' (see Figure 4). In general, the complete contour of the pre-formed tool electrode is copied with a high metal removal rate (MRR) by a linear in-feed in one pass. Given the high current density (10-100 A/cm²), machining cycles take seconds or minutes instead of hours.

During actual, low-temperature (20-50 °C) metal removal, there is no physical contact between product and tool electrode (cathode with an undercut) because of the working gap. The process is known for its high reproducibility and high speed without tool wear. It delivers well-defined glossy surface finishes or textures (R_a 0.5 µm normal, 0.05 µm in the polishing mode), without burr formation and induced internal stresses. There are no loose particles in the parts, which are in turn easy to clean and sterilise. If the process parameters have been properly set, variations are negligible. This ensures that the profile consistency remains unmatched and that extreme



dimensional stability can be reached when combined with no-wear conditions using only one electrode (tool) on thousands of parts.

The first main improvement was changing from sodium chloride (common salt, NaCl) to sodium nitrate (NaNO_3). Additional process-enhancing changes in machining parameters were introduced after a comprehensive test period resulted in 'good vibrations'. To stay upfront, pulsed current was introduced in an innovative way as a trick of the trade, as was a defined oscillation of the tool electrode (see Figure 5; 10% on-time). Since then, this upgraded low-temperature technology with increased accuracy and durable tools has been accepted much more widely in the metalworking industry. More improvements from the lab are on the way, e.g. bi-polar pulsing, extended real-time modelling, improved gap control by using cavitation effects and expanding to other materials such as carbides.

One prerequisite is a perfectly controlled electrolyte handling system for quality conditioning. This includes preparation in terms of temperature, constant chemical composition, concentration and pH value, constant flow rate, control in-/outlet pressure, filtering and removal of the fluid process medium and process particles at all elements of the contour to be machined, no matter how intricate and precise. The resulting waste material is mainly (~95%) composed of thin sludge consisting of electrolyte solution and insoluble metal hydroxides and oxides. The common practice is to use a centrifuge or separator to obtain dry sludge that must be treated as chemical waste.

Dutch connection

The Netherlands is home to a remarkably large number of small and medium-sized companies that are actively researching and applying different versions of the ECM process. The largest user by far is the world-renowned Philips corporation, which is using its own P-ECM to produce the rotary shaving systems in Drachten. This is

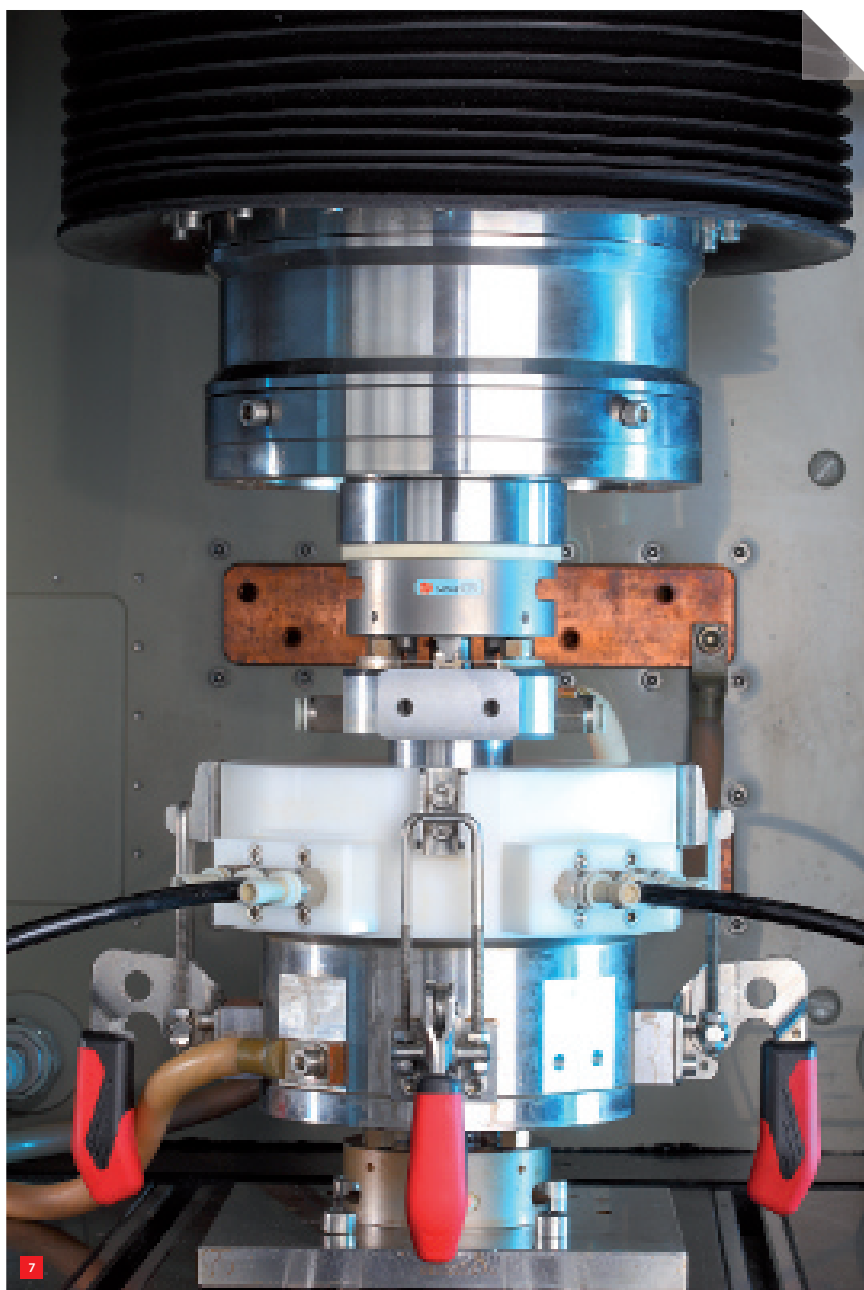
4 Schematic principle of precision electrochemical machining.

5 Crucial elements in actual PEM-ing.

6 Early Philips rotary shaving cap and cutter set.

where it all started (see Figure 6). Eldim, part of the Sulzer Metco company, uses ECM and other processes to produce precision bores with extreme length-over-diameter ratios in difficult-to-machine advanced materials. The Lomm-based OEM supplier is also well known for the crucial engine components of both stationary and mobile gas turbines, such as baffles, seals, inserts, compressor vanes and assemblies. Dutch engineering firms such as Irmato, ECM Technologies and DutchAero are developing working relationships with partners and/or OEM suppliers (ECM Productions).





7 Fixtures play a crucial role, as this set-up underlines.

Machine configuration

As an application-related process, ECM requires a range of equipment in different sizes. In all of their modern machines, PEMTec went for a completely modular, attractive and ergonomic design. Four subsystems can be distinguished, starting with the PEM Mechanic section as the actual machine base and the PEM Power electronic supply. A sturdy, force-closed, solid base structure made of natural granite emphasises the chemically inert and temperature-immune configuration.

Also taken into account in the design is the fact that anodic dissolution is not discriminatory, so all the parts have been

made of stainless steel and synthetic materials. The over-dimensioned, vertical ram with the in-built patented oscillator, which takes care of the linear feed movement, sits on the solid granite portal. At first sight, you might question the relatively large diameter of the quill. However, when you think about it, you realise that it is absolutely essential to connect both the work and the often quite voluminous tool electrode set-up to the table and the ECM head respectively using quick-change interfaces.

Absolute process and operator safety is integrated by way of a fully closed processing area, frontal sliding doors and a fume extraction system. The processing system with MMI touch panel is called PEM Control. By monitoring current, voltage, pulse settings, pH value (preferably pH 7), flow, conductivity, sparking, short-circuiting and temperature, the process cycle is perfectly in control. A self-contained, autonomous electrolyte conditioning system called PEM Aqua incorporates reservoirs, pump and filtration units (fit for flushing pressures from 0.5-6 bar up to 25 bar).

In any production chain, single and multiple fixtures (Figure 7) form a crucial part of the manufacturing process. Secure, stable and well-defined clamping and correct flushing tasks largely determine the end result. Precision ECM is no exception in this case. The quick-change possibilities of both tool and part(s) are facilitated by way of 'easy to set up' palletised fixtures as standard interfaces. Several automation concepts – from singular or multiple cells to robotised custom-made solutions – are available in-house on demand as a turnkey solution. Nowadays, the majority of standard machine tools feature one to three axes; five-axis versions are being developed

ISEM and INSECT

The growing interest in a non-traditional machining technique such as PEM is perhaps best underlined by the fact that in the second half of 2013 two major international seminars in Europe stressed the increasing importance of non-conventional processes in general and precision ECM in particular.

The 17th International Seminar on Electro Physical and Chemical Machining (ISEM), which covered all non-traditional machining processes, was held on the premises of the esteemed Leuven University, Prof. Jean-Pierre Kruth and Prof. Bert Lauwers, acting as chairman and organiser. Sponsored by CIRP (International Academy for Production Engineering) [1], this three-yearly seminar provided the ideal place for the academic and industrial world to meet. Meanwhile, the 9th International Symposium on Electrochemical Machining Techniques (INSECT) at the Fraunhofer IWU Institute in Chemnitz served as a platform



- 8 Specially adapted, silenced crown gears show a promising application field
- 9 PEM-made elements help to compact a complex die (Bihler).

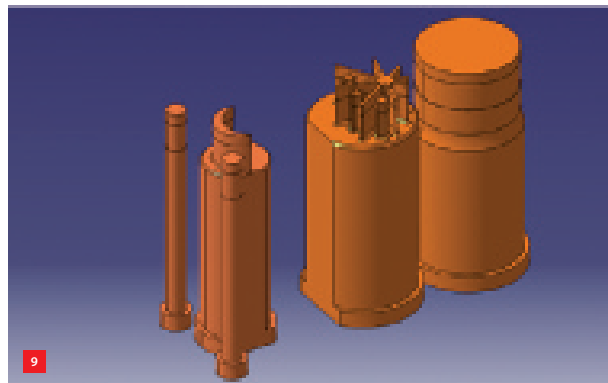
for researchers and engineers in the ECM field [2]. The main themes of both seminars were the technical aspects of micro and macro applications, machine tool developments and the fundamentals of the process at the electrolyte/electrode interface.

ECM revival

Actual PEM applications cover a huge range of materials, sizes and geometries. Sharing new expertise has brought about a kind of ECM revival. Well-known and proven applications are aero- and hydrodynamic surfaces, as well as pneumatic and hydraulic components in automotive, medical and chemical equipment and in the energy sector (e.g. fuel cells). In the turbine industry, high-pressure nozzles, complex fuel injectors and airfoils that are selectively reduced in their cross-section, and even sophisticated blisks – complete stages from a solid blank – are all processed. Successful projects proved that ‘PEM-ing’ is a very promising solution for axial and radial gears, especially corrected crown gears with an impossible-to-mill tooth flank geometry for considerable noise reduction (see Figure 8)

There is a rapidly growing market in micro and precision systems and delicate structures up to 20-30 µm in size, for instance in the watch industry. Miniature spiral bearings both radially and as a thrust journal are state-of-the-art nowadays. Using precision ECM allows for thinner walls and finer geometric elements, resulting in very compact, yet sturdy dies, as Bihler shows (see Figure 9).

On top of this, recent improvements in tool making achieved with PEM now make it possible to process moulds and (cold-forming) dies featuring integrated hologram-like



embossing in micron dimensions for the very first time. The Swiss company Bräm leads the innovation pack in this. Certain users take advantage of the generally less well-known absolute absence of machining forces and induced internal stresses to improve results while working with hardened or weak magnetic materials to preserve the initial material properties. In everyday practice, the PEM capability for removing heat-affected zones stemming from EDM and laser-machining is a relatively new application.

REFERENCES

- [1] www.mech.kuleuven.be/ISEM2013
 [2] www.tu-chemnitz.de/mb/MikroFertTech/insect.php

NOT TO LOSE SIGHT OF A SUB-MICRON SAMPLE

The scanning tunnelling microscope (STM) is a widely used tool for imaging sample surfaces at atomic level, but for a very long time observing live experiments at varying temperatures was virtually impossible. The Leiden Kamerlingh Onnes Laboratory has, however, succeeded in designing a high-speed STM providing images at temperatures ranging from 40 K to 1,000 K. An STM observes a surface of up to $2 \times 2 \mu\text{m}^2$ only. That is why precision technologists will recognise the thermo-mechanical challenge not to lose sight of a sample when working at such wide-ranging temperatures.

AUTHOR'S NOTE

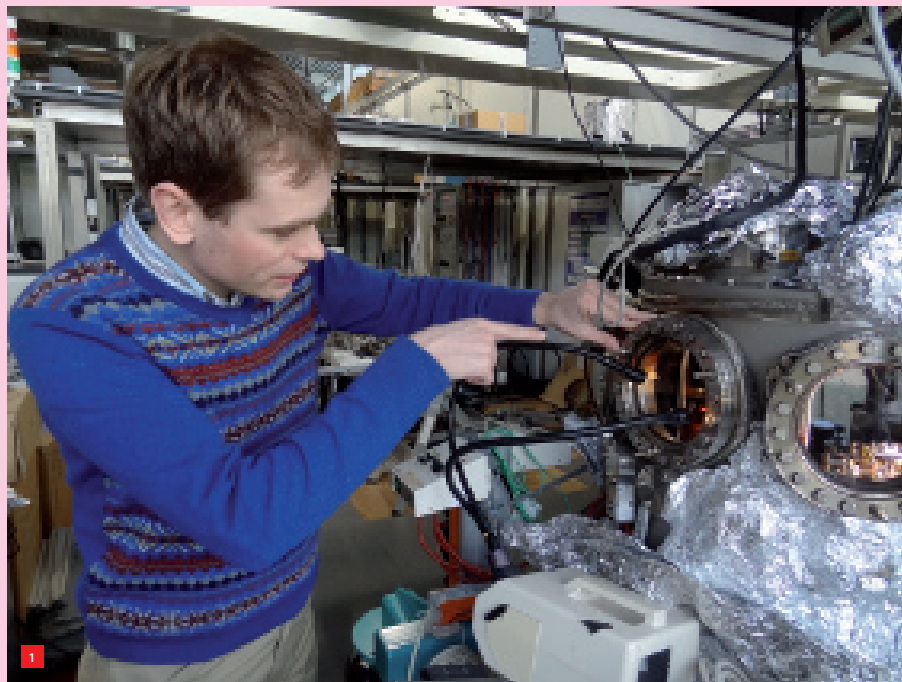
Frans Zuurveen is a freelance text writer who lives in Vlissingen, the Netherlands.

FRANS ZUURVEEN

Leiden

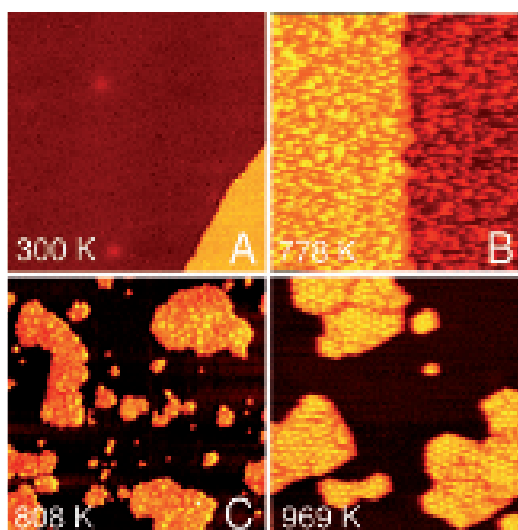
In 1986, Gerd Binnig and Heinrich Rohrer were awarded the Nobel Prize in Physics for their invention of the STM. An ultra-high vacuum set-up in the Kamerlingh Onnes Laboratory of the Leiden Institute of Physics, the Netherlands, has housed successive generations of STMs for twenty years. Experiments performed here have given several students the opportunity to earn their Ph.D. in Physics, supported and guided by Prof. Joost Frenken.

Frenken, also head of the Leiden Center for UltraMicroscopy, and his students perfected the Leiden University STM set-up by introducing sample-temperature variation. After graduating, Marcel Rost, who was one of Frenken's students, started a company, Leiden Probe Microscopy, for the development and marketing of the truly variable-temperature STM. Gertjan van Baarle, who graduated from the same institute, is the current director of this company. His younger brother, Dirk is currently finishing his Ph.D. in Physics in the variable-temperature STM project (see Figure 1).

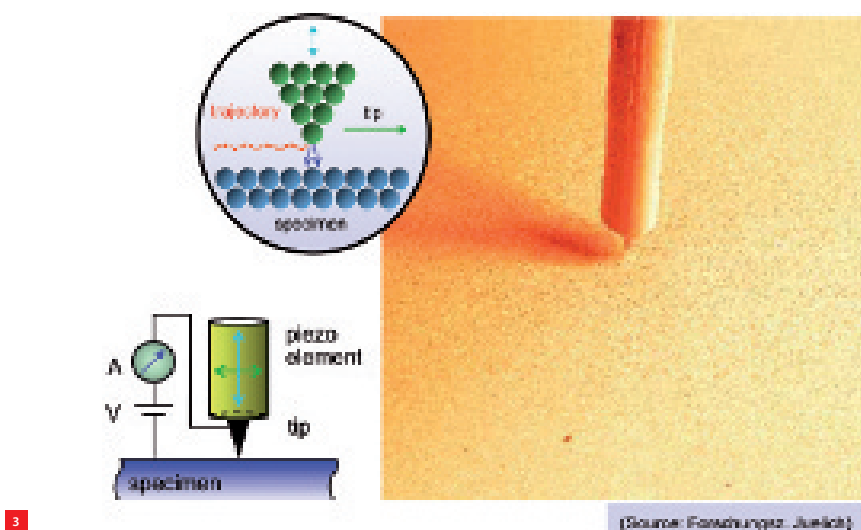


1 Dirk van Baarle working on the vacuum chamber with the Leiden variable-temperature STM.

BAARLED@PHYSICS.LEIDENUNIV.NL | LCU.PHYSICS.LEIDENUNIV.NL | WWW.LEIDENPROBEMICROSCOPY.COM

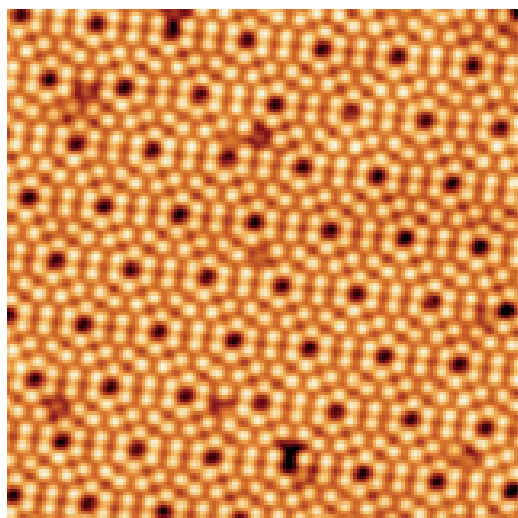


2



3

[Source: Forschungszentrum Jülich]



4

2 STM images of graphene produced during continuous heating from 300 K to 1,000 K, after ethylene decomposition on a (111)-oriented mono-crystalline rhodium surface. (G. Dong, Ph.D. thesis, Leiden University, 2013)

3 Principle of STM. Bottom left: control loop for maintaining a constant distance between the tip and sample surface, providing a height map of that surface (top left). Top right: SEM image of set-up.

4 STM image of $20 \times 20 \text{ nm}^2$ Si with (111)-orientation showing atomic resolution. (V. Fokkema, Ph.D. thesis, Leiden University, 2011)

Principle of STM

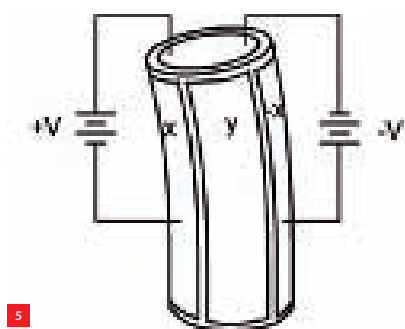
Figure 3 shows the principle of a scanning tunnelling microscope. An extremely sharp tip moves across the sample surface at a constant distance with respect to that surface. The concept of quantum tunnelling is responsible for retaining this constant height. Classically, objects cannot penetrate an impenetrable barrier. According to quantum mechanics, however, the position of an electron, with wave-like characteristics, is distributed with a well-defined probability over a wave function of its atom. If the wave function of an atom at the end of the tip overlaps the wave function of the sample surface, an electron may 'hop' from the tip to an unoccupied wave function of the sample. This quantum effect is known as tunnelling. When a direct voltage is applied between the sharp tip and the conductive sample surface, this tunnelling effect provides a small current between the tip and the surface. The current as a function of applied voltage exhibits very 'steep' exponential behaviour, making it possible to maintain the constant distance of the tip in a feedback control loop.

The setpoint for the tunnelling current typically amounts to no more than 100 pA, 10^{-10} A. The vertical displacement Z of the tip is monitored while the tip scans the sample surface in a raster pattern in the horizontal X and Y directions. When correlating the values of Z for each (X,Y) position to grey-scale values in an image, a height map of the sample surface is provided, making it possible to observe the arrangement of atoms in crystal lattices (see Figure 4).

Typical atomic features measure about 0.1 nm in the X and Y directions and 0.01 nm in the Z direction. To achieve a resolution that is high enough to resolve such features, an

The enormous advantage of introducing sample-temperature variation in an STM is the option to study physical and chemical processes at atomic level by continuous observation of the sample surface as a function of temperature.

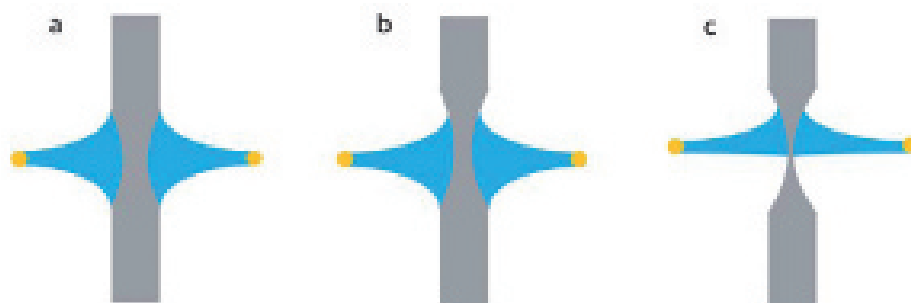
The sample then remains in the ultra-high vacuum environment of 10^{-10} mbar, but, for example, gases like ethylene, C_2H_4 , can be introduced to deposit carbon atoms on the sample surface, when this is sufficiently hot. This means that the formation process of graphene, consisting of a one-atom-thick network of carbon hexagons, can be observed at different temperatures (see Figure 2). Other chemical and physical processes can be studied in situ as well, including CVD (chemical vapour deposition).



5 A piezoelectric transducer of PZT, lead zirconium titanate, with a continuous inner electrode and segmented outer electrodes.

6 The three stages in the etching process of a 250- μm thick tungsten wire to produce an STM tip. (R. van Rijn, M.Sc. Thesis, Leiden University, 2007) Yellow: ring-shaped electrode. Blue: NaOH etchant.

7 Etched STM tips made of tungsten. (a) Light-microscopic image and its reflection. (b) SEM image.



(X,Y,Z)-scanner made of piezoelectric material is used, typically PZT ceramics: lead zirconium titanate. The sample is kept stationary, whereas the tip connected to the scanner covers the three degrees of freedom required. Several ceramic producers deliver piezoelectric tubes with radial polarisation for that purpose; these tubes are fitted with one electrode on the inner wall and four electrodes in the outer wall (see Figure 5).

Applying a voltage between the continuous inner electrode and the four outer electrodes taken together makes the tube wall expand, causing the tube to elongate: Z-movement.

Applying a voltage between one of the outer electrodes and the inner one changes the wall thickness of the tube at that outer electrode only. This effect makes the tube bend sideways, facilitating X- and Y-movements.

An extremely sharp point

Manufacturing a tip with an extremely sharp point is essential to be able to produce an STM with a good resolution (especially when samples are not extremely flat). The radius of the tip should be no more than a few nanometers. This guarantees that one and the same atom is responsible for the current that flows towards the sample

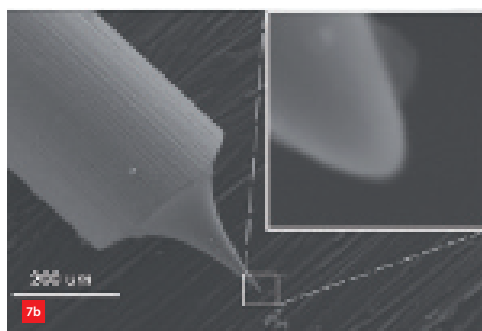
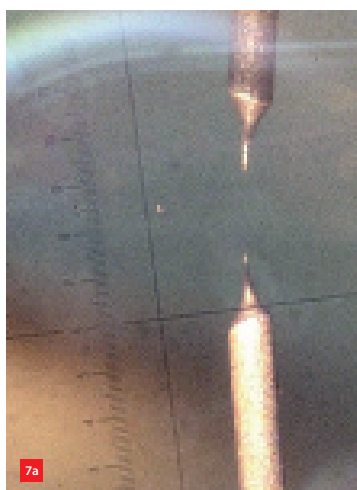
when the tip scans the sample surface. The materials used for this purpose are tungsten and platinum-iridium. The benefit of the latter material is that it stays inert without oxidising, whereas tungsten may corrode in an oxygen-rich atmosphere.

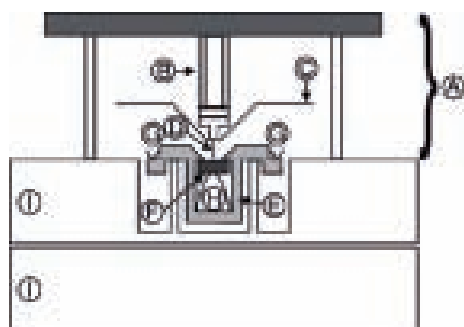
Manufacturing an STM tip made of PtIr is a somewhat haphazard process. Cutting PtIr sheet material may result in the intended ravel-like wires. However, this is a rather cumbersome procedure. STM tips from tungsten can be made by etching with NaOH (sodium hydroxide) in an electrolytic process (see Figure 6). A thin film of etchant is enclosed within a ring-shaped electrode around a 250- μm thick tungsten wire. Carefully adjusting the height of the electrode with respect to the wire provides an extremely sharp tip, which gently falls into a beaker with razor foam. By studying their field emission characteristics, the ultimate behaviour of a valuable STM tip made of W or PtIr can be tested (see Figure 7).

Avoiding thermal catastrophes

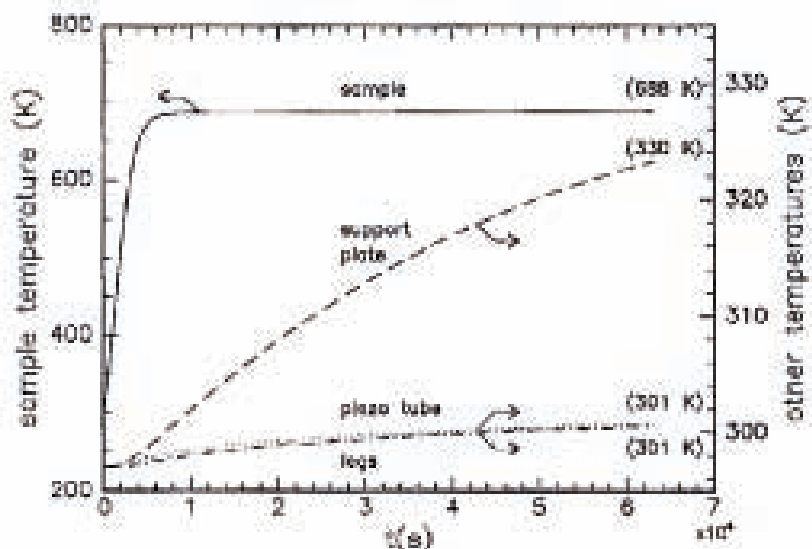
Achieving a temperature range from 40 K to 1,000 K or even 1,200 K means cooling the sample through a heat-conducting connection to liquid nitrogen or helium, or heating the sample by generating an electric current through a filament below the sample. The thermal deformation of the mechanical parts of the STM when changing the temperature will change the position of the tip with respect to the sample if no extra measures are taken. The catastrophes that might happen may include the destruction of the tip because of contact with the sample and – less radically – losing sight of the sample area to be studied if the total thermal drift exceeds the Z-range of the scanner.

Figure 8 shows the basic STM configuration adopted to minimise these unwanted thermal effects. This configuration was thermally optimised by applying a finite-element method (FEM) analysis calculation. The configuration aims to thermally isolate the sample as much as possible from the environment and to minimise the thermal expansions within the rest of the STM.





- A scanner top
- B piezoelectric tube
- C heat shield
- D STM tip
- E molybdenum sample holder
- F sample
- G leaf springs pushing the sample holder into the STM base
- H leaf spring pushing the sample onto the reference plane
- I molybdenum STM base



Another feature of this configuration is the cylindrical symmetry with respect to the vertical axis through the tip, minimising the shift due to thermal expansion in the sample centre, which is the area to be studied. Furthermore, the upper surface of the support plate I – coinciding at room temperature with the sample surface – was chosen as a reference plane from which all thermal expansions are directed away. Ledges at the sample holder E guarantee that the sample surface remains coplanar with the support plate, despite the large thermal gradients.

The FEM analysis aims to keep the thermal expansion of the outer legs of the scanner top A equal to the cumulative expansion of the piezoelectric tube, the tip mount and the tip itself, thus keeping the tip point continuously in the reference plane.

FEM analysis results

In the FEM analysis, all the components from Figure 8 were taken into account, i.e. 22 volume elements and 62 surface elements. Heat conduction was the main phenomenon taken into consideration, but the effect of radiation could not be neglected at sample temperatures over 500 K. Therefore, the solid angles with which each surface element could 'see' all other surface elements were calculated. A matrix was constructed with the radiative coupling constants between all pairs of surface elements, each dealing with their respective surface emissivities. Thus, the temperatures of all elements could be calculated by integrating the conductive and radiative heat flows with time steps of 50 ms.

Figure 9 shows some of the results of the FEM calculations: temperatures of the most important STM elements as a function of time. The heating rate of the sample is three

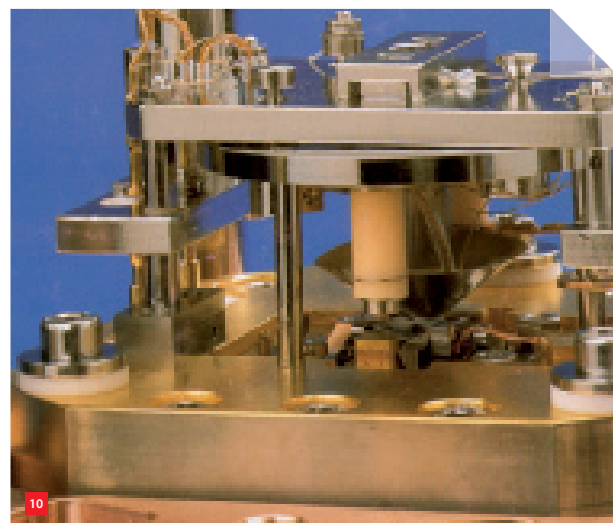
8 Schematic cross section of the STM, used in FEM analysis. (K. Schoots, Ph.D. thesis, Leiden University, 2007)

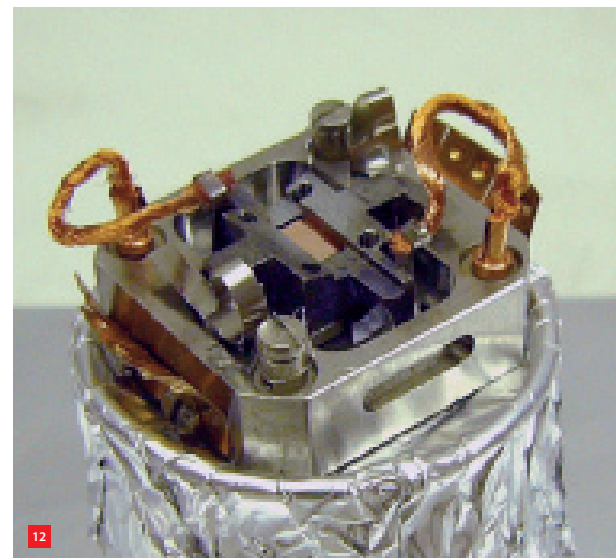
9 Calculated temperatures as a function of time after switching on the filament at $t = 0$ s with 3.36 W power. The numbers between brackets indicate the final temperatures after 37.5 hours of thermal equilibration.

10 The practical set-up of the variable-temperature STM on a molybdenum base block. The radiation shield is visible above the sample.

orders of magnitude higher than the one of the support plate. This proves the effective thermal decoupling of the sample holder with respect to the rest of the system. After 4,000 s, the sample has almost reached its final temperature, while the rest of the STM still increases in temperature at a more or less constant rate. Although the tip nearly touches the sample surface, its temperature remains below 301 K.

When optimising the configuration of Figure 8, close attention was paid to the composition and dimensioning of the outer legs of the scanner top. Legs made of molybdenum (low thermal expansion) and stainless steel (high thermal expansion) with different dimensions were taken into consideration. The microscope performed best with legs made completely out of molybdenum.





11 A sample in its holder, heated to a temperature of over 1,000 K.

12 The universal STM sample holder (coloured dark) with the sample in its centre.

13 The vacuum chamber housing the variable-temperature STM.

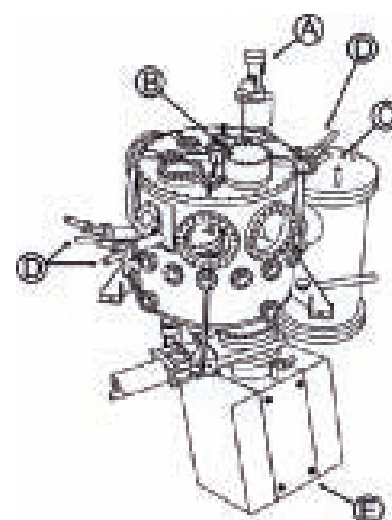
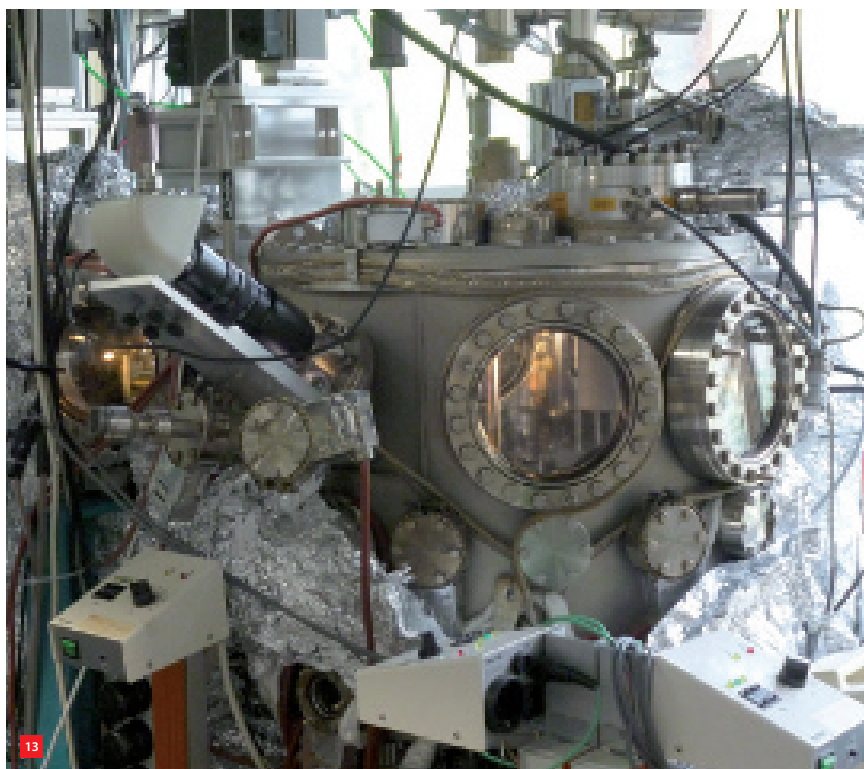
14 Schematic drawing of the ultra-high vacuum chamber. (K. Schoots, Ph.D. thesis, Leiden University, 2007)

Calculations showed that all drifts could be kept well below 0.05 nm/s after only 90 minutes, long before all the parts of the STM reached their final temperature.

Experimental set-up

Figure 10 shows the variable-temperature STM assembly in its current practical set-up surrounded by the molybdenum base block. At elevated temperatures, i.e. 1,000 K and higher, the sample emits visible radiation (see Figure 11).

To facilitate observation of different samples and processes, a universal sample holder has been designed (see Figure 12). Its design ensures minimal thermal contact as well as reproducible position accuracy in relation to the base plate and the tip holder. The sample holder ledges are positioned in such a way that thermal expansion always uses the sample centre as zero reference. What is not illustrated is a (relatively) coarse approaching system to bring the relevant



- A** focussed-ion gun for sputter-cleaning the sample surfaces
- B** LEED system (low-energetic electron diffraction) for determining grid distances
- C** titanium sublimation pump with integrated cold trap
- D** Knudsen cells for vaporising metal layers
- E** ion getter pump

sample area within the positioning range of the piezoelectric tube controlling the tip movements.

Achieving a vacuum environment without contaminating gases and with a pressure of no more than 10^{-10} mbar is very time-consuming, as it includes baking out the recipient walls to get rid of adsorbed and absorbed water molecules. That is why the vacuum chamber that houses the STM is fitted with a locking system to bring in the sample holder without severely disrupting the vacuum conditions. Figure 13 shows the complete experimental set-up in the Leiden Kamerlingh Onnes laboratory and Figure 14 presents a schematic 3D drawing.

Three magnetic-levitation turbo-molecular pumps are the 'workhorses' maintaining the ultra-high vacuum. Their magnetic bearings are completely free of contamination, unlike the conventional bearings normally used in turbo-molecular pumps. These pumps are assisted by ion getter

pumps. The system is also fitted with titanium sublimation pumps for absorbing hydrogen, which is generated when ethylene (C_2H_4) is injected to deposit carbon on the sample surface for producing graphene. When the turbo-molecular pumps, which might cause unwanted vibrations, are switched off, the aforementioned supplementary pumps are able to maintain the required vacuum conditions on their own for up to eight hours.

To conclude

It is quite remarkable that research instruments to observe extremely small objects are getting larger as the objects to be studied become smaller. Examples range from ASML wafer steppers to the CERN Large Hadron Collider – and the large experimental STM set-up in the Leiden Kamerlingh Onnes Laboratory, with which atomic level details can be observed. It is good to bear in mind that all these scientific achievements would be impossible without dedicated precision technology. ■



Your single source supplier for ultra precision engineering, design & metrology.



- Ultra precision design services
- From concept to pilot manufacturing support
- Expert verification and tooling
- Managed transfer to volume producer

WWW.IBSPE.COM

PROPER HANDLING OF THERMAL ERRORS

One of the major challenges of improving the positioning accuracy of machine tools and precision devices is the proper handling of thermal errors. Thermal error refers to the mismatch between the real and predicted displacement and/or the displacement differences of the point of interest due to temperature fluctuations in space and time. Typically, the design objective is to decrease the thermal error within a timeframe of interest. This article takes two design cases to demonstrate the potential of topology optimisation.

EVERT HOOJKAMP, EMIEL VAN DE VEN, MATTHIJS LANGELAAR AND FRED VAN KEULEN

One of the major challenges of improving the positioning accuracy of machine tools and precision devices is the proper handling of thermal errors [1]. In general, there are three types of design solutions for thermal error reduction [2]: heat flow control, design optimisation and real-time compensation. The first includes conditioning of the system or shielding the crucial parts to decrease the influence of the internal and external heat sources. The second aims to reduce the temperature fluctuations and the resulting displacements in the crucial parts of the system. This can be done by proper material selection or smart geometries. The last type of design solution compensates the thermal error using thermal or mechanical actuators during operation. In practice, a combination of all three types is used to reduce thermal error in precision devices.

This paper focuses on design optimisation, specifically on the automated design of geometry to decrease the thermal error. This is done using topology optimisation. Here, the aim is to introduce topology optimisation and its application to precision systems under thermal loading. As such, the paper first presents the basics of topology optimisation. It then outlines implementation for thermo-mechanical systems and then illustrates the potential of topology optimisation, presenting two test cases. It concludes with a discussion of the challenges for thermo-mechanical topology optimisation.

Topology optimisation

Topology optimisation (TO) refers to a relatively recent branch of design optimisation techniques that can be used to generate design concepts for a variety of engineering problems. Although the first academic work on TO appeared in the late eighties, it is only in the last 10-15 years that TO has been used more and more by sectors such as the automotive and aerospace industries (e.g. [3]). In recent years, the focus has also shifted to the needs of the precision engineering field, e.g. by considering thermo-mechanical design problems. This text highlights some of these developments.

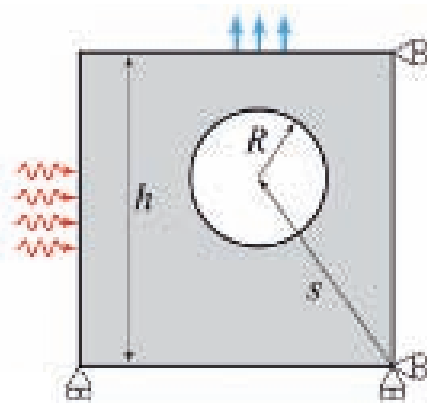
To define what TO is, we first outline what it is not. In classical shape optimisation (Figure 1a), the *shape* of a given design concept is optimised using a set of geometrical design parameters defined by the user. In TO, however, the *distribution of material* in a given design volume is considered, and the optimisation process generates

AUTHORS' NOTE

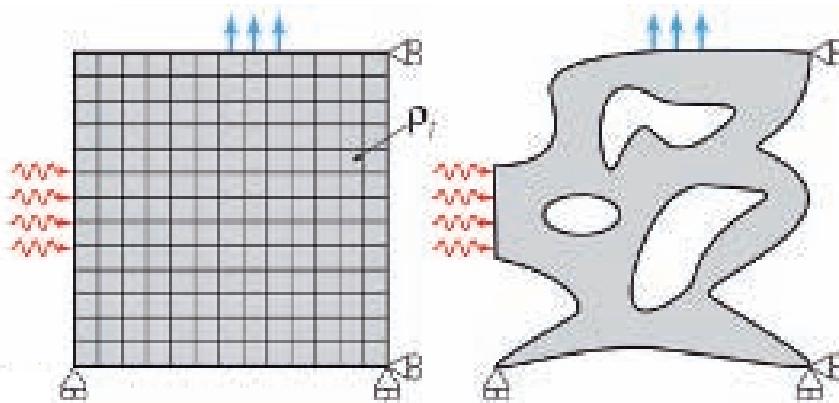
All authors are part of the Structural Optimization and Mechanics (SOM) group, which is an integral part of the Precision and Microsystem Engineering Department of Delft University of Technology, the Netherlands. Headed by Prof. Fred van Keulen, the group's research concerns both mechanics and optimisation. Matthijs Langelaar is an assistant professor in the SOM group; he specialises in

topology optimisation. M.Sc. student Emiel van de Ven is doing his graduate project on the topology optimisation of thermo-mechanical systems. He is being supervised by Evert Hooijkamp, who is finishing his Ph.D. on thermo-mechanical system design.

m.langelaar@tudelft.nl
www.pme.tudelft.nl



1a



1b



2a



2b

properly performing designs that do not require an initial concept. The design volume is discretised in a large number of subvolumes (Figure 1b).

In the case of a finite-element analysis model, each element is typically considered a subvolume. The local presence or absence of material is controlled by a normalised *density* design variable defined in each subvolume. A value of 0 indicates that the subvolume is empty, while a value of 1 indicates completely solid material. After the user defines the design problem in terms of objective, constraints, design domain and performance simulation, an optimisation process can determine the optimal values for

- 1 Schematic illustration of optimisation for a particular thermo-mechanical loading situation (see text for explanation).
 - (a) Shape optimisation.
 - (b) Topology optimisation.
- 2 Fully functional compliant gripper.
 - (a) Created by topology optimisation.
 - (b) Produced using additive manufacturing (AM).

all density variables, corresponding to the optimal material layout. Generally speaking, the number of density variables is large, thousands for 2D models and up to millions for 3D cases. An efficient adjoint design sensitivity analysis [4] and gradient-based optimisation are essential ingredients that enable the TO process.

In short, in TO virtually any topology can be generated using a material distribution parameterisation based on local density variables.

One key advantage of TO is the enormous variety of geometries that can be generated, allowing the process to approximate the ideal geometry very closely. Moreover,

because it is not limited by initial assumptions or shape parameterisations, TO can produce innovative solutions for complex design problems. However, geometrically complex designs are often expensive or impossible to manufacture using conventional techniques, and manufacturing constraints may need to be included in the TO problem formulation to prevent this.

Fortunately, upcoming new manufacturing technologies such as additive manufacturing (AM) are making it increasingly possible to realise the generated complex geometries with minimal modifications, thus preserving optimal performance. Figure 2 shows an example of a compliant gripper created by TO and produced using AM.

Most TO applications involve the static or dynamic performance of structural designs. However, it is also possible to include other physical aspects in the design problem. By employing a thermo-mechanical analysis model, we show that TO techniques can also be applied to reduce thermal error.

Thermo-mechanical model

The thermo-mechanical model of a system relates the thermal and mechanical loads to the temperature and displacement fields. The systems (e.g. precision devices) in question allow the assumption of small temperature fluctuations with respect to the reference temperature (i.e. $|\theta| = |T - T_e| \ll T_e$). Consequently, temperature-independent and linear isotropic material is considered, and the effects of heat convection and radiation are linearised. Thus, the thermal system is assumed to be linear and the temperature field is governed by the heat conduction equation. After spatial discretisation (by finite elements for instance), the nodal temperature vector $\theta(t)$ is determined by:

$$[C_T] \frac{d\theta(t)}{dt} + [K_T] \theta(t) = Q(t) \quad (1)$$

Here, $[C_T]$ and $[K_T]$ denote the heat capacity matrix and the thermal conductivity matrix, respectively, and $Q(t)$ denotes the nodal transient thermal load. The initial condition is also known and denoted by $\theta(t=0) = \theta^0$. The boundary conditions, such as a known temperature or heat flux, are included in the heat conductivity matrix and thermal load vector. The transient response of the temperature field is determined by applying a numerical integration scheme to Equation 1.

The transient temperature response causes displacements due to thermal expansion. The transient displacement field is governed by the mechanical equilibrium equations. The inertia and damping effects are neglected because the

thermal time response is much slower than the structural dynamics of the system. Hence, the spatially discretised mechanical equilibrium equation is:

$$[K_u] u(t) = F(t) - [A] \theta(t) \quad (2)$$

Here, $[K_u]$ denotes the mechanical stiffness matrix, $[A]$ denotes the thermo-mechanical coupling matrix capturing the thermal expansion and $F(t)$ denotes the nodal mechanical load. Note that the reference temperature chosen is the temperature in the undeformed configuration. The thermal error is computed from the displacement vector as the mismatch between the real and predicted displacements of the point of interest. Hence, the thermal error is highly dependent on the predicted displacements, which can be equal to a reference point or determined from sensor information.

Material model

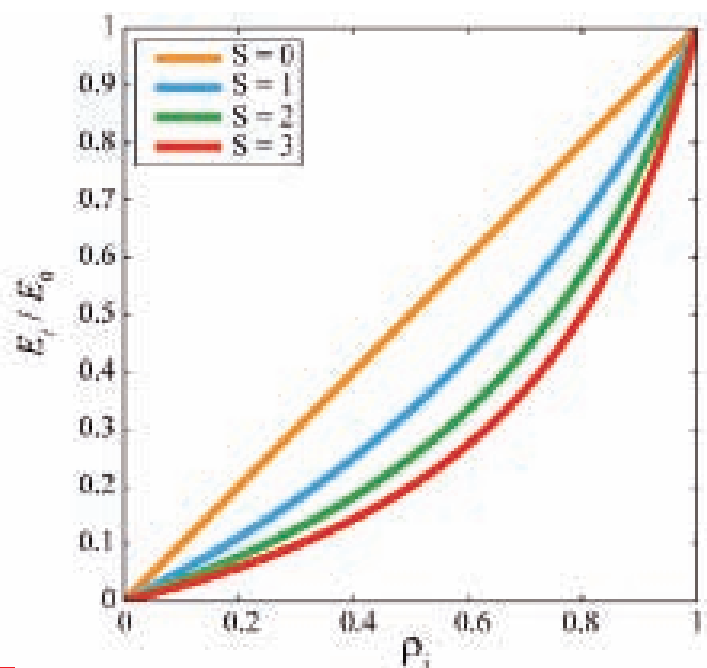
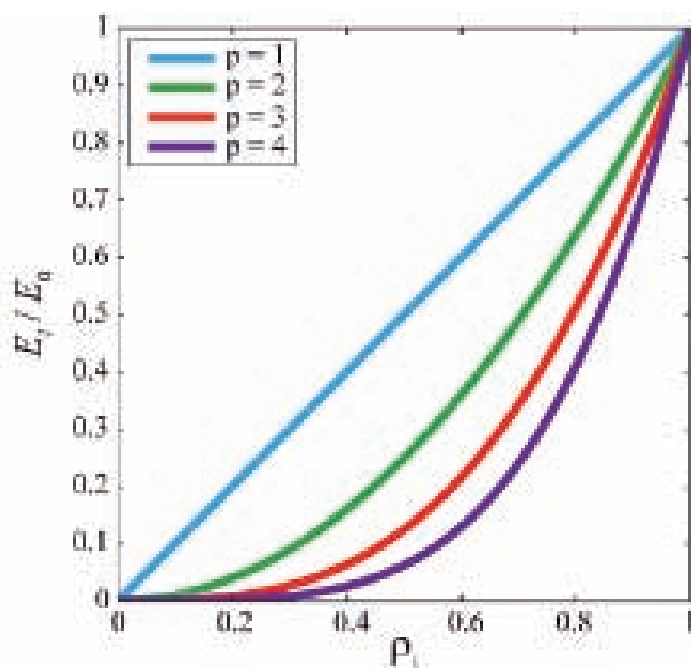
As described before, the design variables in TO are the element densities, which are defined between zero and one (i.e. void and material). In the density method, these design variables may vary continuously from one to zero and vice versa. Therefore, a material interpolation model is needed to capture the material behaviour of the so-called grey elements, i.e. the elements that are neither one nor zero. In literature, different material interpolation models can be found. Here, we discuss the models currently most often used in TO for thermo-mechanical systems.

The *linear interpolation model* adjusts the material behaviour of the element in proportion to the element density. Thus, for a grey element with a density value of 0.5, the material property, like the mass, stiffness or heat conduction, is half of its original value. For example, the elasticity modulus of element i can be expressed as:

$$E_i = \rho_i E_0 \quad (3)$$

Here, ρ_i denotes the design variable of element i and E_0 is the elasticity modulus of the material. The mechanical stiffness matrix of Equation 2 is then assembled, combining all element contributions that depend on the element density. In 2D systems, the effect of the change in element density by the linear interpolation model can be interpreted as a change in thickness of the element.

TO is regularly used to design a structure with a material layout without grey densities, i.e. a so-called black-and-white design. Therefore, the material performance of the grey density element must be less favourable than black or white elements. Currently, *solid isotropic material with penalisation* (SIMP) is used the most [5]. This material



interpolation model expresses the elasticity modulus of element i as:

$$E_i = \rho_i^p E_0$$

Here, p indicates the material penalisation parameter. Thus, for a grey element with a density value of 0.5 and a penalisation of 2, the material property, like the mass, stiffness or heat conduction, is a quarter of its original value. Figure 3a shows the interpolation curves for different values of the penalisation. Note that when the penalisation is 1, SIMP is equal to the linear interpolation model. In practice, a penalisation of 3 is the common choice.

For thermo-mechanical problems, SIMP may cause some difficulties because of the zero slope at zero density. This leads to zero sensitivity for void elements, making it difficult for designs to evolve. One solution that is often used is the *rational approximation of material properties* (RAMP) [6]. The main difference with SIMP is the non-zero slope at zero density, as shown for different penalisations in Figure 3b. Note that when the penalisation is 0, RAMP is equal to the linear interpolation model.

In the TO of transient thermo-mechanical systems, four material properties can be interpolated: heat conduction, heat capacity, thermal expansion coefficient and elasticity modulus. The four penalisation parameters can be chosen independently. Consequently, the grey elements can have specific properties depending on the penalisations, such as

stiff isolating or hyper expanding conductive properties, that deviate from the properties of the solid material.

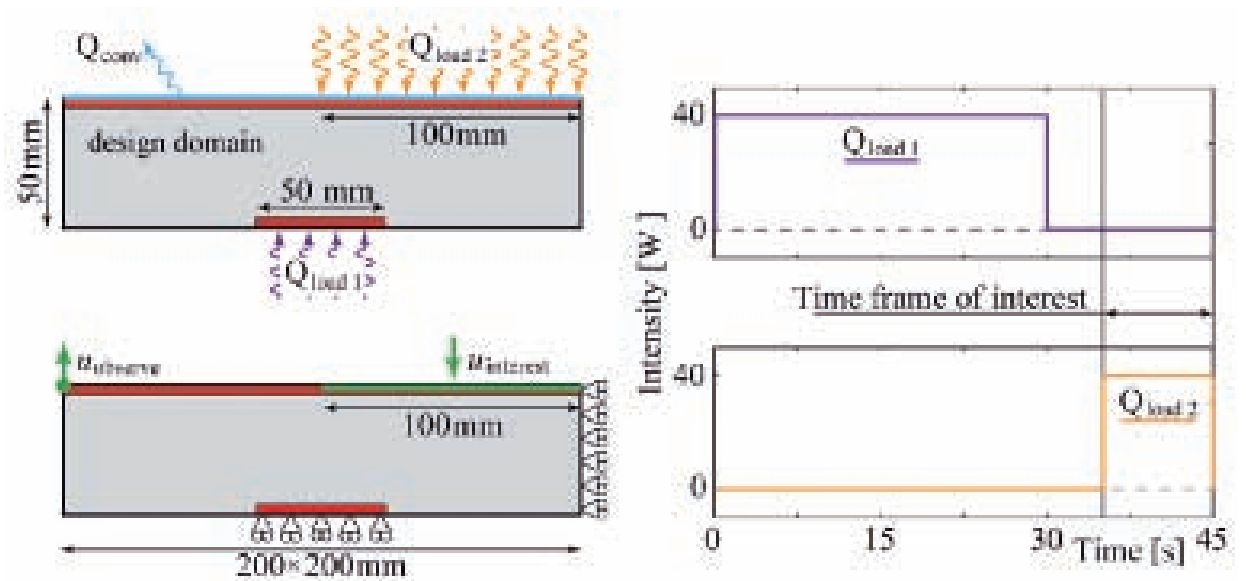
- (4) As mentioned before, the aim of penalisation is to generate black-and-white designs. Hence, a penalisation should be chosen so that the specific properties have a negative effect on the objective. However, this depends on the problem and can be different everywhere in the system (e.g. at one side of the system, high-conducting material may have a negative effect on the system, whereas isolating material may have a negative effect on the other side). In our experience, when reducing the thermal error, better results were obtained using RAMP in combination with a penalisation of around 2 for all four material properties.

Design cases

The potential of TO to reduce a thermal error is presented by means of two thermo-mechanical problems that could arise in precision devices. Design case 1, as shown in Figure 4, is an aluminium structure subjected to two heat loads (one at the bottom followed by one at the top), mimicking a positioning and process step in a precision device. The top of the structure exchanges heat by convection, with a heat transfer coefficient of 5 W/(m²K), while the remainder is thermally isolated.

Mechanically, the structure is supported horizontally on the right-hand side and vertically at the bottom. The thermal gradients will cause the structure to deform, resulting in a thermal error. The thermal error is defined as the vertical displacement difference between the area of interest and a

3 Material interpolation curves for different values of penalisation.
(a) SIMP.
(b) RAMP.



4



5a

5b

4 Design case 1: the system is subjected to two thermal loads at the bottom and the top of an aluminium structure (see text for explanation). On the right the time course of the heat loads is shown.

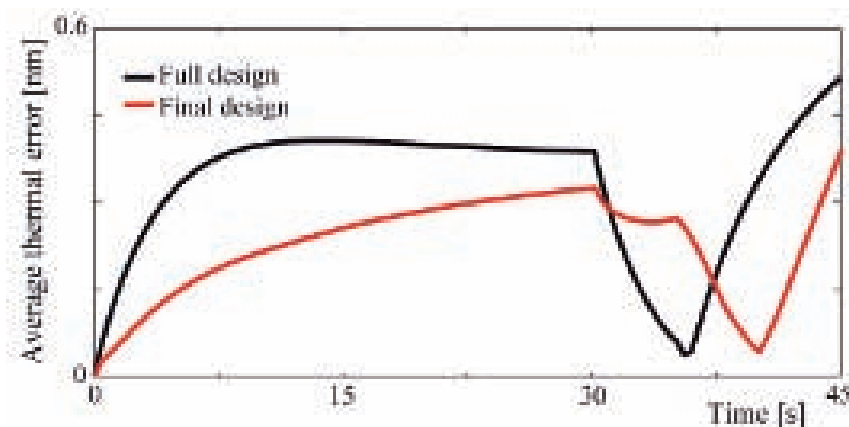
5 The final design.
(a) The black and grey elements show the material layout.
(b) An illustration of the temperature field in colours and scaled displacement field at the end time.

point of observation (measurement point). The design objective is to reduce this thermal error within the timeframe of interest by optimising the material layout within the design domain. The optimised designs are compared to the so-called full design, in which the design domain is completely filled with material.

Besides having good thermo-mechanical behaviour, the structure must also be able to handle samples at the top. Therefore, two non-design areas were assigned, indicated by the red blocks in Figure 4, and two stiffness constraints were included in the optimisation. One stiffness constraint limits the deformations thanks to a vertically distributed load at the top and the other does so thanks to a horizontally distributed load at the top. Both constraints are set to half the stiffness of the full design. The optimisation starts from a design with all the densities set to 0.5. This initial design is used a lot and helps to avoid local minima that might be present at a completely filled or empty design domain.

For this case, we used RAMP as the material interpolation model with a penalisation of 2 for all four material properties. Using the thermo-mechanical model, the objective is evaluated and the sensitivities of the objective function with respect to the design variables (element densities) are calculated. The design sensitivities are fed to an optimiser, in our case the method of moving asymptotes (MMA, [7]), which then determines a design modification. This process is repeated until design convergence.

The final design of design case 1 is shown in Figure 5. With half of the stiffness and less than half of the volume with respect to the full design, the final design reduces the time-integrated thermal error by 60%, and the peak error by 25%, as shown in Figure 6. The principle used by the optimiser is to design a truss structure so that the stiffness constraints are met and heat is stored at the bottom. The stored heat reduces the temperature gradient at later stage and, consequently, the deflection of the structure in the timeframe of interest (i.e. the thermal error).



6

Figure 7 shows design case 2, which is a square aluminium plate that is 1 cm thick. A thermal load is applied sequentially to the four quadrants Q_1 , Q_2 , Q_3 and Q_4 , as indicated by the red squares. The plate is cooled from below, which is modelled by convection with a heat transfer coefficient of $100 \text{ W}/(\text{m}^2\text{K})$. The plate is mechanically supported in y-direction at the bottom and in x-direction on the right (see Figure 7).

A 25 W heat load is applied to each quadrant for 8 seconds, with an 8 second break between each loading. This could represent a kind of measuring process for instance. The thermal expansion will cause the areas of interest (i.e. the

6 The thermal error of both designs as a function of time.

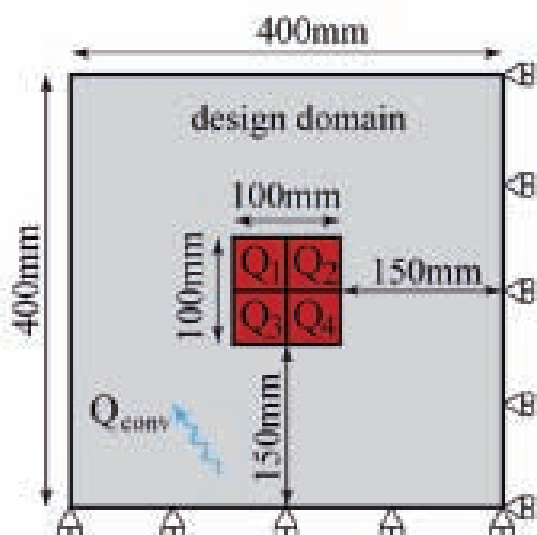
7 Design case 2: the system is subjected to four thermal loads in quadrants 1 to 4, sequentially. On the right the time course of the heat loads is shown.

four quadrants) to displace, causing a misalignment during the process. The thermal error of a quadrant is measured as the absolute displacement of its centre point due to thermal loading.

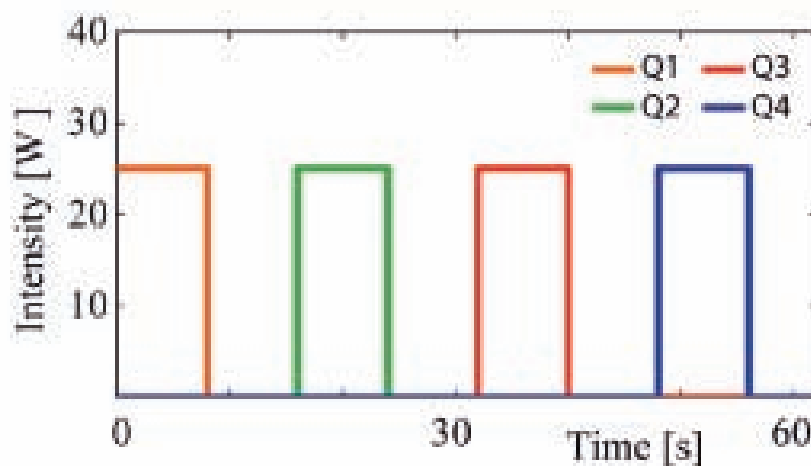
The objective of the TO is to minimise the thermal error of the quadrants during their individual loadings. This will be done by optimising the material layout around the four quadrants, i.e. in the design domain. As with the previous case, the optimised designs will be compared to the so-called full design, in which the design domain is completely filled with material.

Compared to design case 1, the optimisation in this model only differs because the convection is design dependent. Using the same optimisation settings as in design case 1, the final design is shown in Figure 8. The topology optimisation resulted in a design that used about half of the total volume and uses a combination of two principles to reduce the thermal error. For the first two quadrants, a circular plate-like structure is used to expand freely and transfer heat to the environment, whereas a mechanism is used to counteract the thermal deformation for the third and fourth quadrant. Figure 9 shows the thermal error in time; the time-averaged thermal error of the final design decreased by 45% compared to the full design.

Both design cases demonstrate that using smart material layouts can reduce the thermal error in thermo-mechanical problems. Hence, topology optimisation is a good option for thermal error reduction in precision devices.



7

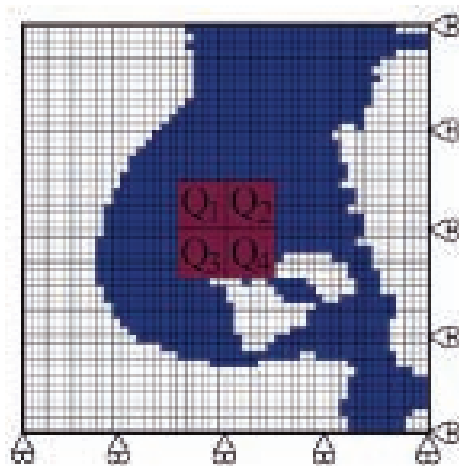


8 The final design.

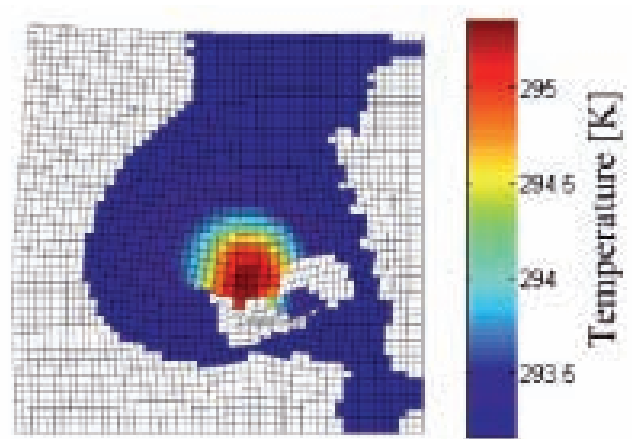
(a) The blue and red elements show the material layout when the red elements were fixed.

(b) An illustration of the temperature field in colours and scaled displacement field at the end time.

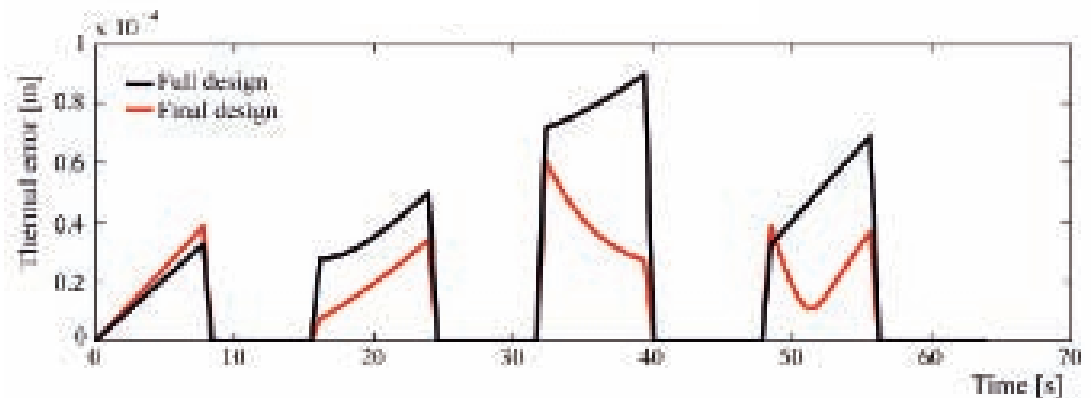
9 The thermal error of both designs as a function of time.



8a



8b



9

Outlook

The examples in this article highlight the opportunities that topology optimisation (TO) techniques offer to reduce thermal errors in precision devices. Now that the principle has been established, the next challenge is to extend this approach to finer meshes and 3D configurations while keeping the computation time manageable. This would allow designers to make use of TO as an additional tool in the design process.

Furthermore, placing heat sources and sinks in the design problem, e.g. the routing of cooling channels, could also be considered. To more accurately model the convection at free surfaces, the modelling should also be refined further. Another current aspect of research is how to include AM manufacturing constraints (e.g. overhang angles) in the problem formulation.

In various upcoming research projects, the Structural Optimization & Mechanics group at Delft University of Technology aspires to further develop the capabilities of these techniques. Working together with end users, it also hopes to increase their applicability. ■

REFERENCES

- [1] Mayr, J., Jedrzejewski, J., Uhlmann, E., Alkan Donmez, M., Knapp, W., Härtig, F., Wendt, K., Moriawaki, T., Shore, P., Schmitt, R., Brecher, C., Würz, T., and Wegener, K., "Thermal issues in machine tools", *CIRP Annals-Manufacturing Technology* 61 (2): pp. 771-791, 2012.
- [2] Lamers, R., "When precision cannot stand the heat", *Mikroniek* 50 (5): pp. 39-43, 2010.
- [3] Cavazzuti, M., Baldini, A., Bertocchi, E., Costi, D., Torricelli, E., and Moruzzi, P., "High performance automotive chassis design: a topology optimization based approach", *Structural and Multidisciplinary Optimization* 44 (1): pp. 45-56, 2011.
- [4] Van Keulen, F., Haftka, R.T., and Kim, N.H., "Review of options for structural design sensitivity analysis. Part 1: Linear systems", *Computer Methods in Applied Mechanics and Engineering* 194 (30): pp. 3213-3243, 2005.
- [5] Bendsoe, M.P., and Sigmund, O., "Material interpolation schemes in topology optimization", *Archive of Applied Mechanics* 69 (9-10): pp. 635-654, 1999.
- [6] Gao, T. and Zhang, W.H., "Topology Optimization Involving Thermo-Elastic Stress Loads", *Structural and Multidisciplinary Optimization* 42 (5): pp. 725-738, 2010.
- [7] Svanberg, K., "The method of moving asymptotes – a new method for structural optimization", *International Journal for Numerical Methods in Engineering* 24 (2): pp. 359-373, 1987.

DSPE CONFERENCE ON PRECISION MECHATRONICS 2014

Second edition of conference on precision mechatronics, organised by DSPE. The target group includes technologists, designers and architects in precision mechatronics, who are connected to DSPE, Brainport Industries, the mechatronics contact groups MCG/MSKE or selected companies or educational institutes. This year's theme is 'Revolution vs. Evolution', because progress is always a mix of evolution (optimisation) and revolution (disruptive technologies).



Tuesday 2 September

Invited speaker

- Prof. Dr. S.V. Sreenivasan (Professor of Mechanical Engineering and the Thornton Centennial Fellow in Engineering at the University of Texas at Austin, United States / Co-founder and CTO of Molecular Imprints)

Session 1 - System Design 1

- Jeroen de Boeij (FEI), *TEM Piezo short-stroke stage – a design based on error budgetting*
- Gijs van der Veen (Delft University of Technology), *Conceptual design of high performance motion systems using topology optimization*
- Cor Ottens (ASML), *Inside the EUV Source, design to specification and costs*

Session 2 - Thermal / Cryo

- Maurice Teuwen (Janssen Precision Engineering), *Lets move in cryo*
- Felix Bettonvil (Astron), *Accurate cryogenic opto-mechanical system for MATISSE*
- Marco Koevoets (ASML), *From evolutions in motion control to revolution in thermal control*

Session 3 - Robotics

- Jacco van der Spek (Alten Mechatronics), *Flexible industrial robotics through imitation learning*
- Maarten Arnolli (Demcon), *A CT-compatible transmission for a needle placement system*
- Bart Dirkx (WittyWorkx), *Low cost hexapod platform for consumer robot applications*

Wednesday 3 September

Invited speaker

- Dr. Xiaodong Lu (Precision Mechatronics Lab, University of British Columbia), *Planar Stage 2.0*

Session 4 - Advanced Applications

- Henk Mol (SKF Engineering and Research Centre), *Sensorised Wheel Bearing*
- Max Café (Delft University of Technology), *Nanometer precision Six Degrees of Freedom Planar Motion Stage with Ferrofluid Bearings*
- Ben van den Elshout (VDL ETG), *High-Performance Web Handling for Flexible Electronics*

Session 5 - Metrology

- Ivo Hamersma (IBS Precision Engineering), *Ultra-high precision metrology of 3D surfaces with wavelength scanning interferometry*
- Rick van der Maas (Eindhoven University of Technology), *Model-Based Calibrations for Medical 3D Reconstructions*
- Hamed Sadeghian (TNO), *Parallel scanning probe microscope comes of age*

Session 6 - Control

- Tom Kok (NXP Semiconductors), *Iterative Learning Control as part of an industrial motion framework*
- Gert Witvoet (TNO), *High performance control of mirror segment actuators for the European Extremely Large Telescope*
- Frank Pasteuning (Philips Innovation Services), *A numerical and experimental*

study of passive damping of a 3D structure using viscoelastic materials

Session 7 - System Design 2

- Ab Visscher (FEI Company), *Revolutionary evolution in the isolation of a Turbo Molecular Pump on an Electron Microscope*
- Ivan Smits (Océ-Technologies), *Mechatronic Approach Project Velocity*
- Peter van der Krieken (TMC), *Autonomous Fast Tool Servo on a standard turning lathe*

WWW.DSPE-CONFERENCE.NL

Having fun

"Here, we are having fun across the boundaries of many interesting disciplines, including electromechanics, precision machine design, metrology, structural dynamics, electronics, real-time computer design, signal processing, estimation, and advanced control algorithms."

Invited speaker, Dr. Xiaodong Lu: "Planar Stage 2.0"



Associate Professor Mechatronics at the University of British Columbia, Canada, and Head of Precision Mechatronics Lab

Roadmap for Digital Fabrication available on-line



Most products are produced by means of the established mass production infrastructure. Traditionally, this involves large stocks, high manual labour, large capital investments, high energy use, long-distance transportation. Although many advanced new materials have unique functional properties that hold a great promise for innovation, they often need to meet the criteria and characteristics of this established mass production paradigm. This delays the exploitation of the huge potential of whole new classes of materials. Combined with major

societal trends and consumer needs like customisation, personalisation, on-demand fulfillment and the fact that the world is becoming ever more digital and networked, there is a need for a paradigm shift in manufacturing called Digital Fabrication.

Digital Fabrication can be defined as a new kind of industry that uses computer-controlled tools and processes to transform digital designs and materials directly into useful products.

The European Diginova project was started to establish the current status across material domains and application domains in Europe in order to identify the most promising technology and business propositions for Digital Fabrication. The project consortium, consisting of four large companies, seven SMEs and nine

research institutes identified and connected main stakeholders through the establishment of innovative networks centred around concrete business cases to determine the added value and feasible routes to commercialisation. Marcel Slot, Director Technology Planning & Partnerships, Océ-Technologies, the Netherlands, acted as project coordinator of Diginova.

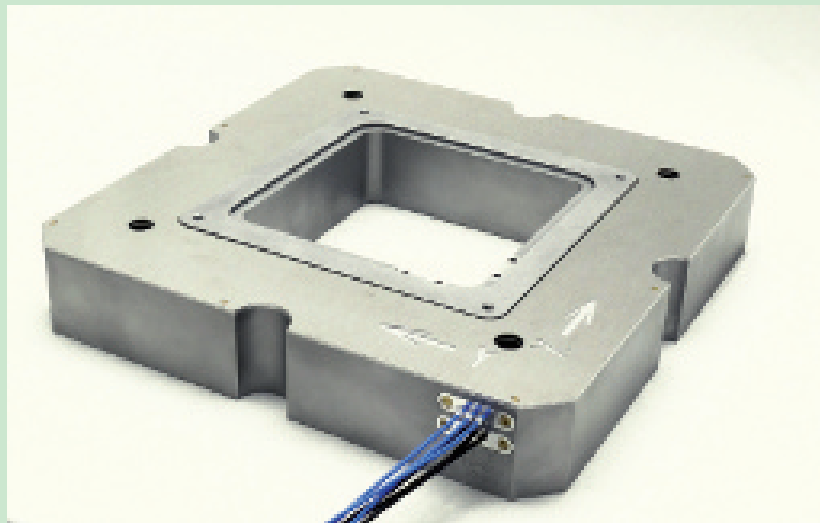
This spring, the Diginova consortium published the Roadmap for Digital Fabrication. It is available on-line. In the December 2014 issue of Mikroniek, dedicated to Additive Manufacturing, more on this roadmap.

WWW.DIGINOVA-EU.ORG

High-accuracy positioning of large loads

Laser 2000, based in Vinkeveen, the Netherlands, now offers the TRITOR 320 CAP from piezosystem Jena, Germany, one of the worldwide leading providers in the field of nanopositioning. This 3D piezo positioning system offers 50/50/400 (x/y/z) μm motion in open loop, 40/40/320 (x/y/z) μm motion in closed loop, for masses up to 20 kg, with a 150 x 150 mm² free aperture. Applications include automation, vacuum environments and non-magnetic applications, in the semiconductor and other industries.

The 3-axis positioning element was developed for high accuracy positioning of large loads. Highly dynamic properties were achieved as a result of finite-element-method optimisation. As with all elements from piezosystem Jena, the performance of the TRITOR 320 can be attributed to its construction with flexure hinges that are completely free of friction. Vacuum and cryogenic versions are available upon request, as well as material variations with invar, super invar, aluminum, or even titanium.

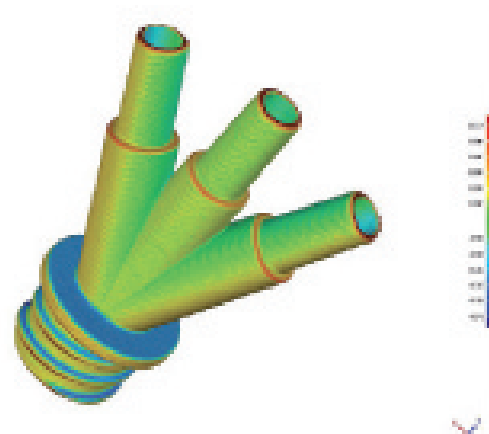


WWW.LASER2000.NL

WWW.PIEZOSYSTEM.COM

Plastic IT brings new 3D measuring technology to UK and Europe

Injection moulding specialist, Plastic IT, Shropshire, UK, has been awarded the sole rights to distribute in the UK and Europe a 3D measurement and validation technology – produced by CGI, Eden Prairie, MN, USA – for the accurate measurement of the internal and external geometries of small, precision, and micro plastic parts. The 3D scanning machines are the CGI Pearl 700 machine with a scanning envelope of 60 x 40 x 75 mm, and the CGI Pearl 900 machine with a scanning envelope of 85 x 65 x 150 mm. According to a press release, these 3D cross-sectional desktop scanners overcome many of the drawbacks found when using traditional measuring technologies such as CMMs, x-rays, and optical comparators for validation of small plastic parts.



■ The CGI Pearl 900 machine and an image from the CGI colour mapping software used to compare a 3-way connector scanned part data with the original CAD design. Green areas are within tolerance, red and blue are too big and too small respectively.

CGI's 3D cross-sectional scanner captures precise part measurements through the creation of 100% accurate 3D data sets. The nature of the technology also allows for multi-cavity / multi-part inspection, which eliminates the necessity for medical device OEMs to make the dangerous assumption that results from each cavity will be the same. It is possible using this technology to ensure that each cavity is independently and precisely tuned to mould parts, instead of 'averaging' across cavities.

To gather complete internal and external 3D data sets on the cross-sectional scanner, the part to be inspected is first encased in a slow-curing plastic resin. The encased or 'potted' part is then placed in the CGI machine, before being sliced into ultra-thin 25 micron layers. As each layer is removed, an optical scanner captures the newly exposed 2D profile at an extremely high resolution of 1 million pixels per square inch. Cutting and imaging is repeated until the part is consumed. The collection of 2D images is then processed to build a 100% accurate 3D point cloud that details exterior and interior geometries. The data can then be inspected, allowing verification of features that are both visible and concealed in the part geometry. Measurement repeatability is +/- 12.75 microns. The 3D scanner enables verification of CAD design intent and deviation cost-effectively and quickly.

A Complete Precision Gear Range



High precision cut gears, precision ground gears from 0.5 module and a competitive range of brass spur gears and pinions. Fine pitch gears, 0.2 to 1.5 module.

Worms and wheels, bevels and internal gears designed to complement the spur gear range.

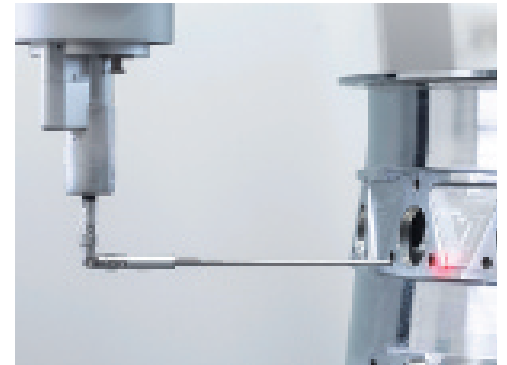
Reliance
Precision Limited

www.relianceprecision.nl
NL +31 (0) 76 5040790
sales@reliance.co.uk

Non-contact measurement with 'tactile' accuracy

Hexagon Metrology (based in Cobham, Surrey, UK) has launched the HP-O technology solution, a new scanning technology on stationary CMMs based on frequency-modulated interferometric optical distance measurement. According to a press release, HP-O features an accuracy and reliability comparable to tactile scanning probes, a higher scanning speed, increased measurement range and the generic optic advantage of non-contact measurements. It is an alternative for high-precision tactile measurements when speed is important, parts are difficult to access for tactile probes or when parts are deformed or get damaged by tactile probing.

The HP-O solution is multi-sensor compatible – multiple optical heads or tactile probes are interchangeable in a single program using the standard tool changer. Optical measurements can be made in single point or scanning mode with 3- or 4-axis scanning in open loop mode. The solution is launched as a complete system including Hexagon Metrology software QUINDOS and Leitz PMM-C high-accuracy CMM. The new lightweight probe head works with an acceptance angle of up to $\pm 30^\circ$ and offers repeatability below $0.3 \mu\text{m}$. The probe diameter is as small as 3 mm and the measurement range up to 20 mm provides access to points inaccessible by tactile probes.



WWW.HEXAGONMETROLOGY.COM

High-Tech Systems 2014 highlights

Early May this year, High-Tech Systems 2014 in Den Bosch, the Netherlands, focused on the high-tech systems industry. The event was organised by Techwatch and featured an exhibition with nearly 100 companies, knowledge institutes and consultancies from the Netherlands and various other European countries. Other highlights were the launch

of the High Tech Systems Center (HTSC) by Eindhoven University of Technology, demos of robot soccer, and sessions on high-level supply chain management, system architecture, robotics and ultra-precision.

WWW.HIGHTECHSYSTEMS.NL WWW.TUE.NL/HTSC WWW.ROBOTSPORTS.NL



■ High-Tech Systems 2014 was held in the pleasant atmosphere of the 1931 Congressentrum Brabant venue in Den Bosch. (Photos courtesy of Techwatch; photographer: Bart van Overbeeke)



■ Eindhoven professor Maarten Steinbuch presented the High Tech Systems Center initiative.



■ Ton Peijnenburg, manager Advanced Developments at VDL ETG and DSPE board member (in charge of the DSPE Special Interest Group Robotics) represented VDL Robot Sports, the industrial RoboCup team that was (re)launched last year.

UPCOMING EVENTS

25-29 August 2014, Leiden (NL)

Summer School Manufacturability

Summer school, organised by LiS Academy, dedicated to the manufacturability of precision components and targeted at young professional engineers with a limited knowledge of and experiences with manufacturing technologies and associated manufacturability aspects.

WWW.LISACADEMY.NL

**2-3 September 2014,
Sint-Michielsgestel (NL)**

DSPE Conference on Precision Mechatronics

Second edition of conference on precision mechatronics, organised by DSPE. The target group includes technologists, designers and architects in precision mechatronics, who are connected to DSPE, Brainport Industries, the mechatronics contact groups MCG/MSKE or selected companies or educational institutes. This year's theme is 'Revolution vs. Evolution', because progress is always a mix of evolution (optimisation) and revolution (disruptive technologies). See page 67 for the programme.



WWW.DSPE-CONFERENCE.NL

4 September 2014, Eindhoven (NL)

Annual conference High Tech Platform

First edition of the annual conference of the Mikrocentrum platform.

WWW.MIKROCENTRUM.NL/HIGH-TECH-PLATFORM

**30 September - 3 October 2014,
Utrecht (NL)**

World Of Technology & Science 2014

Four 'worlds' (Automation, Laboratory, Motion & Drives and Electronics) will be exhibiting in the Jaarbeurs Utrecht. With the co-location of Macropak, European Dairy Industry Show and Industrial Processing the largest industrial show of the Netherlands arises.

WWW.WOTS.NL

9-14 November 2014, Boston (MA, USA)

29th ASPE Annual Meeting

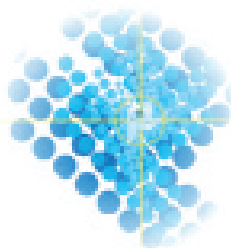
Meeting of the American Society for Precision Engineering, introducing new concepts, processes, equipment, and products while highlighting recent advances in precision measurement, design, control, and fabrication.

ASPE.NET

12-13 November 2014, Veldhoven (NL)

Precision Fair 2014

Fourteenth edition of the Benelux premier trade fair and conference on precision engineering, organised by Mikrocentrum. Some 275 specialised companies and knowledge institutions will be exhibiting in a wide array of fields, including optics, photonics, calibration, linear technology, materials, measuring equipment, micro-assembly, micro-connection, motion control, surface treatment, packaging, piezo technology, precision tools, precision processing, sensor technology, software and vision systems.



Precision Fair

WWW.PRECISIEBEURS.NL

19-20 November 2014, Den Bosch (NL)

Bits&Chips Smart Systems 2014

First edition of the annual event on embedded systems and software, focused on the development of networked technical information systems. Combination of Bits&Chips Embedded Systems (since 2002) and Bits&Chips Hardware Conference (since 2008). The target group includes academia, researchers, designers, engineers and technical management.



WWW.BC-SMARTSYSTEMS.NL

20 November 2013, Utrecht (NL)

Dutch Industrial Suppliers Awards 2014

Event organised by Link Magazine, with awards for best knowledge supplier and best logistics supplier, and the Achievement Award.

WWW.LINKMAGAZINE.NL

25-27 November 2014, Nuremberg (DE)

SPS IPC Drives 2014

International exhibition and conference on electric automation, systems and components.

WWW.MESAGO.DE/EN

Bearing and Linear Technology



Schaeffler Nederland B.V.

Schaeffler Nederland B.V.

Gildeweg 31

3771 NB Barneveld

T +31 (0)342 - 40 30 00

F +31 (0)342 - 40 32 80

E info.nl@schaeffler.com

W www.schaeffler.nl

Schaeffler Group - LuK, INA and FAG - is a world wide leading company in developing, manufacturing and supplying of rolling bearings, linear systems, direct drives and maintenance products. Applications: automotive, industrial and aerospace.

Development



TNO

T +31 (0)88-866 50 00

W www.tno.nl

TNO is an independent innovation organisation that connects people and knowledge in order to create the innovations that sustainably boost the competitiveness of industry and wellbeing of society.

member **DSPE**

Development and Engineering



ACE ingenieurs- & adviesbureau

werktuigbouwkunde en

elektrotechniek BV

Dr. Holtropaan 46

Postbus 7030, 5605 JA Eindhoven

5652 XR Eindhoven

T +31 (0)40 - 2578300

F +31 (0)40 - 2578397

E info@ace.eu

W www.ace.eu

ACE has developed into a leading engineering and consultancy firm with a strong focus on mechanics and mechatronics. Services include conceptualization, development, engineering and prototyping.

member **DSPE**



Lencon Engineering

Hondsdiik 3,

2396 HG Koudekerk aan den Rijn

Postbus 28

2396 ZG Koudekerk aan den Rijn

T: +31 (0)71 341 65 55

F: +31 (0)71 341 65 58

E: sales@lencon.nl

W: www.lencon.nl

Lencon provides maximum flexibility in high-end mechanical engineering and product development. Turn-key projects and detachment of experienced productengineers and precisionengineers.

member **DSPE**

Education



Leiden school for Instrument-makers (LiS)

Einsteinweg 61

2333 CC Leiden

The Netherlands

T +31 (0)71-5581168

F +31 (0)71-5681160

E info@lis-mbo.nl

W www.lis-mbo.nl

The LiS is founded in 1901 by the famous scientist prof. Kamerlingh Onnes. Nowadays the LiS is a modern school for vocational training on level 4 MBO-BOL. The school encourages establishing projects in close cooperation with contractors and scientific institutes, allowing for high level "real life" work.

member **DSPE**



PAO Techniek

Stevinweg 1, 2628 CN Delft

Postbus 5048, 2600 GA Delft

T +31 (0)15 27 88 350

F +31 (0)15 27 84 619

E info@paotechniek.nl

W www.pao.tudelft.nl

Lasers, Light and Nano-motion



Laser 2000 Benelux C.V.

Voorbancken 13a

3645 GV Vinkeveen

Postbus 20, 3645 ZJ Vinkeveen

T +31(0)297 266 191

F +31(0)297 266 134

E info@laser2000.nl

W www.laser2000.nl

Laser 2000 Benelux considers it her mission to offer customers the latest photonics technologies available.

Their areas of expertise are:

- Lasers and laser systems for industry and research
- Light metrology instruments for LED and luminaire industry
- Piezo- and stepper motion products for nano- and micro-positioning
- LED illumination and high speed inspection in machine vision applications

Laser Systems



Applied Laser Technology

De Dintel 2

5684 PS Best

T +31 (0)499 375375

F +31 (0)499 375373

E techsupport@alt.nl

W www.alt.nl

member **DSPE**

3D Measurement Services



Mitutoyo Nederland B.V.
Storkstraat 40
3905 KX Veenendaal
T +31 (0)318-534911
F +31 (0)318-534811
E info@mitutoyo.nl
W www.mitutoyo.nl

Mechatronics Development



centre for concepts in mechatronics

CCM Centre for Concepts in Mechatronics
De Pinckart 24
5674 CC Nuenen
T +31 (0)40 2635000
F +31 (0)40 2635555
E info@ccm.nl
W www.ccm.nl

CCM translates technology into technique. Commitment, motivation, education and skills of our employees are the solid basis for our business approach.

member **DSPE**



Janssen Precision Engineering
Azielaan 12
6199AG Maastricht-Airport
T +31 43 3585777
F +31 43 3580036
E huub.janssen@jpe.nl
W www.jpe.nl

Precision engineering and mechatronic solutions in ambient, vacuum and cryogenic environment

member **DSPE**

Mechatronics Development



CREATING MACHINES TOGETHER

Manufacturing Technical Assemblies (MTA) b.v.
Waterbeemd 8
5705 DN Helmond
T: +31 (0)492 474992
F: +31 (0)492 474510
E: info@m-t-a.nl
W: www.m-t-a.nl

MTA is an high-tech system supplier specialized in the development and manufacturing of mechatronic machines and systems.

Our clients are OEM's in the Packaging, Food, Graphics and High-tech industries.

Metal Precision Parts



Etchform BV
Arendstraat 51
1223 RE Hilversum
T +31 (0)35 685 51 94
F info@etchform.com
W www.etchform.com

Etchform is a production and service company for etched and electroformed metal precision parts.

member **DSPE**

Metal Precision Parts



A Member of the SPGPrints Group

Karel van Gelreweg 22
6961 LB Eerbeek
T +31 (0)313 672 911
E info.vec@spgprints.com
W www.vecoprecision.com

Having our own R&D and Engineering Center including clean room manufacturing and full automated inspection facilities Veco is an excellent co-maker for your extreme precision metal components.

member **DSPE**

Micro Drive Systems



Maxon Motor Benelux

The Netherlands

Head Office
maxon motor benelux bv
Josink Kolkweg 38
7545 PR Enschede

South
High Tech Campus 9
5656 AE Eindhoven
T: +31(053) 744 0 744
E: info@maxonmotor.nl
W: www.maxonmotor.nl

Belgium / Luxembourg

maxon motor benelux bv
Schaliënhoedreef 20C
2800 Mechelen - Belgium
T: +32 (15) 20 00 10
F: +32 (15) 27 47 71
E: info@maxonmotor.be
W: www.maxonmotor.be

maxon motor is the worldwide leading supplier of high precision drives and systems. When it really matters! Try us.

Micro Drive Systems



Minimotor Benelux

Belgium
Dikberd 14/6c
B-2200 Herentals
T +32 (0)14-21 13 20
F +32 (0)14-21 64 95
E info@minimotor.be

The Netherlands
Postbus 49
NL-1540 Koog a/d Zaan
T +31 (0)75-614 86 35
F +31 (0)75-614 86 36
E info@minimotor.nl
W www.faulhaber.com

Faulhaber is a leading manufacturer of miniature drive systems based on ironless micromotors with the highest power-to-volume ratio.

member **DSPE**

Micromachining



Reith Laser bv
Bijsterhuizen 24-29
6604 LK Wijchen
The Netherlands
T +31 (0)24 3787564
F +31 (0)24 3787586
E info@reithlaser.nl
W www.reithlaser.nl

For more than 22 years Reith Laser bv is the leading supplier of laser-processed products in Europe. We can offer you a great diversity of lasermaterialprocessing activities:

- Laser- (micro-) cutting
- Laser drilling
- Laser welding
- Laser micromachining

Reith Laser is active in precision industry, medical industry, aerospace, semiconductor- and automotive industry.

Motion Control Systems



Aerotech LTD
Jupiter House, Calleva Park
Aldermaston
Berkshire
RG7 8NN England
T +44 (0)118 9409400
F +44 (0)118 9409401
E sales@aerotech.co.uk
W www.aerotech.co.uk



Applied Laser Technology
De Dintel 2
5684 PS Best
T +31 (0)499 375375
F +31 (0)499 375373
E techsupport@alt.nl
W www.alt.nl

member **DSPE**



IBS Precision Engineering
Esp 201
5633 AD Eindhoven
T +31 (0)40 2901270
F +31 (0)40 2901279
E info@ibspe.com
W www.ibspe.com

IBS Precision Engineering is a high-tech company in precision metrology components, systems and machines. Our solutions include special metrology machines, machine tool calibration systems, non-contact measuring systems and porous media air bearings.

member **DSPE**

Motion Control Systems



Newport Spectra-Physics B.V.
Vechtensteinlaan 12 - 16
3555 XS Utrecht
T +31 (0)30 6592111
E netherlands@newport.com
W www.newport.com

Newport Spectra-Physics BV, a subsidiary of Newport Corp., is a worldwide leader in nano and micropositioning technologies.

member **DSPE**



Reliance Precision Ltd
Florijnstraat 20
4879 AH Etten-Leur
T +31 (0)76-5040790
E sales@reliance.co.uk

- Positioning systems
- Drives
- Mechatronic Assemblies
- Intelligent Motion Control

Reliance Precision Ltd manufactures, assembles and tests precise motion control solutions for high-accuracy applications.



Rotero Holland bv
Pompmolenlaan 21
3447 GK Woerden
Postbus 126
3440 AC Woerden
T +31 (0)348 495150
F +31 (0)348 495171
E info@rotero.com
W www.rotero.com

Rotero is your partner and advisor in the field of high-precision components: stepper- and servomotors up to 1.5kW, ball screws, precision leadscrews and gear boxes.

Optical Components



Applied Laser Technology
De Dintel 2
5684 PS Best
T +31 (0)499 375375
F +31 (0)499 375373
E techsupport@alt.nl
W www.alt.nl

member **DSPE**



Molenaar Optics
Gerolaan 63A
3707 SH Zeist
Postbus 2
3700 AA Zeist
T +31 (0)30 6951038
F +31 (0)30 6961348
E info@molenaar-optics.nl
W www.molenaar-optics.eu

member **DSPE**

Optics and Imaging



Focal Vision & Optics
Institutenweg 25A
7521 PH Enschede
T +31 (0)53 - 428 7880
E info@focal.nl
W www.focal.nl

Focal Vision & Optics provides services for optical system design and advanced image processing. We design and deliver custom made and high speed precision inspection systems to OEMs and industrial manufacturers.

member **DSPE**

Piezo Systems



Applied Laser Technology
De Dintel 2
5684 PS Best
T +31 (0)499 375375
F +31 (0)499 375373
E techsupport@alt.nl
W www.alt.nl

member **DSPE**



Heinmade B.V.
High Tech Campus 9
5656 AE Eindhoven
T +31 (0)40 8512180
F +31 (0)40 7440033
E info@heinmade.com
W www.heinmade.com

HEINMADE develops and supplies piezo system solutions for positioning and vibration damping. HEINMADE cooperates with and is distributor of Nanomotion, Noliac and Piezomechanik.

Surface Technologies



Maan Special Products B.V.
Glueing Precision
Klipperweg 16
8102 HR Raalte
T +31(0)572 362 936
F +31(0)572 364 498
E info@maansp.nl
W www.maansp.nl

Maan Special Products fabricates high-precision products using unique surface-treatment and glueing technology that tests or even exceeds the limits of what is technically possible.

ADVERTISERS INDEX

- | | |
|--|-------|
| ■ DSPE conference | 31 |
| www.dspe.nl | |
| ■ HEIDENHAIN | 76 |
| www.heidenhain.nl | |
| ■ IBS Precision Engineering | 59 |
| www.ibspe.com | |
| ■ Mikroniek Guide | 72-74 |
| ■ Mikrocentrum | 2 |
| www.precisiebeurs.nl | |
| ■ NTS-Group | 19 |
| www.nts-group.nl | |
| ■ Reliance Precision Limited | 69 |
| www.relianceprecision.nl | |

Dutch Society for Precision Engineering

DSPE

YOUR PRECISION PORTAL

Your button or banner on the website www.DSPE.nl?

The DSPE website is the meeting place for all who work in precision engineering.

The Dutch Society for Precision Engineering (DSPE) is a professional community for precision engineers: from scientists to craftsmen, employed from laboratories to workshops, from multinationals to small companies and universities.

If you are interested in a button or banner on the website www.dspe.nl, or in advertising in Mikroniek, please contact Gerrit Kulsdom at Sales & Services.

T: 00 31(0)229-211 211 ■ E: gerrit@salesandservices.nl

DSPE

YOUR PRECISION PORTAL

μ MIKRONIEK

Mikroniek is the professional journal on precision engineering and the official organ of the DSPE, The Dutch Society for Precision Engineering.

Mikroniek provides current information about technical developments in the fields of mechanics, optics and electronics and appears six times a year.

Subscribers are designers, engineers, scientists, researchers, entrepreneurs and managers in the area of precision engineering, precision mechanics, mechatronics and high tech industry. Mikroniek is the only professional journal in Europe that specifically focuses on technicians of all levels who are working in the field of precision technology.

Publication dates 2014

nr.	deadline	publication	special
4.	01-08-2014	29-08-2014	DSPE Conference Precision Mechatronics
5.	19-09-2014	25-10-2014	(issue before the Precision Fair)
6.	07-11-2014	12-12-2014	Additive Manufacturing (-Report Precision Fair 2014)



**For questions about advertising
please contact Gerrit Kulsdom**

Dial: 00 31(0)229-211 211 ■ E-mail: gerrit@salesandservices.nl





HEIDENHAIN



How do you identify
the right measuring
technology?

To identify the right person in a group of thousands, you only need to look at his fingers. But where do you look when you want to find the best measuring and control technology? You can recognize HEIDENHAIN by many characteristics, but especially by our passion for precision. From the everyday encoder in the machine tool to the nanometer-precise length comparator... for more than 120 years, HEIDENHAIN has been the measure for accuracy. We invest continuously in this technical difference. And you profit from products that are not only innovative, economical and reliable, but also characterized down to their smallest details by unmistakable precision.

HEIDENHAIN NEDERLAND BV

6710 BB Ede

Nederland

Telefoon: 0318-581800

www.heidenhain.nl

angle encoders + linear encoders + contouring controls + position displays + length gauges + rotary encoders